

UNIVERSITY OF LONDON

Imperial College of Science and Technology

Technical Optics Section



A TWO-DIMENSIONAL OPTICAL FOURIER ANALYZER
FOR IMAGE EVALUATION

Tuckerman Moss



Thesis submitted for the
Ph.D. Degree

—
1 9 6 3

ABSTRACT

Fourier techniques are frequently used in quality evaluations of optical systems. It is of value to inspect the relationship between these tests and the subjective evaluation of image quality made by the human eye. An instrument for the measurement of the Fourier spectra of photographic images has been constructed. It is based on a modification of Young's experiment involving polarized light and a Wollaston prism; real and imaginary parts of the Fourier spectrum may be obtained over a range of from zero to five lines per millimeter. This equipment has been used to obtain the Fourier transforms of a group of photographic slides whose images suffer from varying degrees of comatic, Gaussian and ~~sph~~ spherical aberration blur. These results are compared with subjective evaluations of the same images obtained by the method of paired-comparisons at three different distances. It becomes clear from this comparison that the methods of Fourier analysis offer a more stringent method of quality evaluation than is offered by subjective testing.

TABLE OF CONTENTS

• CHAPTER I •

Methods of Optical Image Assessment

Introduction	1
Optical Frequency Response	3
Preliminary Studies into Visual Defocus Tolerances Making Use of Fourier Techniques	13
References	22

• CHAPTER II •

Instrumentation

Generation of Fringes	24
Measurement of the Fourier Transform	30
Primary Aberrations Arising from the Wollaston Prism	33
Variation of Fringe Visibility with Slit Width	49
Variation of Average Intensity Over the Fringe Pattern Field	55
Mechanical Design	60
The Line-Plane Reference System	60
Optical Mounts	64
Lamp and Housing	68
Modulator Drive and Mount	73
Cam Drive and Prism Mount	76
Finish	77
Optical Alignment and Set-up	79
Electronics	81
References	91

•CHAPTER III•

An Evaluation Process Compatible to Both
Subjective and Instrumental Testing

Instrumental Evaluations	92
Test Object Production	94
Paired-Comparison Quality Evaluations	102
Response Difference Computations	118
References	148

•CHAPTER IV•

Relating Visual and Instrumental Concepts
of Quality

Fourier Transforms of Test Slides	149
Comparison Between Transforms and Subjective Tests	159
Conclusions	166
<u>Acknowledgements</u>	169

C H A P T E R I

Methods of Optical Image Assessment

INTRODUCTION

By observing and measuring the diameter and structure of the image of a point source a reasonably critical evaluation of the quality of the intervening optical system may be made. From the shape and structure of the image, a knowledge of the types and relative amounts of aberrations present in the system may often be roughly inferred: and from measurements of the intensity distributions within the image quantitative judgements may be made as to the quality of that system. So it is that we recognise the flare patterns of coma, the broadening of the disk from spherical aberration and defective focus, and the line images of astigmatism.

This means of image assessment was a direct outgrowth of the astronomer's need to test and perfect the objectives for his telescope. A perfect stellar image would be one that was limited only by the diffraction parameters of the system, and Rayleigh (1879) and Ströhl (1895) set empirical limits by which an

estimate of the performance of optical systems might be tested.

Although optical objects are not generally composed of isolated point sources, one may certainly think of any scene as being made up of a large number of adjacent points. To obtain an idea of the performance of an optical system which has been tested by a star image one has to sum the interactions of these points over the image field. In practice the structure of the spread functions of these individual points is inclined not only to be complex but variable over the image field. The process of summing these spread functions and interpreting the results would be both tedious and extremely difficult.

The scenic objects presented to photographic objectives and visual observing instruments are of an extended nature. Moreover, a knowledge of the profile of a line spread function, rather than of a point spread function and its variation over the area of the image plane, adequately indicates the performance of an optical system used to observe extended objects. Rather than applying a quality criterion to this spread function directly, it is more directly informative to take the Fourier transforms of the line spread functions for different azimuths to give the frequency response of

the system in these azimuths. Comparison of the resulting response curves of various systems with the curve for an ideal system will supply the bandwidth, or limit of resolution, of the system as well as a description of its performance at all lower frequencies in any azimuth for each point of the image field.

The limit of resolution of a system may be obtained more directly by noting the highest frequency at which a square-line grating can be just resolved by an observer. Numerous ingenious and valuable test charts of the square-bar type have been invented and used for this purpose. Typical are the Cobb test chart and Inglestam's test pattern. But, as was mentioned, these tests only indicate the band width of the system, and, because of effects such as spurious resolution and contrast reversal produced by the interactions of higher frequency harmonics, too many personal equations must be added to the result to make the quality predictions as reliable as one might wish.

OPTICAL FREQUENCY RESPONSE

The usefulness of Fourier analysis, and hence frequency response techniques, in optical systems evaluation is due to two main factors.

The first is that under two simple conditions, which will be discussed below, a grating-like object, across which the intensity varies according to the formula

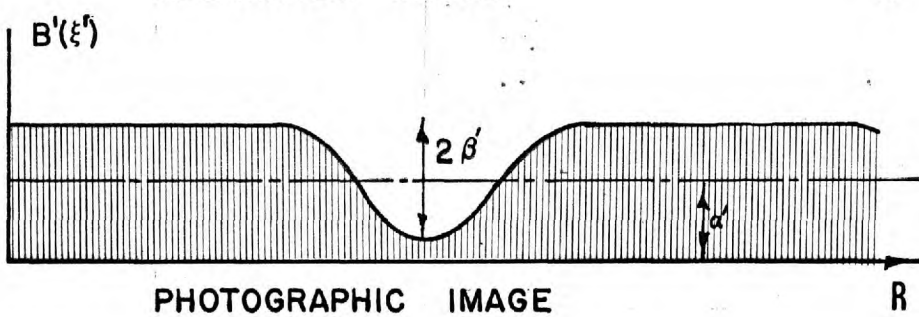
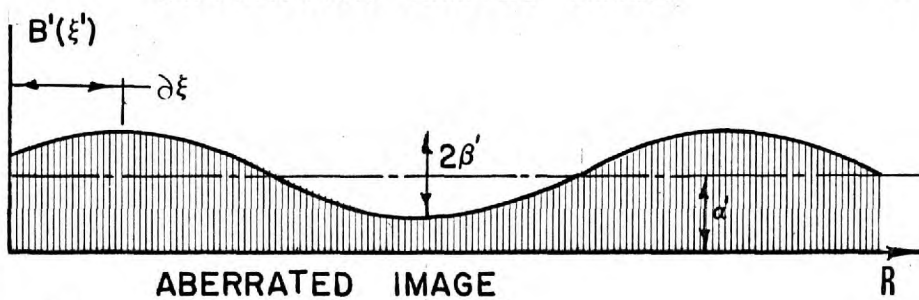
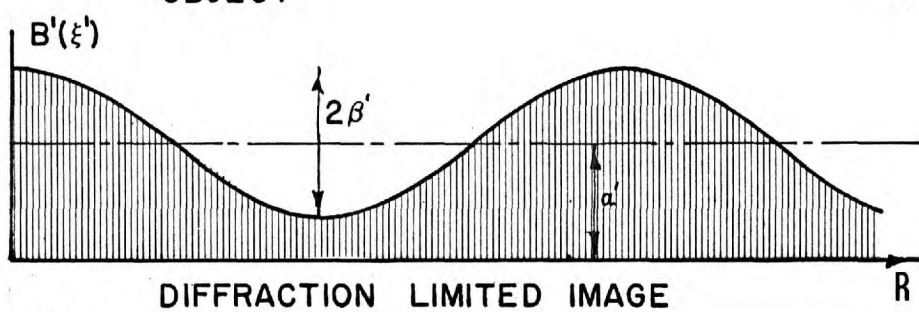
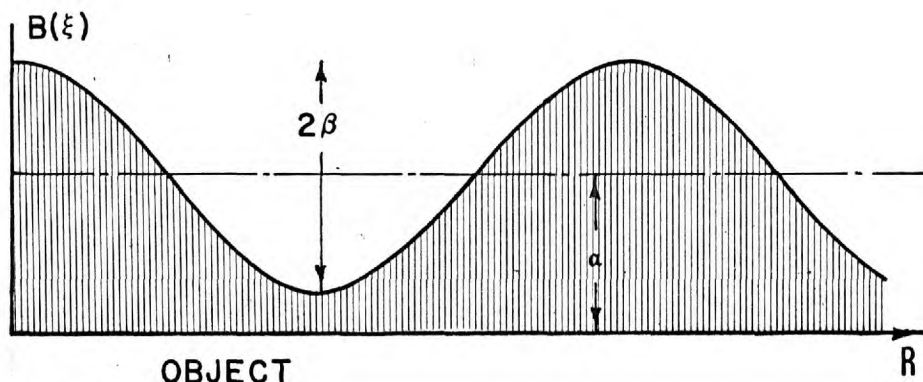
$$B(\xi) = \alpha + \beta \cos(2\pi R\xi).$$

has as its image an intensity distribution, of exactly the same form, namely

$$B'(\xi') = \alpha' + \beta' \cos[2\pi R'\xi' + \theta(R)].$$

The primes refer to the image space in accordance with normal procedure. The contrast transfer function $T(R, \psi)$ of the optical system is equal to the ratio of the image contrast (β'/α') to the object contrast (β/α) , and is always less than unity. The contrast transfer function is dependent on both the azimuthal orientation (ψ) of the grating with reference to the optical system and of the grating spacing $(\frac{1}{R})$. The coordinates (ξ) and (ξ') are usefully chosen to be such that their ratio will equal the magnification of the system. In this case the spatial frequencies R' and R are numerically equal.

This characteristic of a cosinusoidal fringe pattern being transmitted without change of form allows one to avoid all the difficulties of data reduction called for with point or square-wave line test-objects. The effect of aberrations and diffraction caused by the optical system will result in either a reduction of image contrast or in both a contrast reduction and a phase shift. The lateral shift in the image plane may be represented by,



$$\delta \xi' = -\theta(R, \psi) / 2\pi R$$

$\theta(R, \psi)$ being the angular measure of the phase-shift resulting from asymmetry in the spread function. The complex transfer function is then

$$D(R, \psi) = T(R, \psi) \exp \{ i \theta(R, \psi) \}$$

in accordance with the customary formalism.

The second important factor making Fourier analysis so important to optical systems evaluations is that any two-dimensional spatial distributions of intensity (i.e. any extended optical object) may be represented as the super-position of sets of unidimensional cosinusoidal spatial distributions of intensity arranged with the proper azimuth, position and amplitude. In other words, any optical object may be built up out of a variety of Fourier components in such a way that it represents exactly the object. If one were to reduce the object to these components each would be transferred to the image plane in such a manner that they would all suffer a decrease of contrast equal to the contrast transfer function and a shift of lateral position equal to $\delta \xi'$ and these changes would be the direct result of the optical system's failure to produce a perfect image (i.e., a direct point to point correspondence, scaled to the magnification of the system, between the object and image).

The only two conditions which need to be placed upon this treatment of optical images are that the intensities in the image add in a linear fashion (i.e., that the object be of an incoherent nature) and that the aberrations vary smoothly and slowly over the image plane. This latter condition, known as isoplanatism, will be better satisfied as the state of correction of a system is improved, but is generally of an acceptable nature in any event.

Calculations have been made to estimate the frequency response curves of lens systems when they are suffering from defect of focus (Hopkins, 1955), astigmatism (De, 1955) and spherical aberration and coma (Goodbody, 1959). Many of these results have been verified by K.G. Birch (1960) using a slit scanning method and by Kelsall (1959) using an automatically recording interferometer working in monochromatic light. In this case not only was the contrast transfer function, $T(R, \psi)$ measured but, in some experiments, the phaseshift, $\delta\phi'$, was also obtained.

Frequency response curves have also been obtained for photographic emulsions (Eastman Kodak, 1961) making it possible to predict a system's performance by the same method, through to its final recording. There are however, a few peculiarities in the application of frequency response methods to a photographic emulsion.

Firstly the problem is simplified since under most conditions there is no spatial phase shift, between the 'object' cosine-wave and the recorded 'image' cosine-wave. The problem is complicated, however, by the non-linear properties of the photographic emulsion. Because of the non-linear toe and head portions of a normal H-D curve a pure cosine-wave input image may suffer an effect exactly similar to the harmonic distortions found in an audio amplifier. However, unless the gamma is exactly equal to unity, the opacity on the straight portion of the characteristic curve is not proportional to the exposure. There is a linear relation only between the logarithms of these quantities. The signal as recorded on the photographic emulsion now contains harmonics of the original pure cosine-wave. Frieser (1935) suggested that the photographic process could be best thought of in two stages; the exposure of the emulsion to the incoming signal which leads to, in this case, a linear scattering of light in the emulsion; and, secondly the development of the exposed plate. In the first stage a cosine-wave image will only suffer a decrease in contrast but in the second stage the non-linear relation between the effective exposure and the developed density results in the introduction of harmonics to the signal and this effect is a function only of the development process.

Wilczynski's (1960) work on this subject shows that while the best linear contrast transfer function may be obtained over the straight portion of the H-D curve with gamma equal to one, the highest contrast is obtained in the lower, or toe, region of the curve. This confirms the empirical studies made by McKenzie (1931) in connection with studies of variable density sound recording.

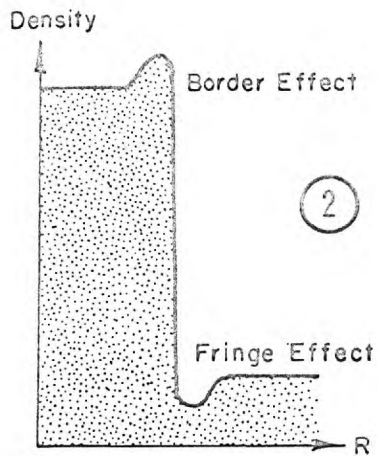
Wilczynski also showed that harmonic distortion occurred in the image for any value of gamma not equal to one by his method of Fourier analysis. His technique of analysis involved the use of laterally moving monochromatic fringes generated by a Michelson interferometer. These fringes were passed through the photographic transparency under test and the light transmitted was collected to obtain the modulus of the Fourier transform of the test object.

The application of the concept of frequency response in the photographic process is further complicated, however, by neighbourhood effects. The effect, first described by Eberhardt (1912), consists in the fact that even for a uniformly exposed image the developed density of small spots was greater than that of large spots. The effect grows with the exposure but is greatly diminished by a background exposure and

the resulting development of fog. During the course of development, the neighbourhood effect rises to a maximum and then decreases as development is continued. The effects were ascribed by Eberhardt to the accumulation, during development, of development products and partial exhaustion of the developer in the region of heavily exposed areas, which tends to slow down the image growth. With very small images, this production of oxidation products and soluble bromide is low. The developer then retains its original concentration and produces greater density than for larger areas. [After Mees (1952b)].

The Eberhardt effect is often pronounced at the edges of high contrast images where both an overshooting and undershooting of the edge may be seen. These effects, known as the border effect and the fringe effect are described by Mees (1952c) as follows:-

- a. The border effect appears as an increase in the density of the margins of a uniformly exposed, sharply defined edge, relative to the density within the image itself. It is caused by the diffusion of the fresh developer into the exposed image from the neighbouring unexposed background.
- b. The fringe effect appears as a diminution in the fog density along the boundary of a well-exposed and sharply defined image as a result of the diffusion of reduction products from the image.



In terms of Fourier analysis this implies, and was shown by Wilczynski to be so, that for low frequency sinewave test objects an increase of even harmonics will occur, giving higher average opacity and lower fundamental amplitude for the same opacity. This in fact,

explains the apparent rise above unity of the frequency response curves, given by Eastman Kodak for the lower portion of the response curve.

While it has been suggested that the overshooting effect tends to correct the contrast transfer function of the optical system by intensifying the mid-range frequencies this is really not generally so. Frequency filtering occurs only in those parts of the image where contrast is high and the resolution would be good in any event. In the low contrast detail no filtering occurs at all. Basically the Eberhardt effect only distorts the image in a non-linear and non-correctable manner. It is frequently the best course to reduce the effect, by brush development, to a minimum value.

As was previously mentioned, the use of Fourier techniques in optics aims to set up an objective method of evaluating the image quality, based on the transfer factors of the system. The lens designer may find the effect on the frequency response of a lens of different aberrations by calculation and testing, and is able, to some extent, to control the frequency response of the system; he will know the effect that the photographic emulsion will have on the image and so will know the limiting and controlling quality factors of the entire system. There remains the important question, namely, whether the sensitivity of frequency response as a means of assessing image quality is greater than the sensitivity of assessment of image quality made subjectively by observers.

An attempt to solve part of this problem was made by Crose (1956) when he filtered out certain spatial frequencies from photographic scenes and observed them over the resulting restricted bandwidth.

Other experiments, such as those by Higgins, Lambert and Wolfe (1959), have been carried out involving controlled degradation of image quality and a variable contrast transfer factor. While these experiments are valuable and useful, they do not seem to establish a direct relationship between the observer's criterions

of quality in a photographic image and the contrast transfer functions of the preceding system.

The purpose of the work described in this thesis has been of a two-fold nature: first, the development of an instrument to obtain the Fourier transform of photographic images (which, although not in itself an entirely new development, does describe a new method of instrumentally obtaining these ends) and secondly, an investigation of the effect that a degradation of image quality by Gaussian blur, spherical aberration and coma will have both on the Fourier components of the image ~~the~~ ^{and} the observer's judgement of the quality of that image. Correlation of these factors will then be made.

PRELIMINARY STUDIES INTO VISUAL DEFOCUS TOLERANCES MAKING USE OF FOURIER TECHNIQUES.

In an effort to obtain a rough idea of the parameters which would be expected in this research a group of preliminary experiments were carried out. These tests all involved the ability of observers to discriminate the minimum defect of focus of a dark strip on a brighter background which could be tolerated when compared with a juxtaposed comparison slit. Crude as these experiments were, the results are of interest.

Ten experienced observers were asked to set a series of dark strips and a knife-edge so that their images, viewed in projection, just became unsharp. They were asked to choose the minimum defocus position that produced a just discernable defocus of the image, whether this involved an apparent loss of contrast or a softening of the edges. The observers were allowed to 'zero-in' on what they felt this position to be. As mentioned, to aid their discrimination, an equivalent image of perfect focus was projected through the system to act as a comparison. See Figure (3).

At the one meter observing distance used, the slit images viewed had a real width of 2.0", 0.250", 0.33", 0.007" and 0.001". The last and narrowest slit, being below the resolution of the eye, exhibited a contrast reversal and was, therefore, not used.

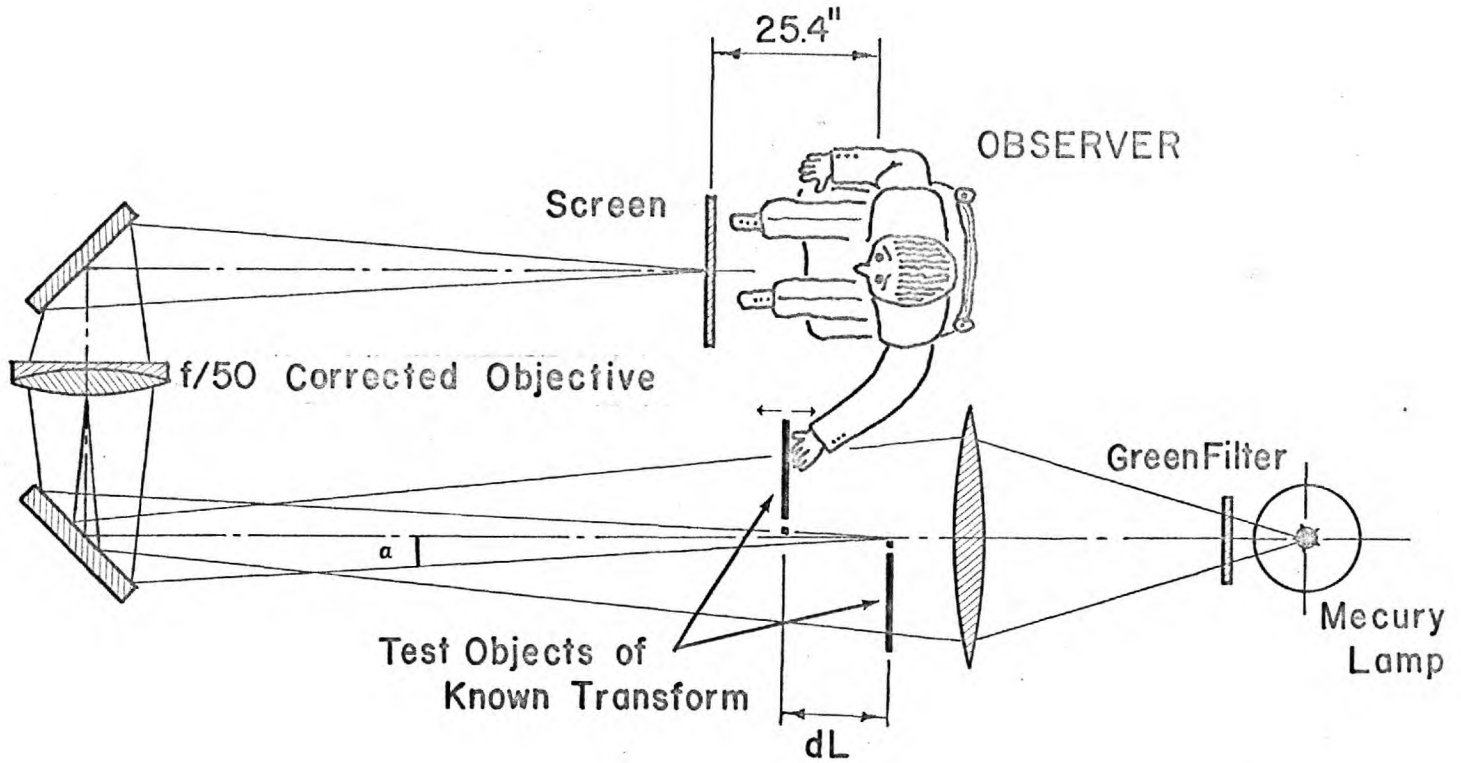
Neglecting phase changes the Fourier transform of the defocused image is given by

$$|b'(s)| = |b(s)| \cdot |D(s)|$$

In Hopkins' convention $D(s)$ is, here, the frequency response of a defocused lens and $b(s)$ is the Fourier transform of an object, $B(u)$. However, due to the comparatively large amounts of defocus required to affect the observer's judgement in these experiments $b(s) \approx 1$ and we may approximate the image transform thus

$$|b'(s)| \approx |D(s)|$$

3



Now $D(s)$ has been calculated by Birch (1959) for various degrees of defocus. If W_{20} is the marginal difference of optical path corresponding to a longitudinal defect of focus, dL , for a lens accepting a cone of rays of semi-angle (α), then

$$W_{20} = -\frac{1}{2} N \sin^2 \{\alpha\} dL = n\lambda/\pi$$

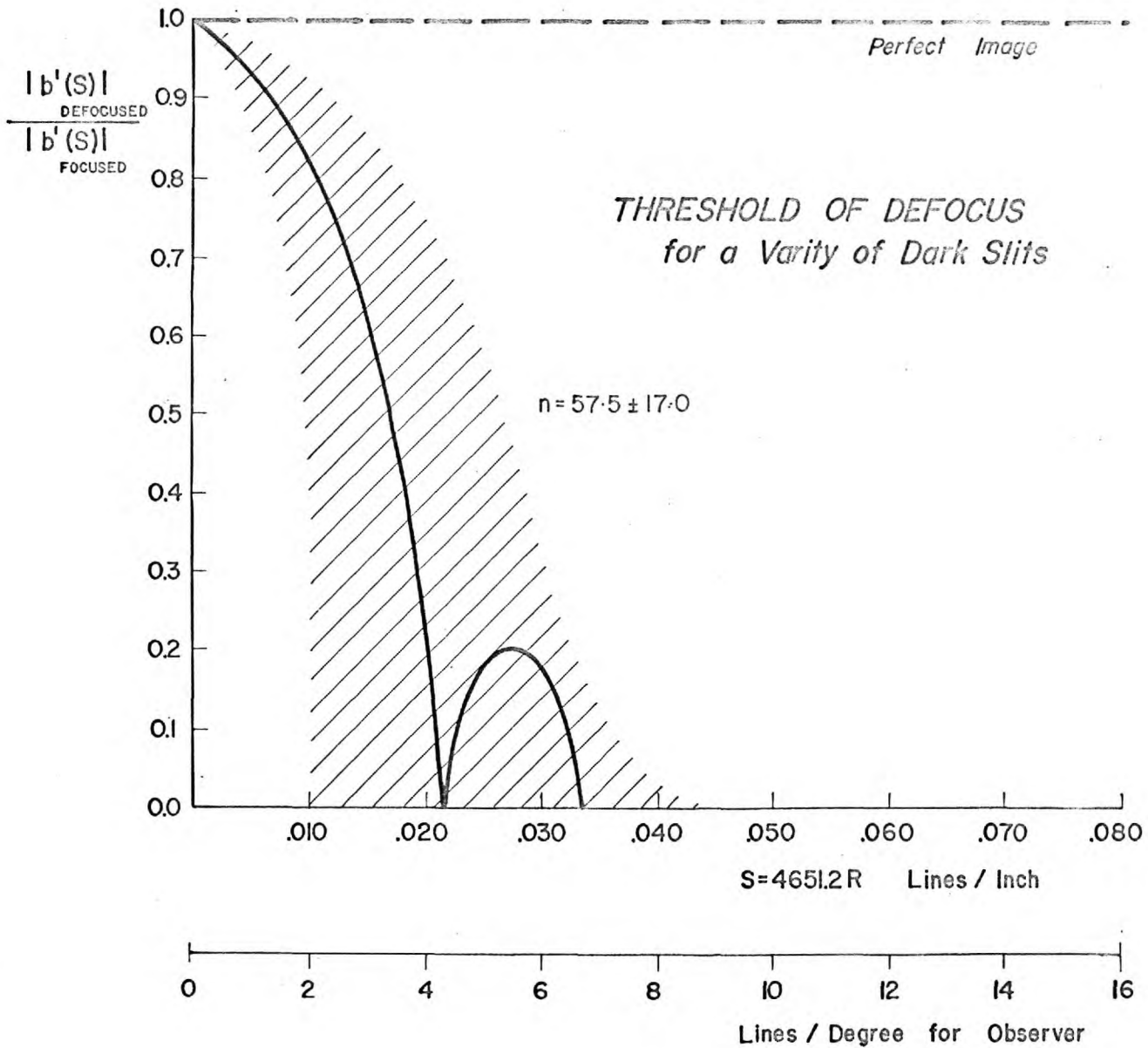
The frequency response of a defocused lens is dependent on (n), and these values may be obtained easily after the substitution, $\sin\alpha = (2F)^{-1}$. In fact

$$dL = 8n \lambda F^2 / \pi N$$

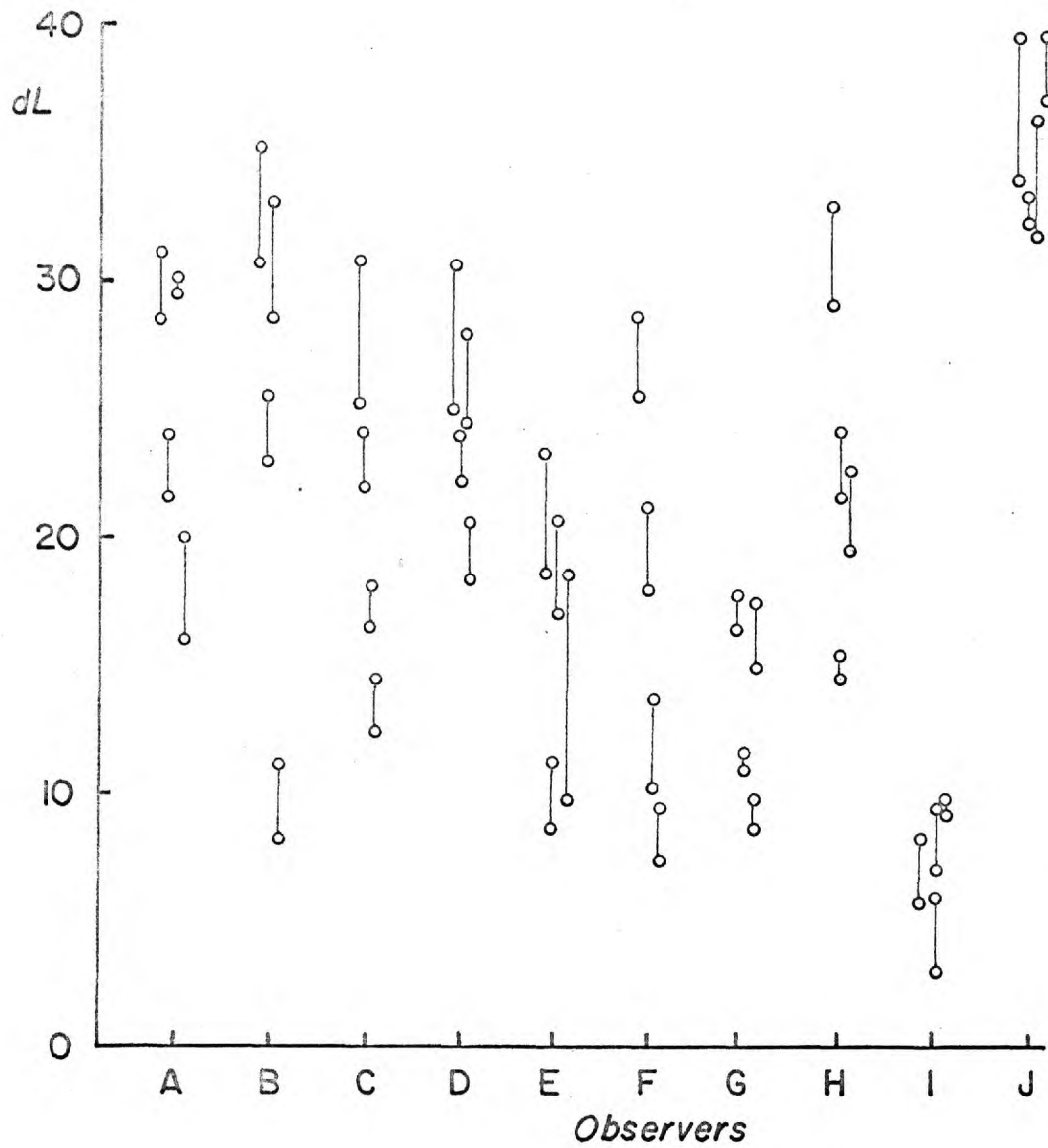
These results are shown in Figure (4), plotted as a ratio of the image frequency loss against the spatial frequency. The size of the error range indicates that the observer is using subtle (to him) variations of image structure as his basic criterion, not gross, rapid changes of frequency content. For this reason, and intensity considerations, it is to be assumed that all variations of the data below $b(s)/b'(s) = 0.1$ are unimportant.

Each observer was asked to make three separate settings for each object. Although the averaged probable error of these settings is only 3.7, Figure (5) shows that this resulted, in part, from his memory of previous settings. While there is a tendency to retain the basic individual criterion for sharpness,

4



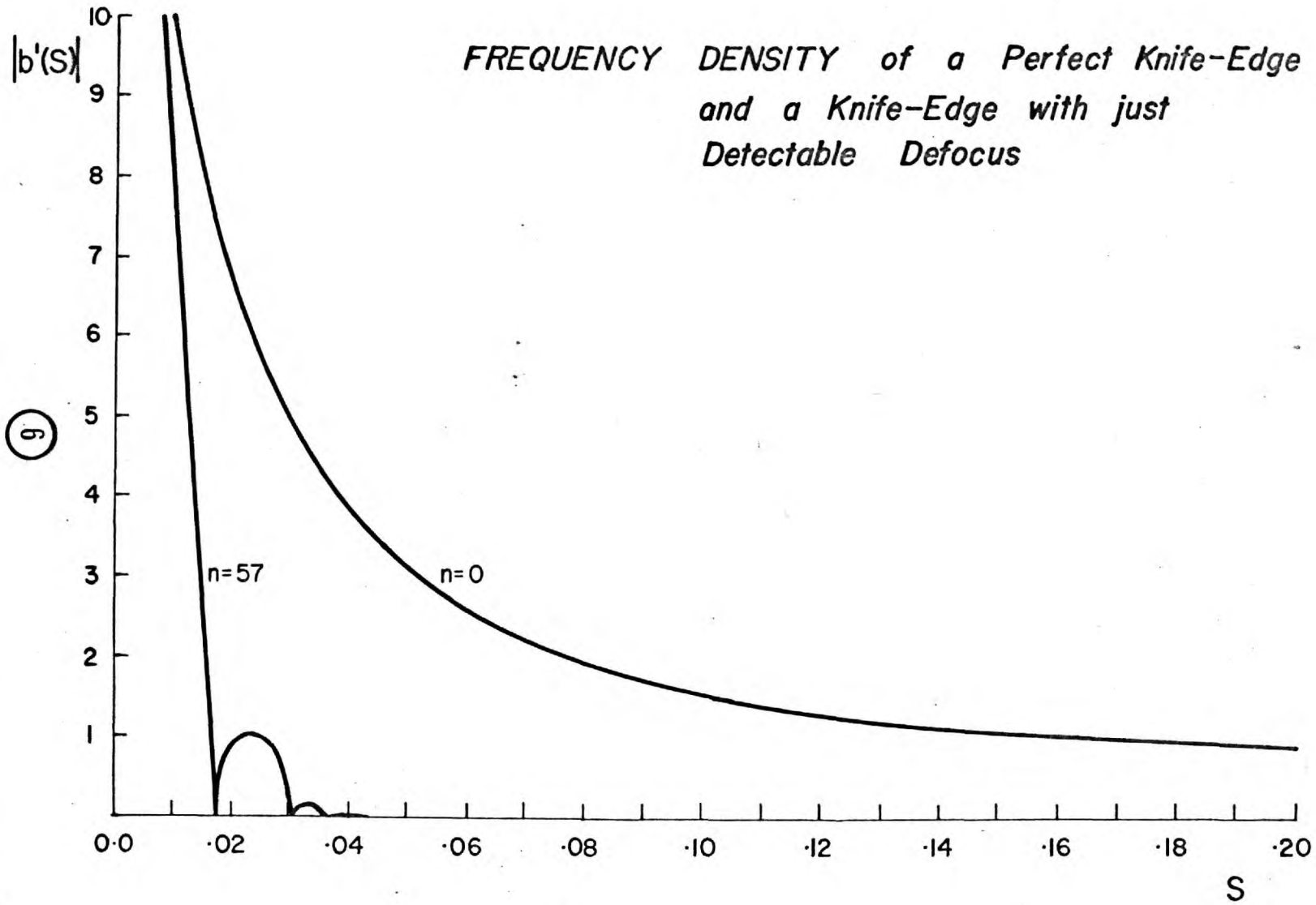
STANDARD DEVIATION OF INDIVIDUAL OBSERVATIONS



it is not of a definitely predictable value. This variation in the focus criterion of an observer indicates the need to keep towards the high side of the response function in order to be sure of satisfying the observer of the comparison image's sharpness.

Figure (6) shows that the frequency content has dropped to nearly 10% of the perfect image for values of (s) ranging about 0.025. This is roughly equivalent to 14 lines/inch at our observing distance. Clearly this value is well within the resolution limits of the eye. Simply by making the crude calculations relating the average separation of the retinal sensory units (which Hecht and Mintz (1939) take to be 2μ) to the best situation of resolution we find that 126 lines/inch should be resolvable at this distance. (It is interesting to note here that the generally accepted value of angular acuity in terms of a grating is $2'$ of arc (Emsley, 1936) or 67.8 lines/inch in our terms. Hecht and Mintz (1939) found that under conditions of extreme contrast and high background illumination a thread of $0.5''$ of arc could just be discerned as existing. Fechner's Law (1860) states that a variation of 1% of light level, at normal illumination may be detected by comparison).

Although no really firm conclusion may be made from these data, they do indicate two things.



First, that the visual criterion for image sharpness is surprisingly crude as compared with the techniques of frequency response. Second, that the threshold lies within a small enough region of the spatial frequency spectrum to allow instrumental techniques of Fourier analysis of good sensitivity.

REFERENCES

- Birch, K.G. (1960) Proc. Phys. Soc.
- Croce, P. (1956) Revue d'Optique, 35, 569-642.
- De, M. (1955) Proc. Roy. Soc. 71, 231
- Eastman Kodak (1961) Laboratory Report, No. 1037
Rochester, N.Y., p.64.
- Emsley, H.H. (1936) Visual Optics, Hatton & Co. Ltd.
London, p.45.
- Fechner, G.T. (1860) Elemente der Psychophysik,
Breitkopf & Härtel, Leipzig
- Frieser, H. (1935) Kinotechnik, 17, 165
- Frieser, H. (1958) Optical Image Assessment Summer
School, Imperial College,
London, p.83.
- Goodbody, A.M. (1958) Proc. Phys. Soc., 72, 1.
- Higgins, G.G.
Lambert R.L. &
Wolfe, R.H. (1962) JOSA, 45, 121.
- Hecht, S. &
Mintz, E.V. (1939) J. Gen. Phys. 22, 595
- Hopkins, H.H. (1955) Proc. Roy. Soc. A. 231, 91.
- Kelsall, D. (1959) Thesis - Univ. of London
- Mees, C.E.K. (1959) The Theory of the Photographic
Process, Revised Ed, McMillan,
N.Y., 875-879.

- McKenzie, D. (1931) J.S.M.P.E., 17, 172
- Wilczynski, J. (1960) Thesis - Univ. of London.

C H A P T E R I I

Instrumentation

GENERATION OF FRINGES

The illumination at any point (A) from two coherent point sources of light, P_1 and P_2 , will depend on the relative phase of the beams from P_1 and P_2 . When they are in phase, constructive interference results; out of phase gives destructive interference. This relative phase depends on the difference of path $AP_1 - AP_2$, which in turn varies with the angle $\angle P_1P_2A$.

If A is at a distance and the angle $\angle P_1P_2A$ is nearly a right angle, the variation of path length with angle is almost linear. So, for monochromatic light, the illumination on a screen parallel to P_1P_2 at some distance will be wholly covered by cosinusoidal fringes. The fringe spacing will be inversely proportional to the separation of P_1 and P_2 and directly proportional to the distance from the screen. These are Young's fringes.

The classical method for production of Young's fringes is the illumination of two slits by a third equidistant slit or by a collimated coherent beam. This has the disadvantage of wasting most of the light on the slit jaws and requiring that the slits be very narrow so that they act as true diffraction sources. The resulting light level is too low to be of great practical use. This problem can be overcome by using two images of one slit. The various standard techniques for this are the Fresnel biprism, Lloyd's mirror, the Billet split lens and Newton's double mirror. A Wollaston (or Rochon) prism may also be utilised.

These prisms are made out of a birefringent material and have the effect of refracting incident light of two different polarizations slightly differently. Thus a slit viewed through such a prism will appear double and can be made to act as effectively two separate coherent sources. It is necessary to place a polarizer oriented at 45° to the optical axes of the prism, on each side of the prism. The first ensures the coherence of the two images; the second removes the orthogonality of their polarizations, permitting interference.

The separation of the two virtual slits is proportional to the distance of the original slit from

the prism interface. For an actual slit this limits the maximum separation of the fringes to a scaling factor times one half of the prism thickness. While in theory it would be perfectly acceptable to use a real image of the slit, which could then be formed inside the prism the practical considerations of high lens speed with small aberration tolerances make this an impractical solution.

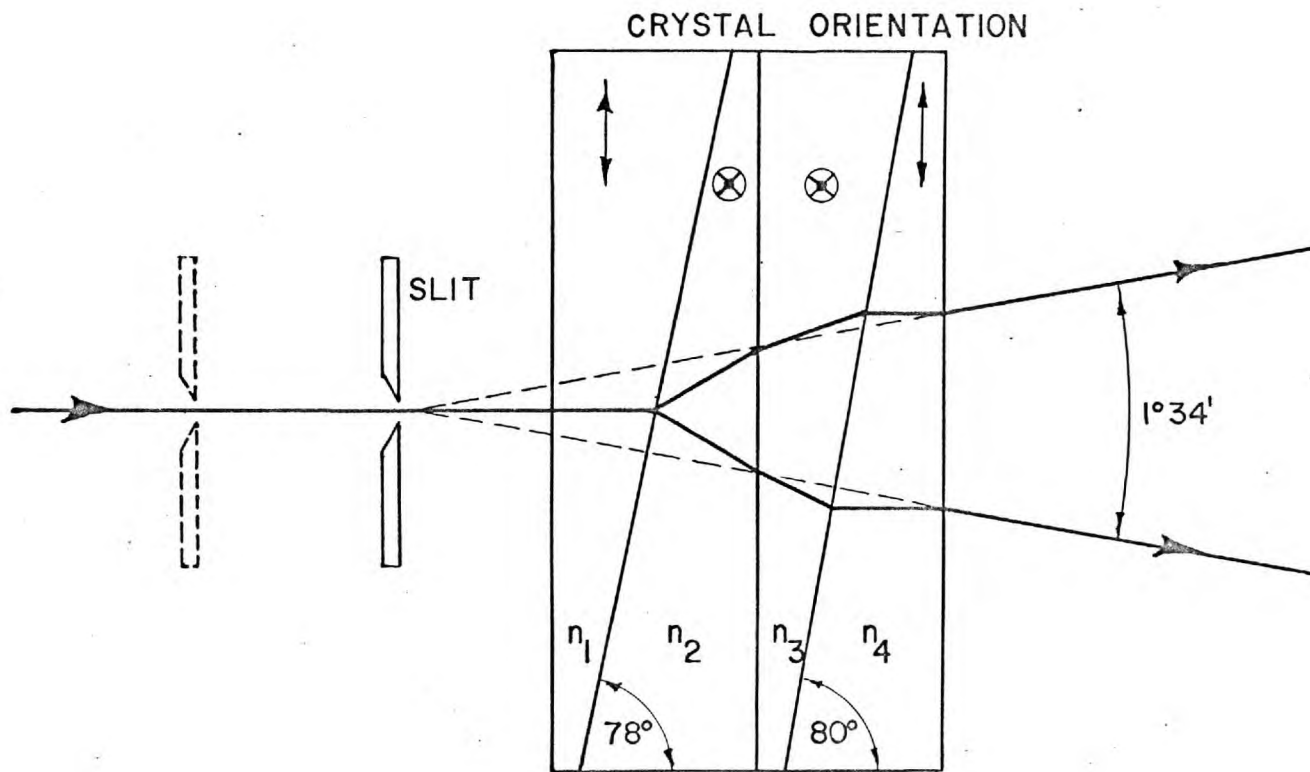
If, however, two Wollaston prisms are placed face to face, in the manner shown in Figure (7), the plane of the apparent slits will lie outside the resulting prism system. This will enable one to obtain a zero fringe spacing position giving no fringes by making the prism to slit distance such that the two images exactly overlap. This was the system finally adopted.

The effect of a lateral shift of the prism may be best thought of by considering an axial ray from the real slit through the center of the prism. This ray will pass through equal thicknesses of the prism halves; the two polarizations of the ray will have equal optical path lengths and so will emerge in phase. If, however, the prism is laterally displaced with respect to the ray, there will be different thicknesses of the two prism halves traversed by the ray. This is equivalent to adding a retardation plate to the early

FOURIER ANALYZER

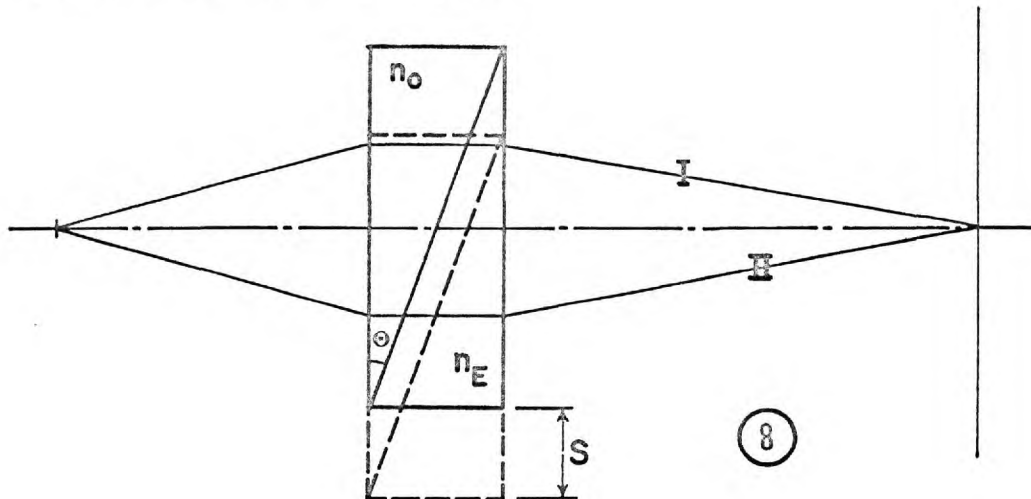
Calcite Double Wollaston Prism

7



PERPENDICULAR POLARIZATION [$n_1 = n_4 = 1.658$
 $n_2 = n_3 = 1.486$

situation; there will be a path difference for the two polarizations and they will no longer emerge in phase. This appears as a sliding of the fringe pattern in the image space.



Neglecting the second order effects caused by the variation in path angle through the laterally shifted prism, the total optical path difference between the orthogonally polarized beams I & II resulting from a lateral prism motion, S , will be of the following form

$$OPD = 2(n_o - n_e) S \tan \theta$$

In practice it is very difficult to make the prism move exactly along the optical axis. A pure translation, with disregard to the direction is, however, reasonably simple to produce. It is of interest then to inspect this case.

A pure translational motion of the prism with respect to the slit will linearly vary both the frequency and the spatial phase of the fringes. This may be described by writing

$$I = \cos^2 \left[f_1(D)u + f_2(D) \right]$$

where (I) is the intensity in the fringe pattern, (D) is the prism position and (u) a coordinate in the fringe plane. The functions $f_1(D)$ and $f_2(D)$ are due to the longitudinal and lateral components of the motion, respectively, and both are linear functions of position. A suitable choice for these functions can be made as follows:-

$$f_1(D) = aD \quad f_2(D) = bD + c$$

then
$$I = \cos^2(aDu + bD + c)$$

Here both the phase and the frequency are changing with the position (D). However, shifting the fringe-plane coordinates to

$$u' = u + \frac{b}{a}$$

gives

$$I = \cos^2(aDu' + c)$$

The phase at $u' = 0$ is now independent of the frequency. Here (a) represents the constant of proportion between the fringe spacing and the longitudinal prism motion and (c) represents the lateral position of the image.

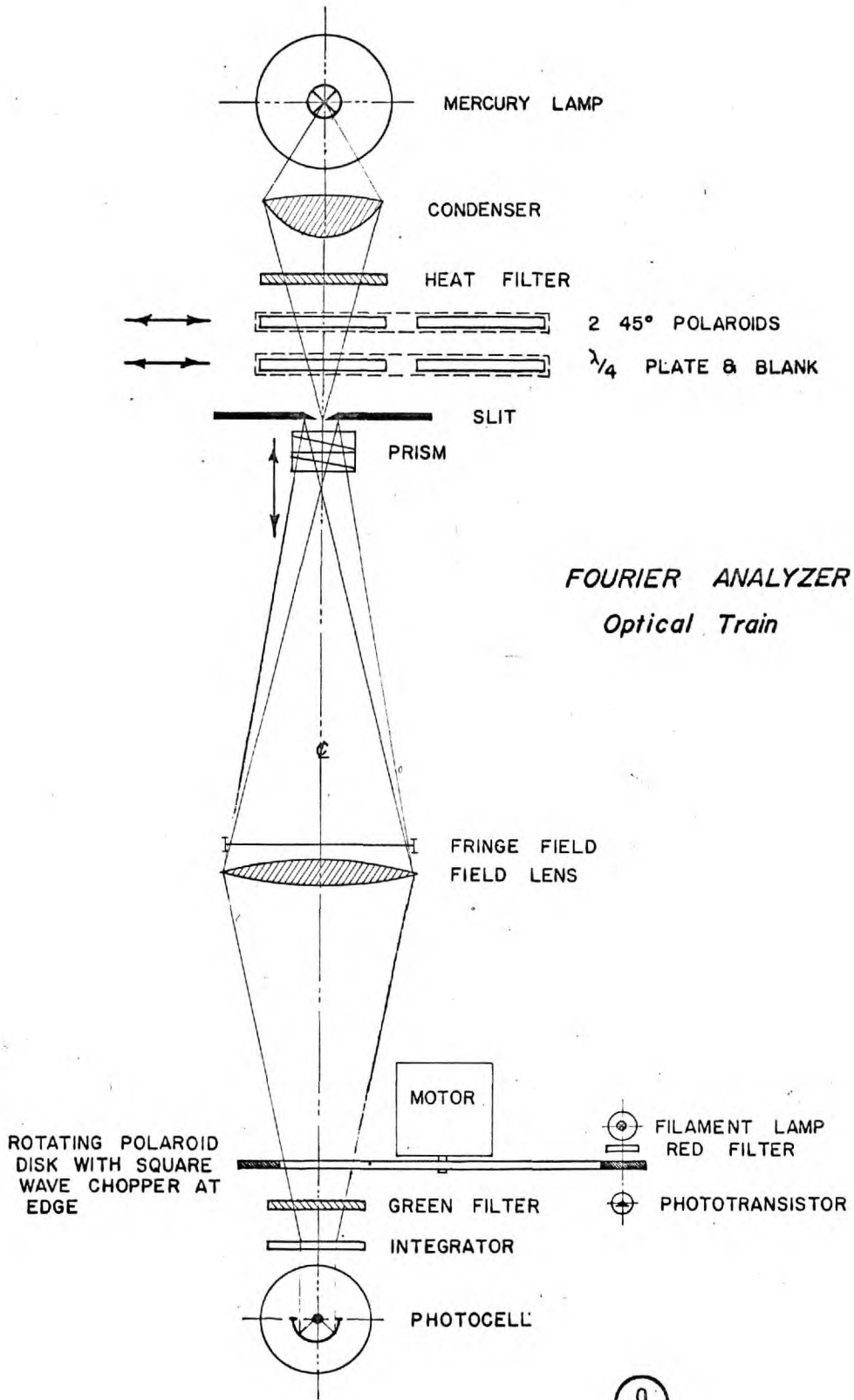
This, in summary, merely says that for a fringe pattern which is linearly changing in frequency and linearly shifting in phase, there is some point at which the phase is constant. If this point is kept to the center of the image space, the lateral shifting of the fringes may be determined and controlled through alignment.

Figure (9) shows the optical system which has been used.

If the analyser is rotated it will appear to the photomultiplier that the pattern in the fringe plane, constitutes what may be described as a standing wave of intensity distribution; the temporal frequency of this standing wave being twice the rotational frequency of the analyser. As we have seen, the spacial frequency will depend on the distance between the actual slit and the prism interface.

THE MEASUREMENT OF THE FOURIER TRANSFORM.

If a transparency which is described by a one-dimensional function of position $B(u)$, which we wish to analyse, is placed at the fringe plane, the flux, $F(t)$, arriving at the receptor will be given



by integrating the product of the transparency and the illumination, that is by

$$F(t) = \int B(u) [\alpha + \beta \cos 2\pi s u \cos \omega t] du \\ = \alpha \int B(u) du + \beta \cos \omega t \int B(u) \cos 2\pi s u du$$

where (α) is the average intensity in the fringe pattern and (β/α) is the fringe contrast, (u) is the spatial coordinate in the fringe plane, (s) is the spatial frequency, (t) is time and $\left(\frac{\omega}{2\pi}\right)$ is the temporal frequency. This last is equal to twice the frequency of rotation of the analyser. The light flux $F(t)$ will give a corresponding time-varying signal from the photomultiplier used to detect the flux. If one filters out the temporal frequency (ω) from this signal, the ratio of its amplitude to that of the constant term is proportional to

$$\int_{-\infty}^{+\infty} B(u) \cos\{2\pi us\} du$$

that is, the Fourier cosine transform of $B(u)$.

If the position of the fringe system is shifted laterally by an amount u_1 , the component of frequency ω will be

$$\beta \cos \omega t \int_{-\infty}^{+\infty} B(u) \cos 2\pi s(u-u_1) du$$

and, if $2\pi s u_1 = \frac{\pi}{2}$ the ratio of the A.C. to D.C.

amplitude will be proportional to

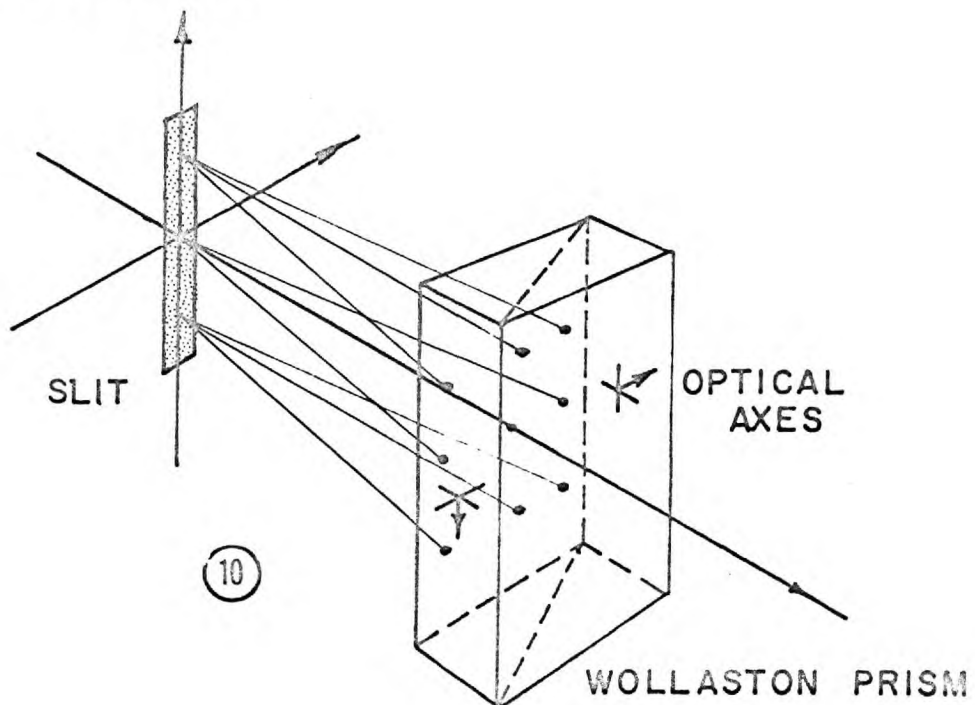
$$\int_{-\infty}^{+\infty} B(u) \sin 2\pi s u du$$

that is, the Fourier sine transform of $B(u)$.

If the phase difference between the two different polarisations from the source is changed by a quarter of a period (by inserting a quarter wave plate) the Fourier cosine transform of $B(u)$ may be measured.

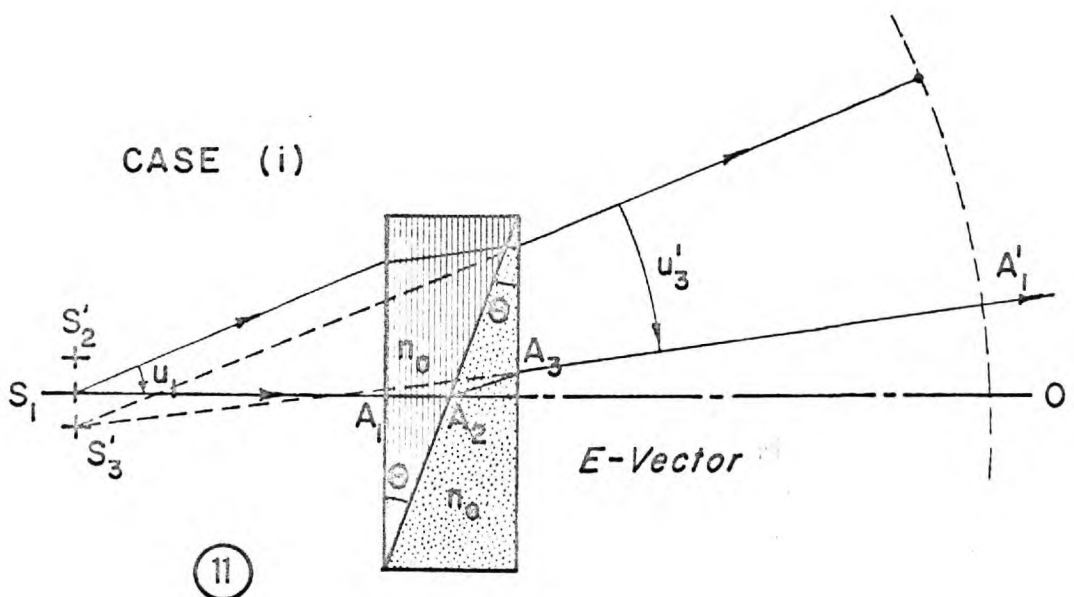
Armed with these facts, plus the knowledge of the variation of the fringe spacing with prism motion, it will be understood that an instrument based on these procedures can measure the Fourier spectra of photographic images over a finite range of spatial frequencies. It remains only to examine the departures from linearity of the system. These will be dealt with as four separate sub-sections.

PRIMARY ABERRATIONS ARISING FROM THE WOLLASTON PRISM.



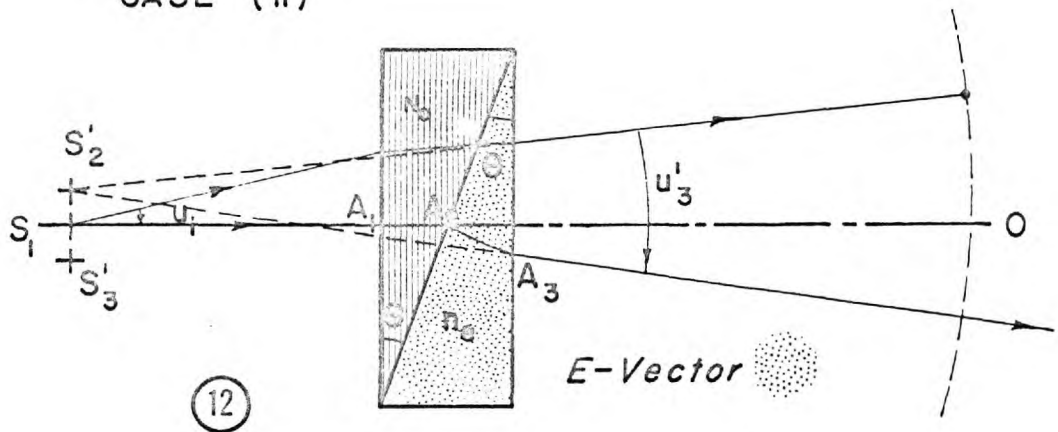
Because of the mode of illumination of the slit all rays are substantially parallel to the horizontal plane. Hence, with optical axes as shown, we shall have the ordinary index of refraction for E-vectors parallel to the horizontal plane. In determining the primary aberrations arising from the Wollaston prism the values obtained from a single horizontal section will be representative of the entire fringe field and these aberrations will appear as a cylindrical wave-front distortion perpendicular to the horizontal plane. See Figure (10).

The action of the Wollaston prism on a wavefront originating at the point S_1 of a slit source may be considered in terms of diagrams (11) and (12). In (11),



for example a wavefront polarized with the E-vector in the plane of the diagram leaves S_1 and is refracted successively at the three surfaces of the prism. It has the ordinary refractive index in the first prism and the extraordinary refractive index in the second prism. In (12), on the other hand, the wave

CASE (ii)



leaving S_1 is polarized with its E-vector normal to the plane of the diagram, so that it has the extraordinary refractive index in the first prism and the ordinary refractive index in the second prism.

Ideally in both cases the wavefronts emerging from the prism should be spheres centred on the image points $S_{2,3}'$. Variations in optical path difference arising from aberrations are easily calculated using the primary aberration formulae

$$W(r) = \frac{1}{8} S_I r^4 + \frac{1}{2} S_{II} r^3 + \frac{1}{2} S_{III} r^2 \quad (1)$$

as given by Hopkins (Wave-Theory of Aberrations, p.79).

It has of course, to be remembered that we are here not dealing with an axially symmetric optical system.

Thus the coefficients

$$\begin{aligned} S_I &= \sum A^2 h \Delta\left(\frac{u}{n}\right) \\ S_{II} &= \sum AB h \Delta\left(\frac{u}{n}\right) \\ S_{III} &= \sum B^2 h \Delta\left(\frac{u}{n}\right) \end{aligned} \quad (2)$$

should strictly speaking use a close sagittal ray for the values of A , h and $\Delta\left(\frac{u}{n}\right)$, and a finite trace of the axial ray $S_1 \overbrace{A_1 A_2 A_3} A'$ in each case to give the values of B . Because of the small angles involved, however, it is permissible as a first approximation to put $B = n \sin \bar{i} = n \bar{i}$, where \bar{i} is the angle of incidence of the reference (axial) ray $S_1 A_1$ at the different surfaces of the prism.

Let θ be the angle of each prism. Then

for the successive surfaces, in case (i)

$$\begin{aligned} \text{(i)} \quad \bar{i}_1 &= 0 & \bar{i}_2 &= \frac{n_o}{n_e} \theta & B_1 &= 0 \\ \bar{i}_2 &= \theta & & & B_2 &= n_e \theta \\ \bar{i}_3 &= \bar{i}_2 - i_2 & & & B_3 &= (n_o - n_e) \theta \\ &= \left(\frac{n_o}{n_e} - 1 \right) \theta & & & & \end{aligned} \quad (3)$$

For the second case

$$\begin{aligned}
 \text{(ii)} \quad \bar{i}_1 &= 0 & B_1 &= 0 \\
 \bar{i}_2 &= \theta & \bar{i}_2' &= \frac{n_e}{n_o} \theta & B_2 &= n_o \theta \\
 \bar{i}_3 &= \left(\bar{i}_2' - i_2 \right) & & & B_3 &= - \left(n_o - n_e \right) \theta \\
 &= - \left(1 - \frac{n_e}{n_o} \right) \theta & & & &
 \end{aligned} \tag{3}$$

The values of B_3 are thus numerically equal.

To find the values of u , u_1' we note that, for plane surfaces,

$$n' u_s' - n u_s = h_s c \Delta(n u s \bar{I}) = 0$$

Thus

$$u_s' = \frac{n u_s}{n'}$$

giving, in the two cases, the following values. The angle u_1 is chosen equal to the full aperture used in forming the fringe pattern.

$$\begin{aligned}
 \text{(i)} \quad u_1 &= u_1 & \Delta \left(\frac{u}{n} \right)_1 &= \left(\frac{1}{n_o} - 1 \right) u_1 \\
 u_1' &= \frac{u_1}{n_o} & & & & \\
 u_2 &= u_1' = \frac{u_1}{n_o} \\
 u_2' &= \frac{n_o u_2}{n_e} = \frac{n_o u_1'}{n_e} = \frac{u_1}{n_e} \\
 \Delta \left(\frac{u}{n} \right)_2 &= \left(\frac{1}{n_e} - \frac{1}{n_o} \right) u_1
 \end{aligned} \tag{4}$$

Similarly we find

$$\begin{aligned}
 \text{(ii)} \quad \Delta \left(\frac{u}{n} \right)_1 &= \left(\frac{1}{n_e} - 1 \right) u_1 \\
 \Delta \left(\frac{u}{n} \right)_2 &= \left(\frac{1}{n_o} - \frac{1}{n_e} \right) u_1 \\
 \Delta \left(\frac{u}{n} \right)_3 &= \left(1 - \frac{1}{n_o} \right) u_1
 \end{aligned} \tag{4}$$

The values of A_1 , A_2 , A_3 are also easily found, since $A = ni = n(hc-u) = -nu$ when $c = 0$.

Thus:

$$\begin{aligned}
 \text{(i)} \quad A_1 &= -n_1 u_1 = -u_1 \\
 A_2 &= -n_2 u_2 = -n_o u_2 = -u_1 \\
 A_3 &= -u_1
 \end{aligned} \tag{5}$$

Similarly

$$\text{(ii)} \quad A_1 = A_2 = A_3 = -u_1 \tag{5}$$

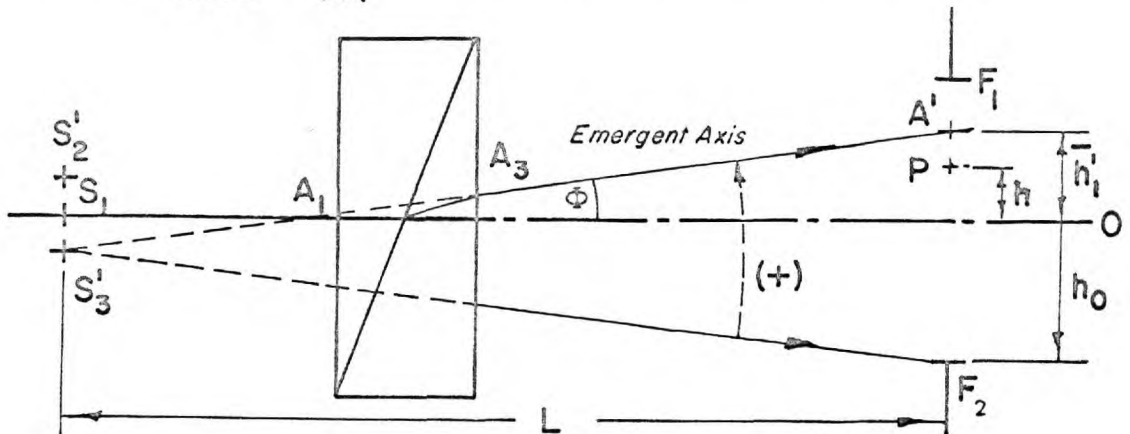
Let d be the half-thickness of the prism, and suppose the distances $A_1 A_2$, $A_2 A_3$ to be equal, and, within the desired approximation, each equal to d . Then, if l_1 is the distance of S_1 from A_1 ,

$$\begin{aligned}
 \text{(i)} \quad h_1 &= [l_1 u_1] \\
 h_2 &= h_1 - du_1' = \left[h_1 - \frac{du_1}{n_o} \right] \\
 h_3 &= h_2 - du_2' \\
 h_3 &= \left[h_2 - \frac{du_1}{n_e} \right]
 \end{aligned} \tag{6}$$

$$\begin{aligned}
 \text{(ii)} \quad h_1 &= [l_1 u_1] \\
 h_2 &= h_1 - du_1' = \left[h_1 - \frac{du_1'}{n_e} \right] \\
 h_3 &= \left[h_2 - \frac{du_1'}{n_o} \right]
 \end{aligned} \tag{6}$$

We now have all the prime data required for the calculation of S_I , S_{II} and S_{III} .

A convenient choice for the numerical value of the angle u_1 is found by consideration of the following diagram. The emergent axis for the polarization
CASE (i)



(13)

(i) appears as $S_3'A_1$, and the ray $S_3'F_2$ is that ray which, emerging, passes through the edge F_2 of the fringe area. The angle u_1 is numerically equal to $\widehat{A_1'S_3'F_2}$, and is

$$|u_1| = \left\{ \frac{\bar{h}_1' + h_0}{L} \right\} \tag{7}$$

where h_0 and \bar{h}_1' are taken to be essentially positive. As the prism moves from left to right, the value of h_1' will decrease, so that the maximum value of h_1'

occurs when the prism is in its extreme position to the left of the diagram. It is in this case that the greatest relative shear exists between the two wavefronts (i) and (ii).

The numerical values of \bar{h}_1 and h_0 are, since $\Phi = 2^{\circ}6' = 0.0367$ radians

$$\bar{h}_1' \approx L\Phi = 19.8 \times 0.0367 = 0.727 \text{ cm}$$

$$h_0 = 0.95 \text{ cm}$$

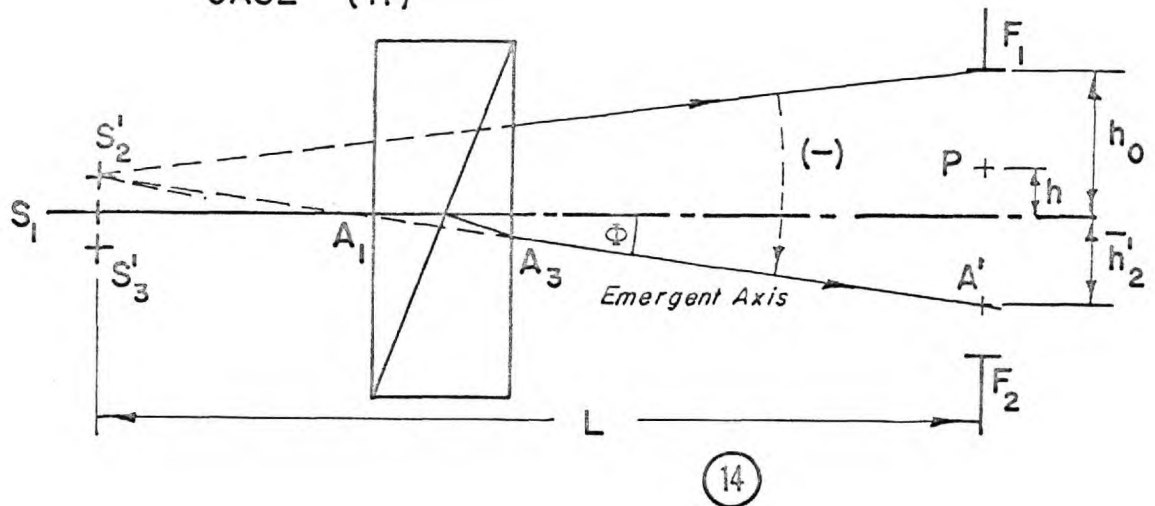
Hence $|u_1| = \frac{1.677}{19.8} = 0.0847$

For any calculation it is useful to choose u_1 to be positive when considered in the customary sign convention of instrumental optics. In this latter the sense of the angle is that of a rotation from the ray to the axis, and this rotation is positive when anti-clockwise. The angle $\widehat{F_2S_3'A_1}$ is thus positive, and $u_1 = + 0.0847$. The calculations of the aberration coefficients S_I, S_{II}, S_{III} are carried through using this angle. Then for any point in the fringe field the aberration of each wavefront is found by substituting an appropriate value of the fractional aperture, r , in the formula (1). For a point P in the fringe plane, at a distance h from the origin O, r will have the values

$$r_1 = \left[\frac{\bar{h}_1' - h}{\bar{h}_1' + h_0} \right] \quad (8)$$

$$r_2 = - \left[\frac{\bar{h}_2' + h}{\bar{h}_2' + h_0} \right]$$

CASE (ii)



where h , the height of a current ray now takes positive or negative values, according as the point P is above or below the axis of symmetry.

It will be necessary to calculate the effects of aberrations for, say, three positions of the prism. This is because there are two opposing factors. As the prism moves to the right, the incidence heights of the ray at the surfaces of the prism increase, and so the aberration coefficients S_I etc., for each polarisation, will also increase.

On the other hand the relative shear between the wavefronts at the fringe plane will decrease as the prism moves to the right. Thus if the prism were moved from an extreme left to an extreme right position, there would be a large shear acting with zero aberration changing to a large aberration with zero shear. In both cases there would be no effect of aberration on the fringes.

Let I, II and III be used to denote the extreme, mean and further positions assumed by the prism in the practical case as it moves from left to right. For each of these cases the values of B will be those given in (3). Now $\theta = 12^\circ = 0.2094$ radians, and $n_e = 1.486$ $n_o = 1.658$.

Thus:

$$\begin{aligned} \text{(i)} \quad B_1 &= 0 & B_2 &= 0.3112 & B_3 &= 0.360 \\ \text{(ii)} \quad B_1 &= 0 & B_2 &= 0.3472 & B_3 &= -0.360 \end{aligned} \quad (9)$$

Again, since only plane surfaces are involved, the angles u , u'_1 are also the same for all the cases I, II and III. By (4), these are

$$\begin{aligned} \text{(i)} \quad u_1 &= 0.0847 \\ \Delta \left(\frac{u}{n} \right)_1 &= -0.0539 \end{aligned} \quad (10)$$

$$\Delta \left[\frac{u}{n_2} \right] = 0.0075$$

$$\Delta \left[\frac{u}{n_3} \right] = 0.0463$$

$$(ii) \quad n_1 = 0.0847$$

$$\Delta \left[\frac{u}{n_1} \right] = - 0.0463$$

$$\Delta \left[\frac{u}{n_2} \right] = - 0.0075$$

$$\Delta \left[\frac{u}{n_3} \right] = 0.0539$$

(10)

Further the value of A is the same for each surface in each case, so that

$$(i) \quad A_1 = A_2 = A_3 = - u_1 = - 0.0847$$

(11)

$$(ii) \quad A_1 = A_2 = A_3 = - u_1 = - 0.0847$$

For case I, $l_1 = 0$, and then, by (6),

$$(i) \quad h_1 = 0$$

$$h_2 = 0.00639$$

$$h_3 = 0.01352$$

(12)

$$(ii) \quad h_1 = 0$$

$$h_2 = .00713$$

$$h_3 = .01352$$

For case II, $l_1 = 1.25$ cm:

$$(i) \quad h_1 = 0.1059$$

$$h_2 = 0.1123$$

$$h_3 = 0.1194$$

(13)

$$(ii) \quad h_1 = 0.1059$$

$$h_2 = 0.1130$$

$$h_3 = 0.1194$$

For case III, $l_1 = 2.50$ cm:

$$(i) \quad h_1 = 0.2118$$

$$h_2 = 0.2182$$

$$h_3 = 0.2253$$

(14)

$$(ii) \quad h_1 = 0.2118$$

$$h_2 = 0.2189$$

$$h_3 = 0.2253$$

The values of the aberration coefficients for the three cases are now found to be:

Case I

$$(i) \quad S_I = .0000048 \quad S_{II} = .0000204 \quad S_{III} = .0000857$$

$$(ii) \quad S_I = .0000048 \quad S_{II} = .0000238 \quad S_{III} = .0000870$$

Case II

(i) $S_I = .0000043$ $S_{II} = .0001908$ $S_{III} = .0007980$

(ii) $S_I = .0000049$ $S_{II} = .0002211$ $S_{III} = .0006219$

Case III

(i) $S_I = .0000046$ $S_{II} = .0003612$ $S_{III} = .0015104$

(ii) $S_I = .0000051$ $S_{II} = .0004136$ $S_{III} = .0013769$

To show the variation in wavefront aberration over the full aperture it will be adequate to obtain five values of r . These will be found at equal intervals of h , such that $h = 0, \frac{1}{4}h_0, \frac{1}{2}h_0, \frac{3}{4}h_0$ and h_0 . As it has been shown $\bar{h}_1^i = L$ and $h_0 = 0.95$ cm; further, it is a good approximation to call $\bar{h}_1^i \cong \bar{h}_2^i$.

From formula 8,

$$r_1 = \left[\frac{\bar{h}_1 - h}{\bar{h}_1 + h_0} \right]$$

$$r_2 = - \left[\frac{\bar{h}_2 + h}{\bar{h}_2 + h_0} \right]$$

For the five separate points the values will be:

Case ICase IICase III

POINT 1 $h = 0$

$r_1 = .4335$

$r_1 = .4175$

$r_1 = .3870$

$r_2 = .4335$

$r_2 = .4175$

$r_2 = .3870$

<u>Case I</u>	<u>Case II</u>	<u>Case III</u>
POINT 2. $h = \frac{1}{4} h_0$		
$r_1 = .2952$.2716	.2336
$r_2 = - .5760$	- .5635	- .5907
POINT 3. $h = \frac{1}{2} h_0$		
$r_1 = .1503$.1263	.0806
$r_2 = -.7168$	- .7088	- .6935
POINT 4. $h = \frac{3}{4} h_0$		
$r_1 = .0083$	- .0196	- .0729
$r_2 = .8587$	- .8546	- .8471
POINT 5. $h = h_0$		
$r_1 = -.1330$	- .1649	- .2258
$r_2 = - 1.000$	- 1.000	- 1.000

By applying formula (1) the variation in optical path difference between the two beams may be obtained for these various points over the fringe field. These results are plotted with the aperture appearing as the ordinate. Formula (1) states:

$$W(r) = \frac{1}{8} S_I r^4 + \frac{1}{2} S_{II} r^3 + \frac{1}{2} S_{III} r^2$$

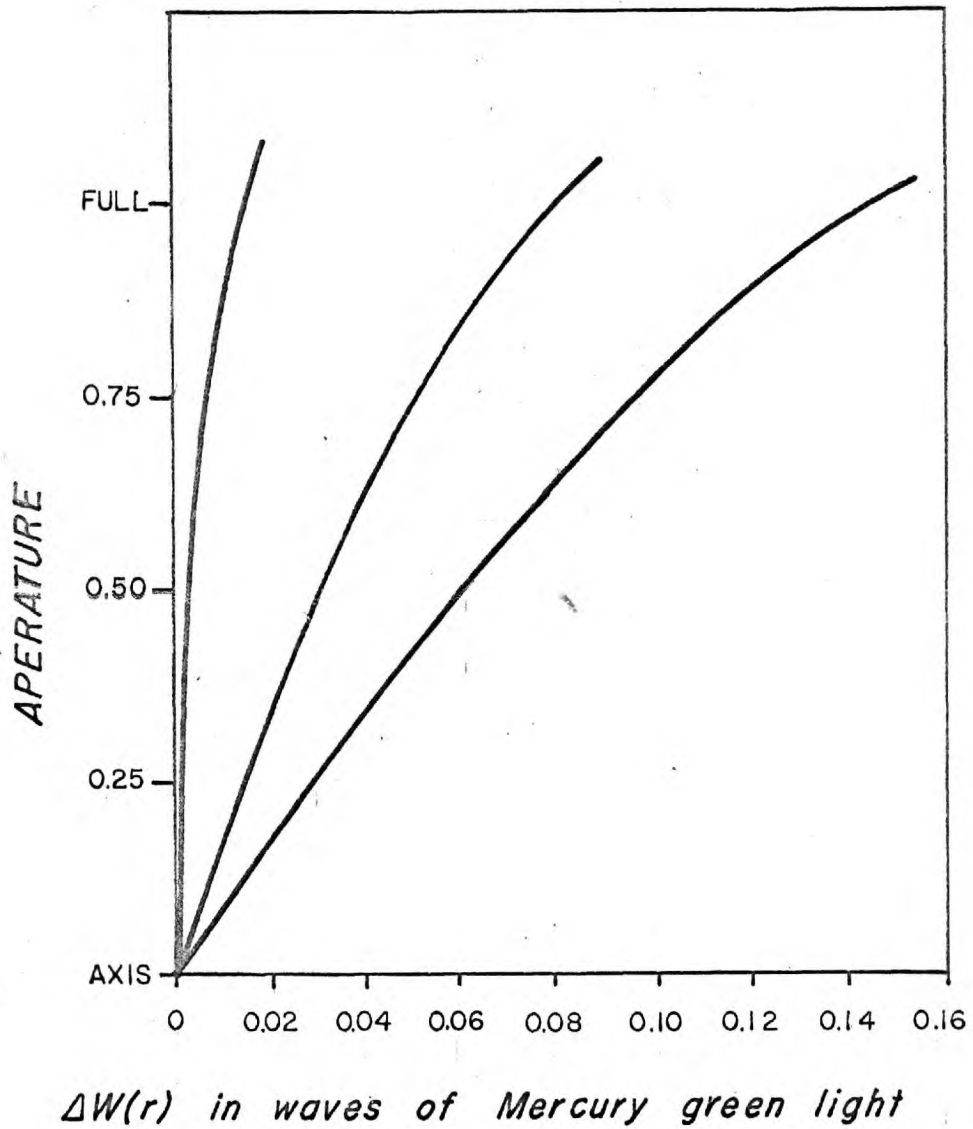
Beam (i)	<u>Case I</u>	<u>Case II</u>	<u>Case III</u>
$W(r_1) = 10^8 \times$	8.90	74.85	129.59
$W(r_2) =$	3.36	31.34	43.50
$W(r_3) =$	1.00	6.55	5.00
$W(r_4) =$	0.01	0.15	3.94
$W(r_5) =$	0.78	10.42	36.42

Beam (ii)			
$W(r_1) = 10^8 \times$	9.15	62.27	115.25
$W(r_2) =$	16.77	118.58	261.94
$W(r_3) =$	26.88	195.74	483.59
$W(r_4) =$	39.92	296.32	621.58
$W(r_5) =$	56.00	422.11	898.39

The total wave-front aberration difference between the two beams, $W(r)$, expressed in wavelengths of mercury green (5461\AA), being:

$W(r_1) =$	0.000	0.002	0.003
$W(r_2) =$	0.002	0.016	0.040
$W(r_3) =$	0.005	0.035	0.078
$W(r_4) =$	0.007	0.054	0.115
$W(r_5) =$	0.010	0.079	0.158

TOTAL PRIMARY ABERRATION
FROM A WOLLASTON PRISM



These aberrations will have virtually no effect on the fringe field and there is no need to make any corrections for them.

VARIATION OF FRINGE VISIBILITY WITH SLIT WIDTH.

Since the signal-to-noise ratio of the final output is directly dependent upon the visibility, (V), of the interference bands, it is of great interest to examine the formula expressing the influence of the width of entrance slit on the visibility of the fringes.

Referring to Figure (16) we find that:

$$(P_1Q)^2 = \left\{ (x + x_0) - \xi \right\}^2 + \left\{ (y - \eta) \right\}^2 + D^2$$

$$(P_2Q)^2 = \left\{ (x - x_0) - \xi \right\}^2 + \left\{ (y - \eta) \right\}^2 + D^2$$

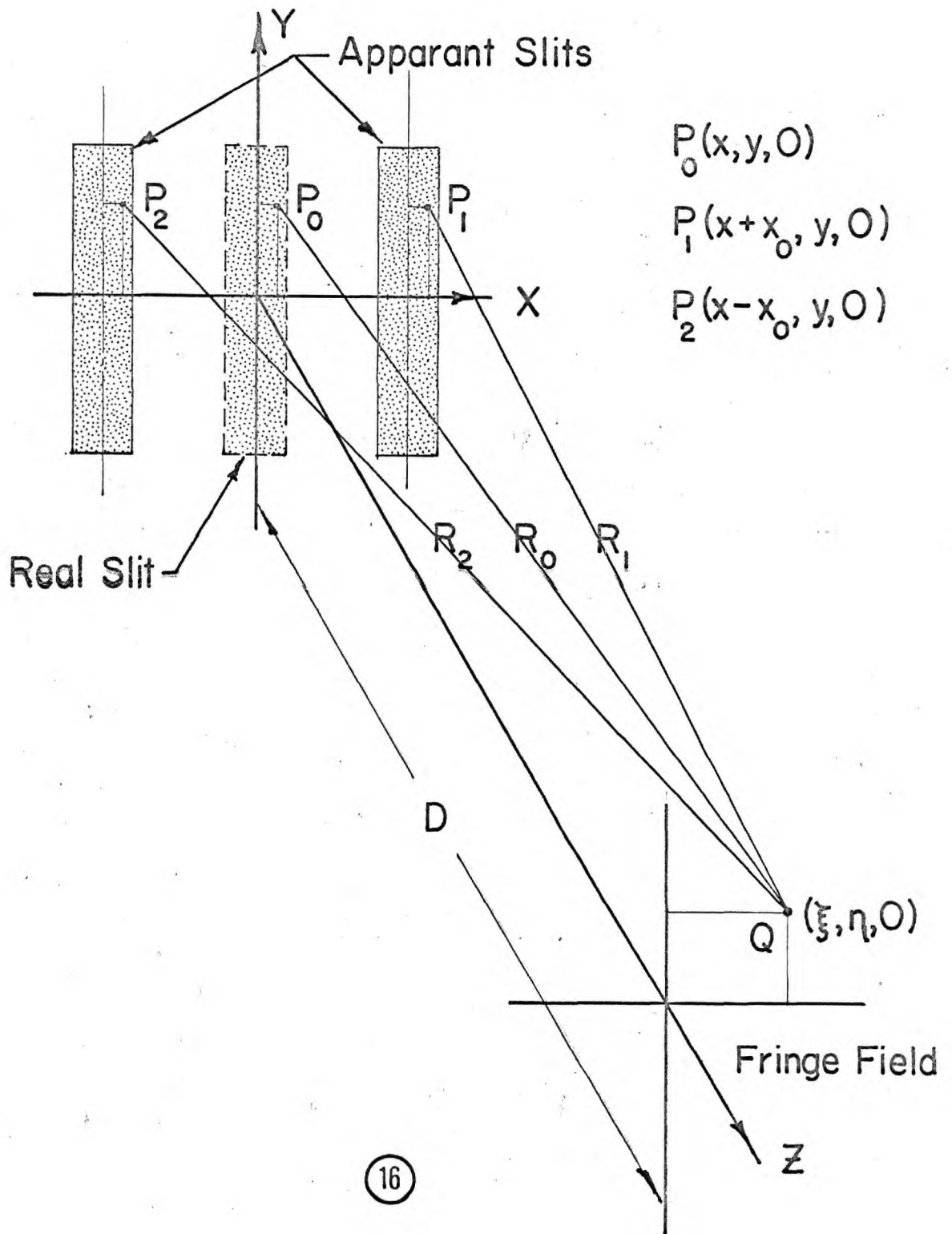
where (x), (y) and (z) are coordinates in the slit field and (ξ), (η) and (D) are coordinates in the fringe field. Subtracting and factoring gives for the path difference to the point Q in the fringe plane,

$$\left[(P_1Q) - (P_2Q) \right] \cdot \left[(P_2Q) + (P_1Q) \right] = \left[2x_0 \right] (2x - 2\xi)$$

$$\left[(P_1Q) - (P_2Q) \right] = \frac{4x_0 (x - \xi)}{\left[(P_1Q) + (P_2Q) \right]}$$

or, with

$$(P_1Q) = R_1 \text{ and } (P_2Q) = R_2,$$



$$R_1 - R_2 = \frac{4x_0 (x - \xi)}{[2R_1 - (R_1 - R_2)]}$$

Since $(R_1 - R_2) \ll R_1$ (R_1 being very nearly equal to R_2), we may write:

$$\begin{aligned} R_1 - R_2 &= \frac{4x_0 (x - \xi)}{(R_1 + R_2)} \\ &= \frac{4x_0 (x - \xi)}{\{2D - (D - R_1) - (D - R_2)\}} \end{aligned}$$

Since also, $|D - R_1| \ll D$ and $|D - R_2| \ll D$ (R_1 and R_2 being very nearly equal to D as well),

$$\begin{aligned} R_1 - R_2 &= \frac{4x_0 (x - \xi)}{2D \left[1 - \frac{2D (R_1 + R_2)}{2D} \right]} \\ &= \frac{2x_0 (x - \xi)}{D} \left[1 + \frac{2D - (R_1 + R_2)}{2D} \right] \end{aligned}$$

Clearly the second term in this statement very nearly equals one, so that we may make the following approximation to obtain an expression for the optical path difference between rays from the two apparent slits

$$R_1 - R_2 = \left[\frac{2x_0 (x - \xi)}{D} \right]$$

The general two dimensional formula for the distribution of intensity in an interference pattern is:

$$I(\xi, \eta) = A_1^2 + A_2^2 + 2A_1 A_2 \cos \Phi$$

where $\Phi = \frac{2\pi}{\lambda} x$ (path difference). Putting $K = \frac{2\pi}{\lambda}$

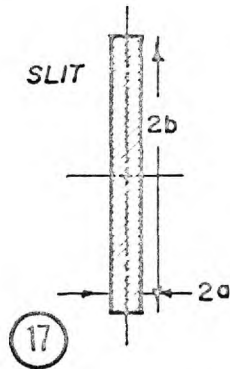
and substituting the above we see that:

$$\Phi = K \left\{ \frac{2x_0 (x - \xi)}{D} \right\}$$

Our fringe pattern is a unidimensional system which is independent of (η) and, so, the expression becomes:

$$dI(\xi) = \left[A_1^2 + A_2^2 + 2A_1A_2 \cos \left(\frac{2x_0 K(x - \xi)}{D} \right) \right] dx dy$$

$$I(\xi) = (A_1^2 + A_2^2) \iint dx dy + 2A_1A_2 \iint \cos \left(\frac{2Kx_0 (x - \xi)}{D} \right) dx dy$$



If the slit half-width is (a) and half length (b) making the area of the slit $4ab$, then:

$$I(\xi) = (A_1^2 + A_2^2) 4ab + 4A_1A_2 (ab) \frac{1}{a} \int_{-a}^{+a} \cos \left[\frac{2Kx_0 (x - \xi)}{D} \right] dx$$

The term under the integral may be expressed as:

$$= \frac{1}{a} \int_{-a}^{+a} \cos \left[\frac{2Kx_0}{D} x - \frac{2Kx_0}{D} \xi \right] dx$$

$$= \frac{1}{a} \cos \left(\frac{2Kx_0}{D} \xi \right) \int_{-a}^{+a} \cos \left(\frac{2Kx_0}{D} x \right) dx +$$

$$+ \sin \left(\frac{2Kx_0}{D} \xi \right) \int_{-a}^{+a} \sin \left(\frac{Kx_0}{D} x \right) dx$$

The second integral, being of a symmetrical form, cancels itself. So, the above expression becomes:

$$\begin{aligned}
 &= \frac{1}{a} \cos\left(\frac{2kx_0}{D}\xi\right) \left[\frac{\sin\left(\frac{2kx_0}{D}x\right)}{\left(\frac{2kx_0}{D}\right)} \right]_{-a}^{+a} \\
 &= \cos\left(2x_0 \frac{K\xi}{D}\right) \left\{ \frac{2 \sin\left(\frac{2kx_0}{D}a\right)}{\left(\frac{2kx_0}{D}\right)a} \right\}
 \end{aligned}$$

Substituting back into the above:

$$\begin{aligned}
 I(\xi) = 4ab & \left[(A_1^2 + A_2^2) + \right. \\
 & \left. + \frac{A_1 A_2}{a} \frac{2 \sin\left(\frac{2kx_0}{D}a\right)}{\left(\frac{2kx_0}{D}a\right)} \cos\left(\frac{2kx_0}{D}\xi\right) \right]
 \end{aligned}$$

or dividing both sides by the slit area

$$\begin{aligned}
 \frac{I(\xi)}{4ab} &= A_1^2 + A_2^2 + \\
 &+ 2A_1 A_2 \left\{ \frac{\sin\left(\frac{2kx_0}{D}a\right)}{\left(\frac{2kx_0}{D}a\right)} \right\} \cos\left(\frac{2kx_0}{D}\xi\right)
 \end{aligned}$$

The maximum and minimum values of (I) will then be:

$$I_{\max} = A_1^2 + A_2^2 + 2A_1A_2 \left[\frac{\sin\left(\frac{2Kx_0}{D} a\right)}{\left(\frac{2Kx_0}{D} a\right)} \right]$$

$$I_{\min}$$

The Michelson definition of (V) the fringe visibility is:

$$V = \frac{I_{\max} - I_{\min}}{I_{\max} + I_{\min}}$$

so that the visibility of the fringes as a function of slit width is:

$$V = \left[\frac{2A_1 A_2}{A_1^2 + A_2^2} \right] \cdot \left[\frac{\sin\left(\frac{2Kx_0}{D} a\right)}{\left(\frac{2Kx_0}{D} a\right)} \right]$$

The first term in this expression expresses the effect of unequal amplitudes in the two interfering waves, and in our case their ratio is essentially equal to one; the second term is due to the finite size of the source slit.

It is of interest to note, at this point, that after the final instrument parameters were settled on the calculations for expected visibility gave reasonable results. For a visibility, (V), of 0.95 (1.00 being perfect) the required slit width was 4.3μ ; while a visibility of 0.84 gave a width

of 8.6μ . Both values are physically possible.

VARIATION OF AVERAGE INTENSITY OVER THE FRINGE PATTERN FIELD.

A variation of the average intensity in the fringes (α), over the field will effectively attenuate the signal output thereby causing a variation of response with the location of the sample object. Since the virtual slits are never greatly separated (0.04" maximum), it was felt that the difference in intensity between the center and the edge of the field which occurs with a single slit would serve to place limits on this error. Thus we need to consider the variation of intensity across the far-field diffraction pattern of a single narrow slit. For the dimensions used, calculations show that the maximum variation across the image space is less than 1%. The effect of this small variation is negligible.

An experimental verification of these calculated results will be given later along with the entire performance record. Before this, however, we must describe the construction of the instrument which was based upon the foregoing considerations.

DESIGN CONSIDERATIONS

It was felt that the position previously reached in the measurement of Fourier spectra of photographic images called for a somewhat more sophisticated instrumental approach. An instrument was needed which would be able to handle a large number of photographic transparencies, of some convenient and standard size, over a useful spatial frequency range, and operating in a semi-automatic manner. This proposed instrument should be easy and foolproof in operation, require low maintenance while possessing a long life expectancy, be self-contained and capable of operation in a fully lighted room while requiring no more than a normal AC input. The output should be linear, scaleable and permanent.

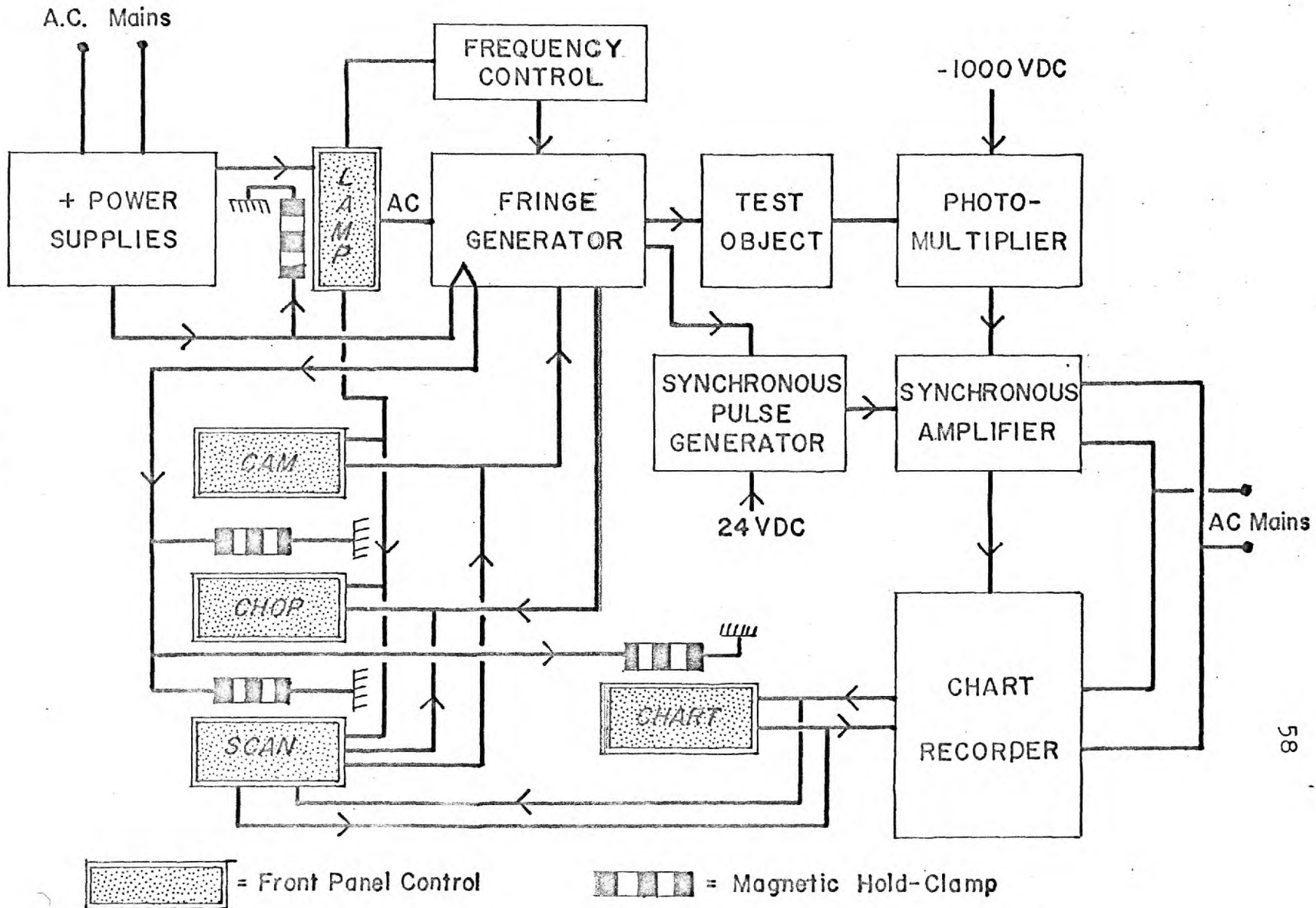
Figure (18) shows the completed instrument.

DESCRIPTION OF EQUIPMENT

Figure (19) is a block diagram of the equipment. Actuation of the Fringe Programme block results in a programmed linear variation of the fringe spacing at a fixed standing wave frequency. The sequence also controls the chart recorder drive and the standing wave generator (or modulator) turning them on and off at the beginning and end of a scan.



19



Over-riding switches for independent operation of these functions are also included on the instrument's front apron.

Each slide magazine will hold thirty transparencies and these may be processed one immediately after the other. The complete sequence of scanning and re-setting is fully automatic and takes just one hundred seconds.

There are two major exceptions to the above times for processing. If, first, the real and the imaginary parts of the Fourier spectrum are required separately two scans will be needed for each object, thereby doubling the time. The choice of solutions is controlled by one of the pull knobs on the cover; the second pull knob zeroes the light level by eliminating the fringe pattern while holding the light level constant. The second exception arises from the design assumption that all test objects would have symmetry about the horizontal axis. If it is of interest to check this quality each slide must be turned upside down and rescanned; the results are then averaged. Any difference in values would be due to a failure of the instrument to maintain a constant light level in the vertical direction.

MECHANICAL DESIGN

The base, prism holder and slit mounts were all poured from a 700 series, medium heat treatment aluminium. This particular alloy series, with its high copper-iron content, was used because of its good machineability, high mechanical stability without ageing and its low relative cost (this because of its popular useage; a melt is nearly always in process at a large foundry). The patterns for these items were all made in the Imperial College shops. It is interesting to note that no cores were required for these casts and that the base was poured with an irregular split line. One small wall failure occurred in the rear apron because of this requirement, but adequate patching was possible. The wall thickness of the apron and bottom webbs, it will be noted, is only $\frac{3}{16}$ ". If a fully cored pattern had been used, with the resulting draw taper, it is doubtful that it would have been castable.

THE LINE-PLANE REFERENCE SYSTEM.

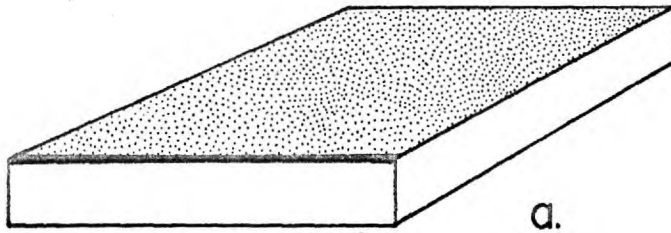
The base casting has been machined in such a way that there is only one reference plane and one reference line from which the optical axis is established. The particular procedure here was

to true the top of the casting with skin cuts to obtain a stable base from which to machine the bottom footings. The base was then strapped down and the top inside pads were all milled to an equal level, establishing a horizontal reference plane. The front outside edge was then cut and cleaned. The lamp center-line was then taken as an artificial location point and all lateral measurements were taken from it.

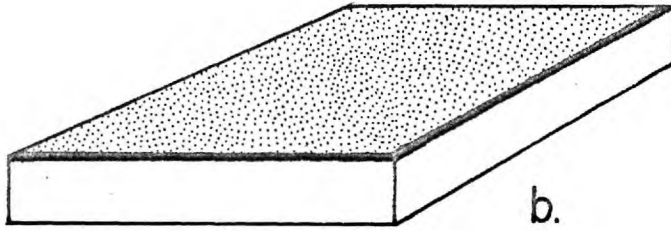
While not wishing to belabor the point, it does seem valuable to understand this concept of plane-line referencing for optical systems. The system is well known and used in good optical benches, but in normal practice it is almost invariably passed over. Since optical elements usually are in the form of short cylinders the designer is too often tempted to mount them in circular cells. A little thought will show how difficult it is to align several of these cells. Once the mechanical center point of a cylinder is lost, through machining, it is very difficult to establish again. This means that the concentricity of the elements is very doubtful. It can be achieved by mounting all the elements inside a totally enclosing outer cylinder, as in the method of the telescope, but this leaves one with either a problem of establishing the perpendicularity of the

element to the enclosing cylinder or of not knowing the spacing between the elements. Full-length, squared-off internal spacers will solve all these problems although one is then left with no chance of adjustment in spacing. Clearly, in all but a few special cases, this design technique is awkward and wasteful of time and materials.

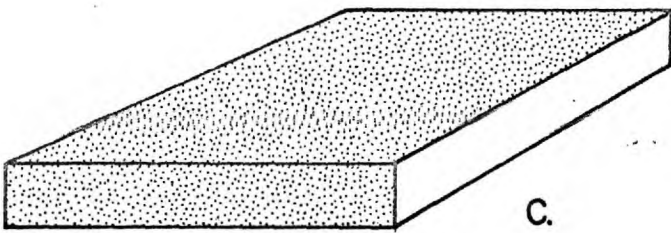
Several other referencing systems are immediately obvious. A few of these are shown in Figure (20). In both cases (a) and (c) some sort of artificial cross line does in fact have to be established. The difference between this and cases (b) and (d) is that the second line is artificial and is not machined into the system. Case (c) is the most commonly encountered reference system for optical systems of high quality while case (e) is rarely used. The main fault with cases (c), (d) and (e) is that one must rely on a machine tool to establish the perpendicular faces. It cannot be strongly enough emphasised that this is one job that machine tools are not in general capable of doing nor is it their purpose. The only common tool which is capable of establishing perpendicularity is a try-square. A designer must never forget this fact.



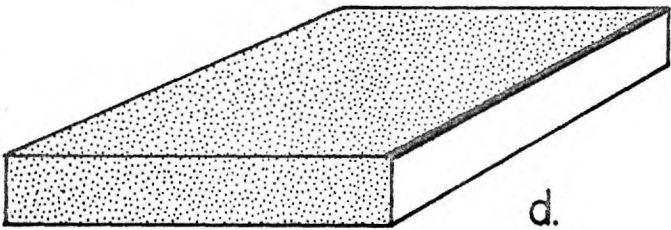
ONE LINE
ONE PLANE



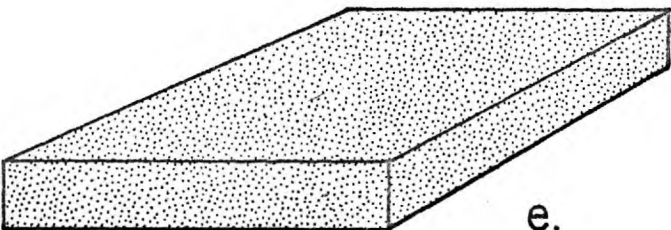
ONE PLANE
TWO LINES



TWO PLANES



ONE LINE
TWO PLANES

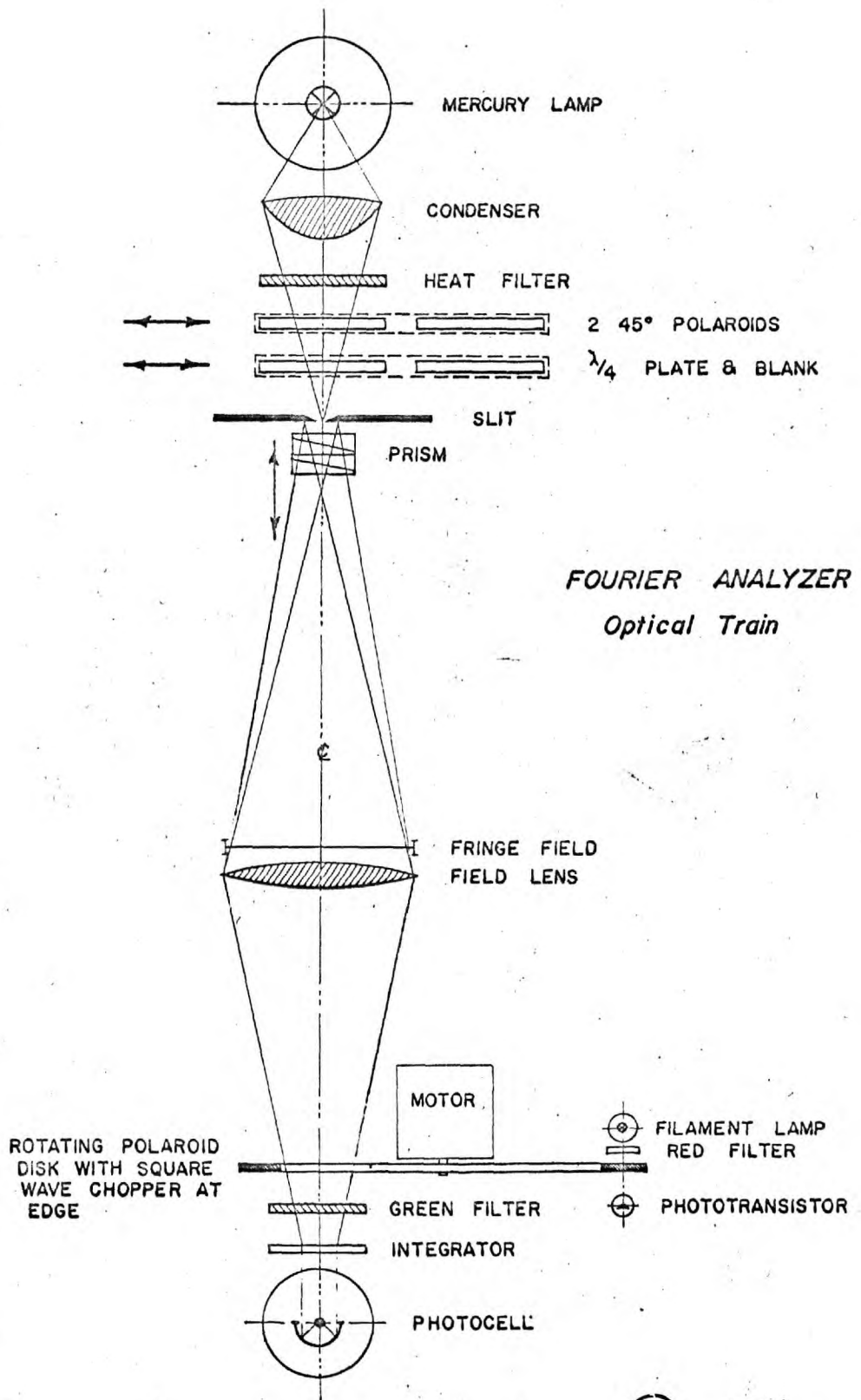


THREE PLANES

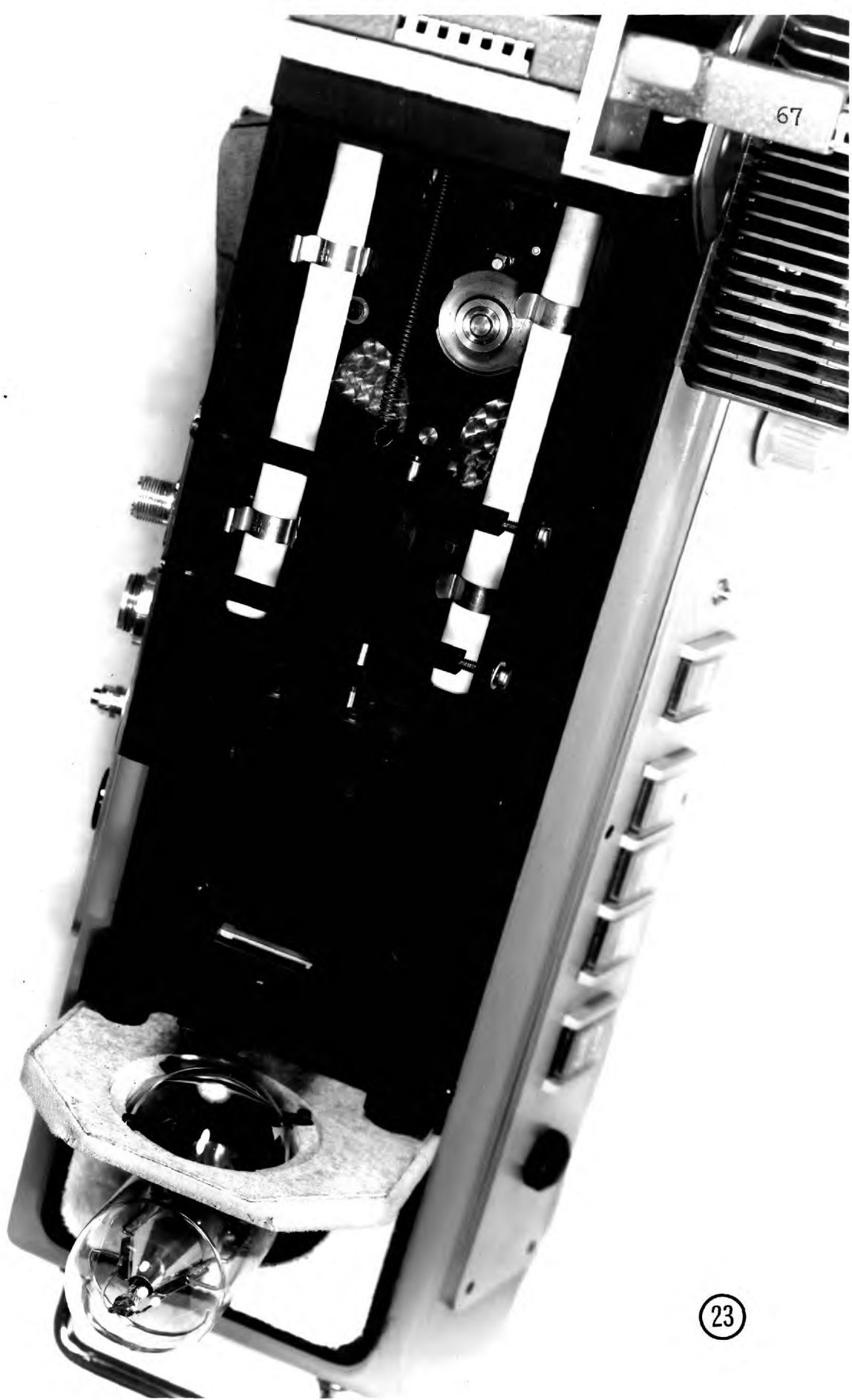
The only fault with case (b) is that if the second line, the cross line, is machined in, one is tempted to measure directly from its edge rather than along the main reference line. With case (a) adequate information is included in the machining to establish an optical axis while no opportunity occurs for mistaken trust in machine generated angles.

OPTICAL MOUNTS.

For convenience a copy of the optical train is included as Figure (21). Three items are mounted without provision for adjustment. These are: the Wollaston prism, P_1 , the condenser C_1 and the objective O_1 . These mountings are shown in figures (22) and (23). These items, as well as the other optical units, were carefully aligned and checked before being finally located. Most of the lens are held into their mounts by phosphor-bronze clips. It might be of interest to mention that when this material is used for clips care should be taken that the rolling mill grain should be perpendicular to the bending lines of permanent deformation or, finally, fracture will occur.







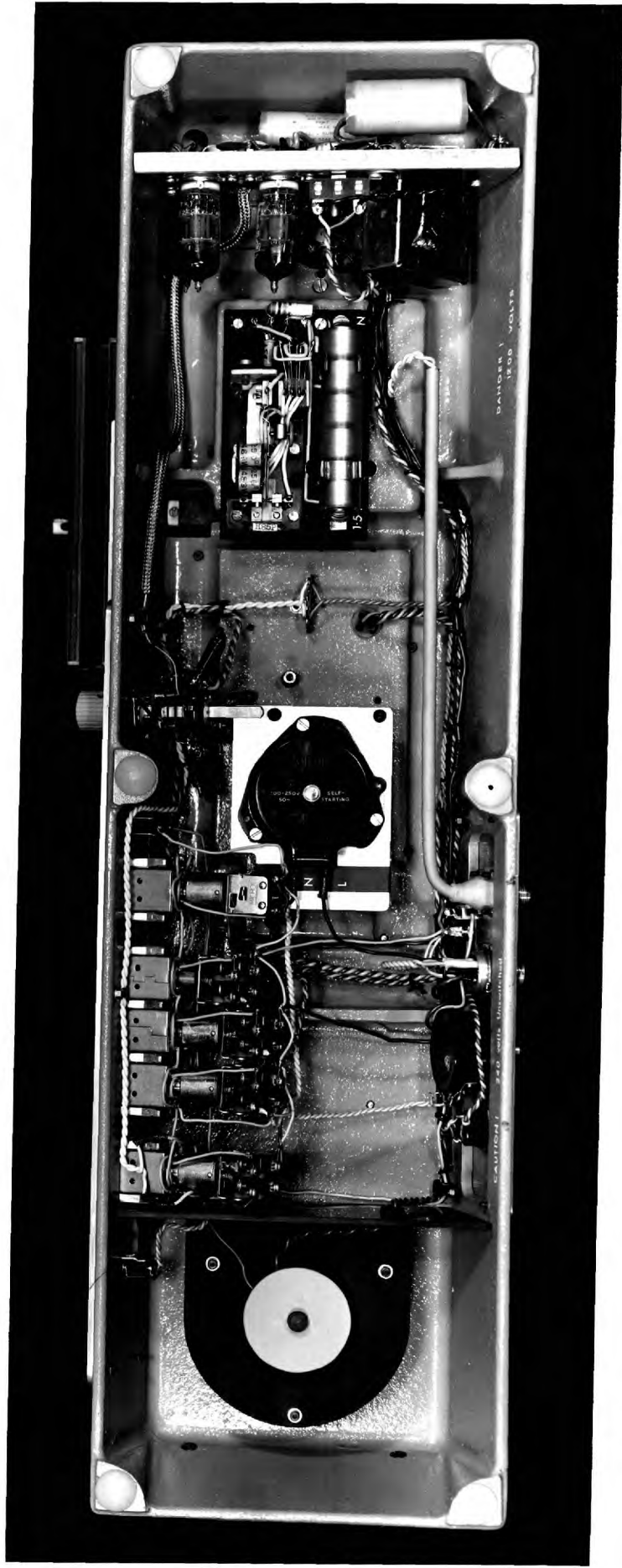
67

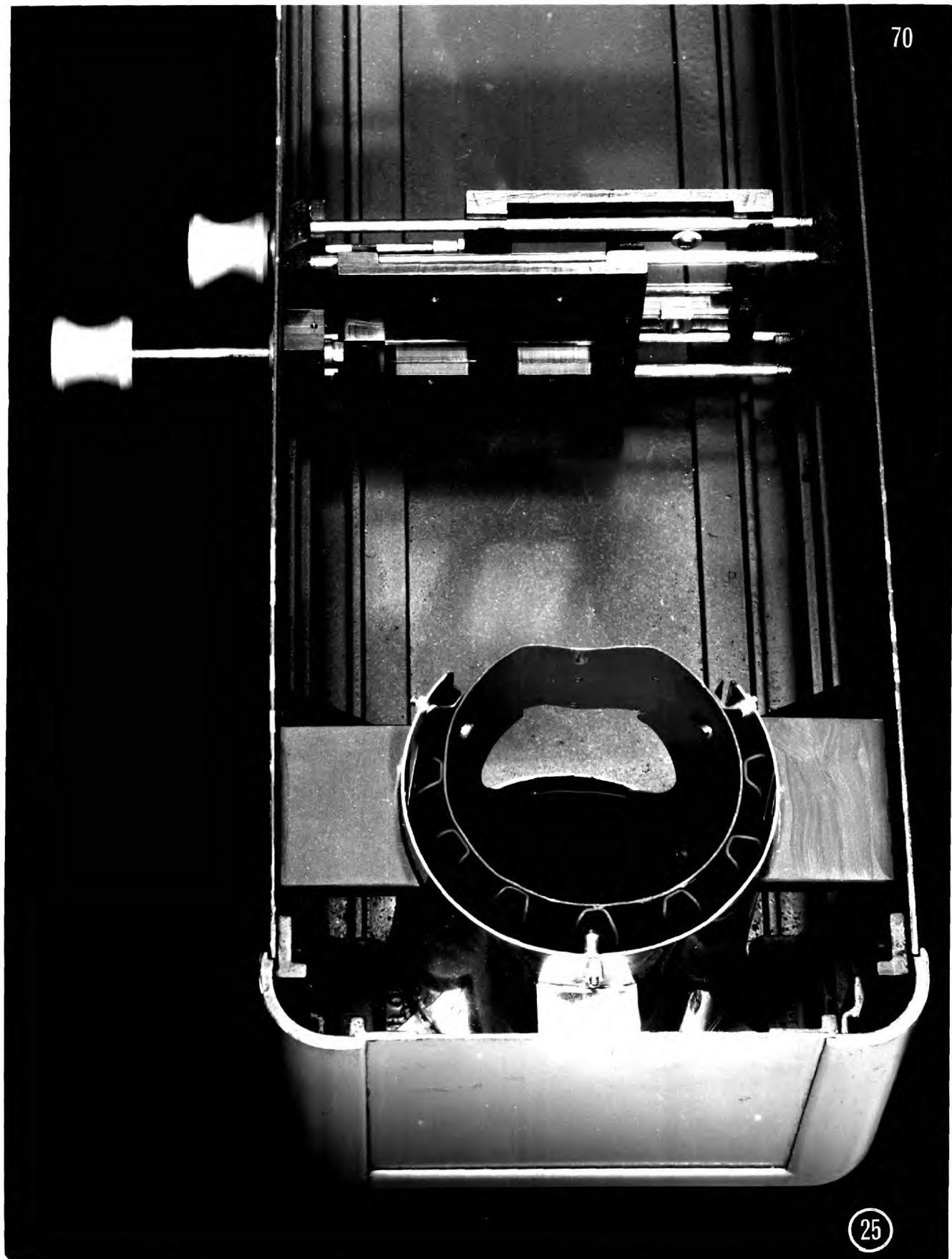
The photomultiplier socket is mounted directly on the base casting and the voltage divider network is directly underneath. The potential at this point is -1000 v. relative to earth when the power supply is on, and appropriate care should be taken when handling. The charges on the condensers decay through the voltage divider with a time constant of the order of a few seconds. This section is shown in Figure (24).

The push-pull slides, shown in Figure (25) control the polarization of the light falling on the slits. One slide holds two pieces of polaroid whose axes of polarization are set at 45° to the slit and parallel to the slit. The other slide holds a quarter-wave plate and a clear position. The slides run on two steel shafts in open "V" grooves, being constrained on the other side by phosphor bronze clips. Centering is accomplished by a combination of spacers and adjusting the knob shaft length. Although the units operate smoothly and firmly they are decidedly too complex for their purpose. Simplifications, however, are often more obvious after the fact.

LAMP AND HOUSING.

The lamp is mounted into a modified three-pin socket. The socket plate, made of Tufnel, is suspended





below the base casting by three pins of the same material as shown in Figure (24). By making the holes in the socket plate decidedly oversize it is possible to adjust the lamp, within limits, in all directions. At the same time a large supply of air is free to pass by the lamp for cooling.

This particular lamp, with its high internal pressure and all glass shell, is capable of fracture during operation. The resulting explosion of glass particles could be serious. It is therefore, important that the lamp never be operated with the cover off.

The cooling of the lamp proved to be a substantially more difficult proposition than was originally thought. The first design allowed a constant air passage of over 3 square inches through a one stage light trap, and relied on convection. The condenser (C_1) mount was made of a machinable furnace material and the walls of the case were lined with asbestos. This system was not satisfactory.

Forced air cooling was considered but it seemed both cumbersome and awkward.

I am indebted to Mr. Shack, currently of this laboratory, for suggesting the final solution. Figure (25) illustrates the lamp housing. The

inner, black cylinder acts as a thermal collector. It encircles the lamp with about $\frac{1}{4}$ " clearance with the only opening being in the optical path. The surface temperature of this part of the chimney rises to about 250°C in the neighbourhood of the lamp. The conditions are so adverse that the black dye, used in anodizing the tube, has been substantially bleached out. The heat that is reradiated on the outside of this tube is reflected by the outer tube. This outer tube has been silver-radium plated and is highly polished. The inner tube cools itself by conduction to the air which passes by it by convective currents and by radiation from the section above the case. The heat transfer that does occur seems to occur mostly along the six spacers separating the inner and outer parts of the housing. The efficiency of the chimney is improved by thermally isolating these spacers and by putting cooling fins on the inner tube. The end of the case becomes warm to the touch after about two hours of operation, but it never seems to rise about 40°C . The free air passage space has remained at about 3 square inches.

A thermal isolation of more than 200°C in $\frac{3}{8}$ " (inner -outer shell separation) by convective air is an impressive result.

MODULATOR DRIVE AND MOUNT

The modulator (standing wave generator), comprising a rotating polaroid, is suspended in a stable balance position from the ears on the top of the base casting by two dural arms. The connection between the arms and the modulator itself is by way of heavily loaded polyethelene pads. These pads are heavily damping in the audible range and they help to prevent the whole unit from "ringing". The polaroid sheet (.010" stock) is surrounded on its perimeter by a light dural ring to which it is glued. The ring prevents the disk from setting up destructive standing waves in its surface at high speeds.

In operation the polaroid disk revolves at between 15000 and 20000r.p.m. to give an output frequency of between 500 and 600 c.p.s. The stability of the particular frequency chosen seems to be better than 1% after a 10 second warm-up.

The prime mover is a size 10 DC servo-type motor. It is mounted to the face plate by the normal two-flange-and-clips servo-motor method. Directly pinned to the shaft is a passivated bronze gear of high quality (A.G.M.A.5). In a step-up of 8:1 this drives an equivalent quality steel gear at 120 D.P. for the pair. This second gear is

pinned to the shaft carrying the polaroid disk. The unit is shown in Figure (26).

It will be noticed that on the periphery of the polaroid disk a black quadrant has been painted. This is used to operate a synchronous transistorized switch which produces a reference beam for use in the electronics. Both the phototransistor and the miniature lamp to activate it are mounted in a brazed brass arm which bolts to the top of one of the chopper hangers. The arm is electrically insulated from the chassis. In the lamp housing section a red Wratten filter and a small, short focus lens have been mounted with Canadian balsam.

The shaft is supported by two very high precision ball bearings (A.B.E.C.7). These bearings have only half shields because of the speed required of them; appropriate care should be exercised. The normalised life factor of the bearings is about 1.7 which should result in a life of about 500 hours.

The majority of the "ringing" in the unit is suspected as coming from the passivated bronze gear. Two dissimilar metals were chosen in an effort to equalise the wear in the two gears. Quieter running would be obtained, at a small sacrifice in life, if the larger wheel had been of a somewhat smaller face width and cut from an anodized aluminium blank.



Control of the unit's speed is held by the screwdriver type rheostat on the rear apron.

CAM DRIVE AND PRISM MOUNT.

The 1 rpm clock motor that hangs below the center of the base casting drives a three-wheel gear-train. There is a 3:5 step-down in the first pair, the second pair being 1:1. The gears are again of dissimilar metals to ensure quiet running and equal wear. Staked to the hub of the second gear is a ground, 2% constant rise cam. At both extremes of the cam travel there is a short flat position for location of the slit-prism separation. The third gear is mounted on an extended shaft. The upper extension carries two adjustable position cams which each actuate a micro-switch. These switches control the scan sequence (lower switch) and the chart drive (upper switch). See Figures(23) and (27). The two independent wheel shafts are housed in bushed nylon flange bearings. This material is very satisfactory for slow-speed, low-load bearings; the motion is exceptionally smooth and soft. Some tricks are involved in its use, however. The bearing should be made with a .002" - .003" oversize O.D. and a decidedly undersize bore (say .010"). After

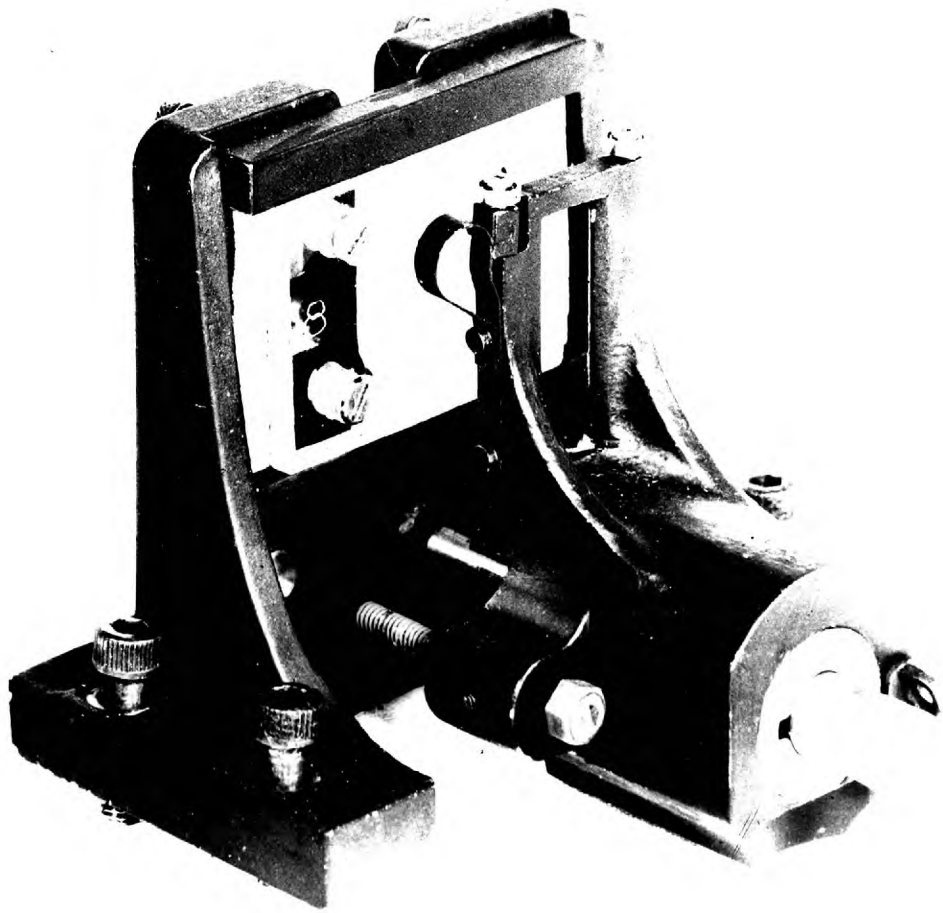
pressing the bearing into the housing a sharp reamer may be put through the bore with a long push and small twist. This assumes the shaft to be of an 'f6' to 'h6' tolerance and will produce reasonably reliable results.

The constant-rise cam mentioned above, drives the prism mount along a splined steel shaft which is held by a heavy force fit in the slit mount. The prism itself is held in the cast mount by a celulose cement. A mild steel sleeve has been pressed into the casting; it has been broached and bored to accept the splined shaft.

This particular design of way was used in an effort to discover whether it produced fewer problems than normal techniques. It is not a total success, for the fitting and lapping require both time and skill far in excess of the quality of the results. It is not a recommended technique where a double-shaft way may be used instead.

FINISH

All of the painted parts have been first primed with zinc chromate and finished with several coats of celulose lacquer. Aerosol bombs (under the trade-name "Rust-o-leum") were used for spraying.



Dural parts have been either clear or acid black anodized. Copper and brass parts have been ammonia blackened or left bright. Some steel parts have been blued, but the majority have been left bright.

OPTICAL ALIGNMENT AND SET-UP

The major components of the optical system have been mechanically located to be in good alignment. The lamp and prism-slit systems, however, must be aligned separately.

The lamp is simply set so that the light falling upon the slit is maximized. By loosening the three screws on the socket board underneath, the whole socket may be slid back and forth or sideways with a freedom of $\pm \frac{1}{8}$ ". Vertical adjustment may be achieved by adding spacers to the support cylinder or by the simple expedient of not pushing the lamp full home. The medium-pressure mercury source must not be operated without a safety cover for reasons of explosive danger. It need hardly be pointed out that the UV output of the lamp is decidedly dangerous to the eyes.

The prism itself must be in a good state of alignment before beginning to adjust the slit. With the photomultiplier housing, modulator disk

and objective removed it is possible to observe the returned images from the prism surfaces and from the slit face, with a dark-ground angle dekkor. Images will be seen from all the interfaces and they must be sorted out to avoid confusion later. The prism holder is adjusted (preferably after removing the front plate as noted previously) until the coloured images (i.e., the doubly transmitted beam reflected from the slit face) coincide in the vertical plane with the images from the last prism surface and the unobstructed image from the slit face. The latter two images should be aligned in the horizontal plane.

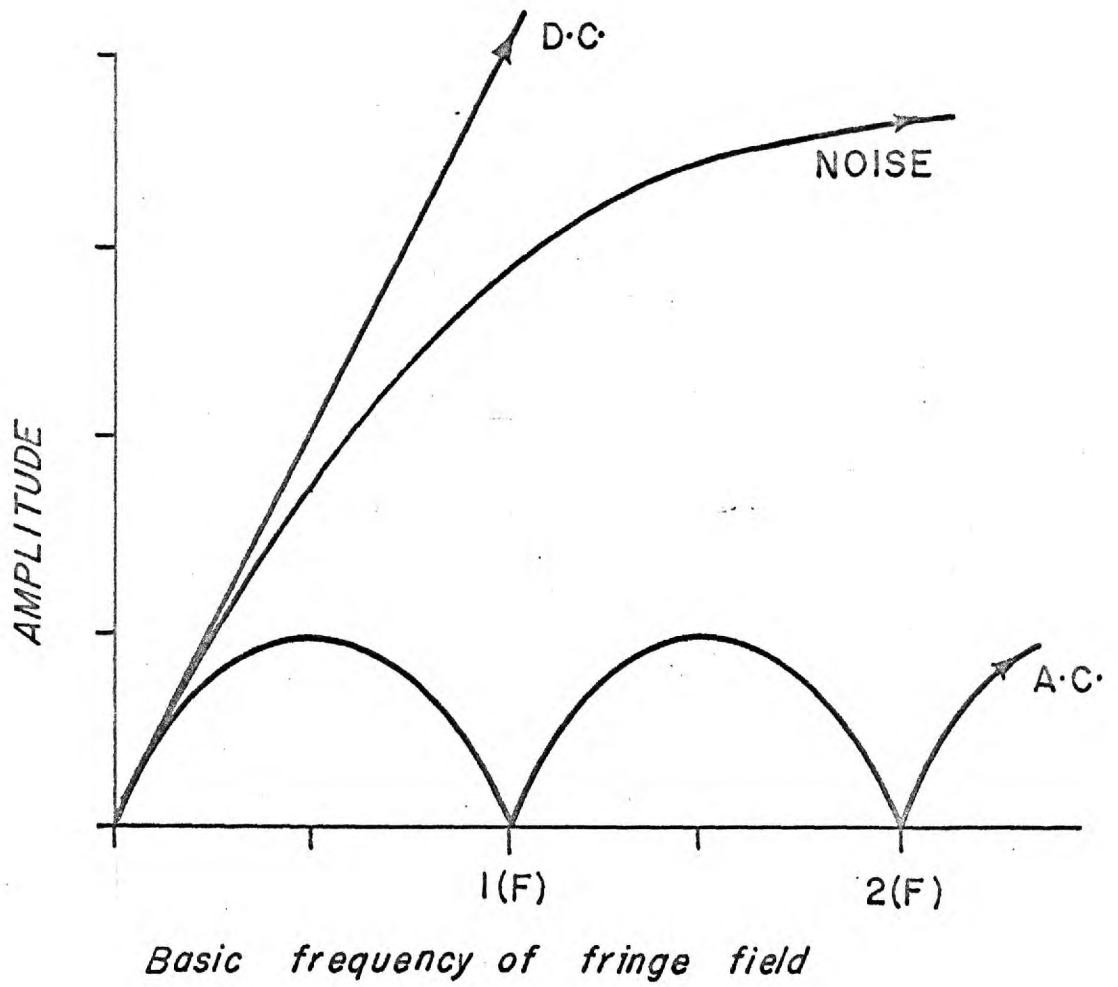
The angle dekkor is then replaced by a low-power microscope focused in the area of the fringe field. With the mercury source and two polarizers in the beam, oriented at 45° to the slit axes, fringes will be seen. Notice first the zero fringe, which will now be near the center of the field, as the prism is driven through its travel. If this fringe wanders strongly to one side it implies that the driving axis is not parallel to the optical axis. This is corrected by rotating the entire prism mount. This assembly is adjusted so that the zero fringe state occurs at the extreme end of the travel. It is probable now that the slit-prism relation will have to be checked again. This time place the prism holder

under operating tension by advancing the cam a little way through its operating cycle. It only remains, then, to set the angle of the prism parallel to the axis of the slit thereby giving maximum contrast to the fringes. This is done by adjusting the sideways motion of the bridge at both ends of the travel. Replacing the removed optics it should be noted whether the optical beam falls clearly on the central area of the photomultiplier's sensitive area.

ELECTRONICS

The signal, as viewed by the photomultiplier, is composed of three parts; the AC signal, a DC background and noise. The AC signal is derived from the variation of transmission of the test object when illuminated by the generated set of standing wave fringes. The frequency is dependent on the rotational speed of the chopper, while the amplitude is related to the spatial frequency content of the object and its transparency. The DC signal, however, is dependent only on the transparency and size of the test object.

Figure (28) illustrates the relationship of these quantities as the width of the object is varied. Clearly the optimum situation for lowest signal to noise ratio is when the object being

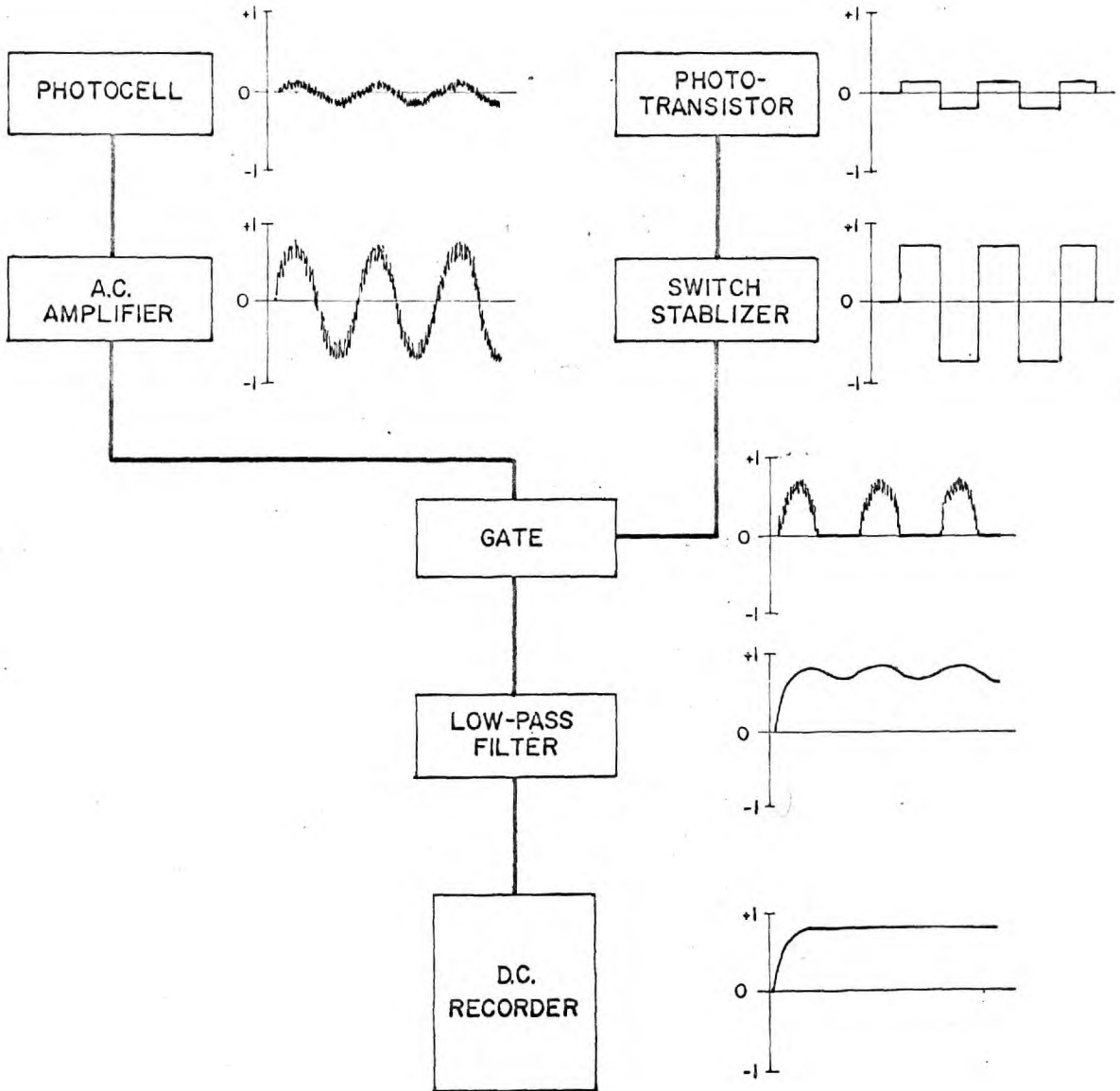


examined has the same width as the basic frequency being generated. This indicates the nature of the optimum type of object that should be presented to the instrument. There is a minimum level of total signal indicated by the dark current below which one should, however, not drop. In other words, while the ratio of AC to DC signal (and thus signal to noise) should be kept as low as possible by not presenting the instrument with an object whose DC content is high (e.g., a simple circle of diameter several decades greater than the fringe width). The other extreme situation could result in such a low intensity of light being transmitted that it is totally masked by the dark current of the photomultiplier.

The output of the photomultiplier is fed directly into an Elliott type B801 Synchronous Amplifier. This instrument comprises a high-gain low-noise amplifier with coarse and fine attenuation of 80 dB in steps of 20dB and 2dB, plus a smooth interpolating attenuation of 6dB at all positions. The amplifier characteristics are stated, by Elliott Bros., to be stabilized throughout by negative feedback circuits. The output is coupled to a phase

FOURIER ANALYZER

Block Circuit Diagram A

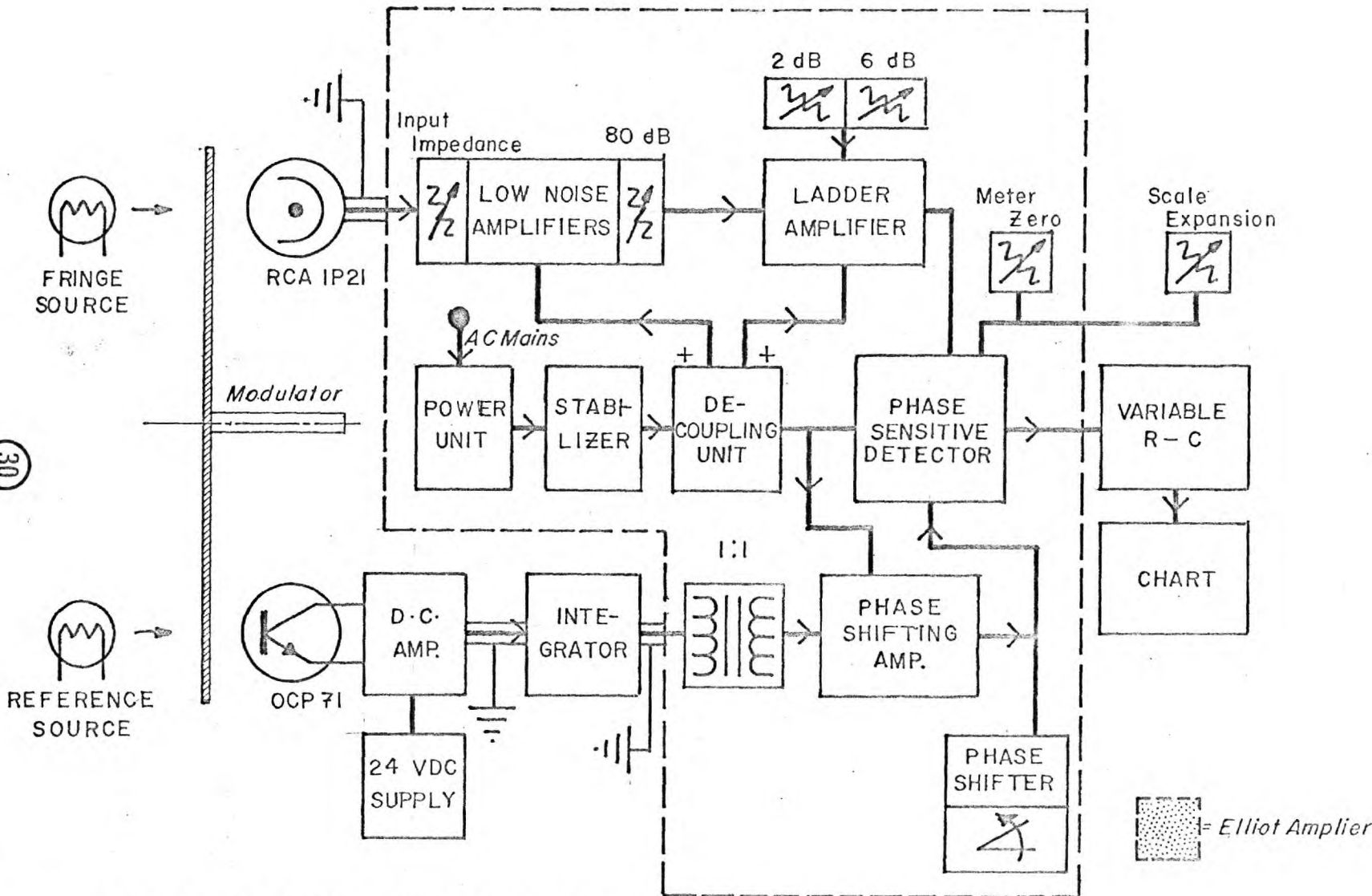


sensitive rectifier which rectifies those components of the signal which are in synchronism with a reference signal which is derived from the polaroid chopper. The reference signal is automatically controlled to a constant level within the instrument and it can be varied continuously in phase before being presented to the phase sensitive rectifier.

Figure (30) is an illustration of the complete electronic circuit showing the basic operations. All those units within the dashed lines are incorporated within the Elliott amplifier. Since only those parts of the signal in phase with the reference signal are rectified all signals in quadrature and at harmonics will give rise to no deflection. Any signals at frequencies different to that of the reference (e.g. noise) will produce an alternating voltage at some beat frequency. If the frequency of these beats is at a lower value than the time constant of the output they will be integrated and not appear. The effective bandwidth (and, therefore, apparent signal to noise ratio) of the amplifier is then controlled by the time-constant of the output.

Following the convention of Smith, Jones and Chasmer the effective bandwidth may be expressed as:

30



ELECTRONICS BLOCK DIAGRAM

$$\Delta f = \frac{1}{2} \pi \int_0^{\infty} \frac{d\omega}{1+\omega^2\tau^2}$$

where $\tau = R_{\text{meter}}C$, the time constant of the output circuit and $\omega = 2\pi f$. Then,

$$\Delta f = \frac{1}{\Delta\tau}$$

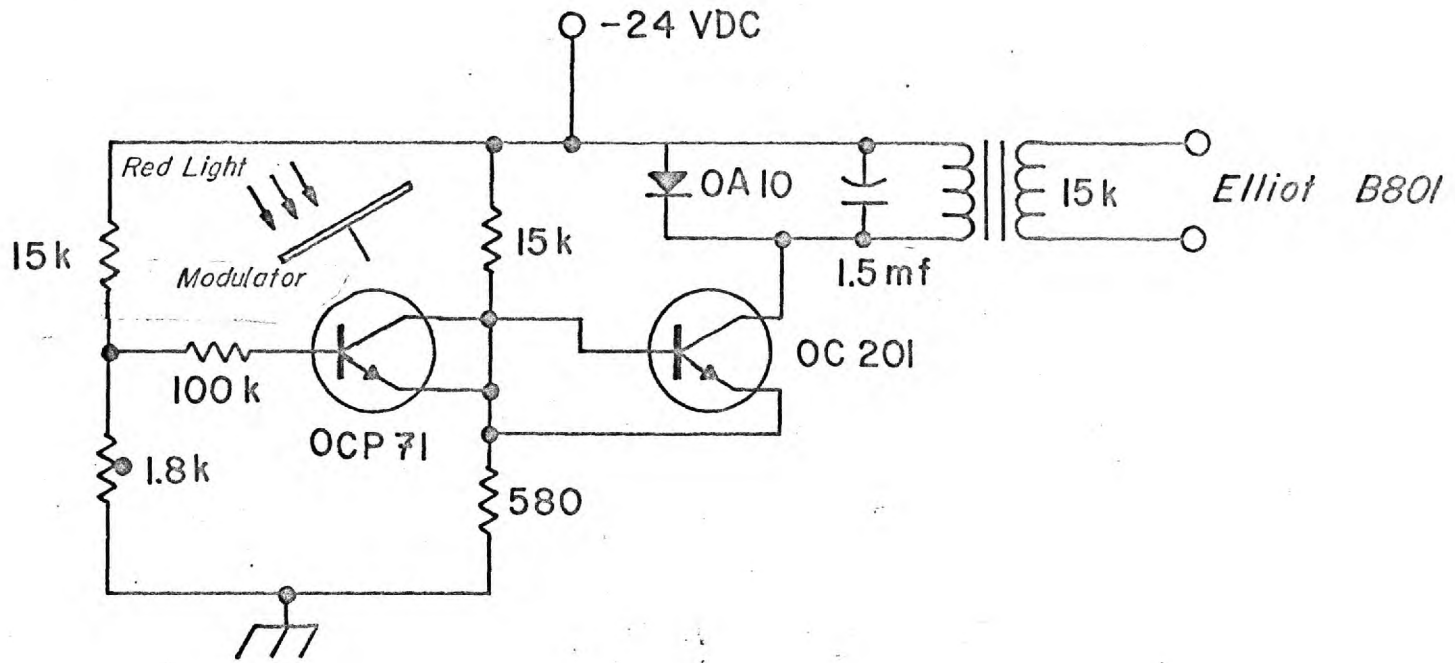
The Brown Potentiometric Recorder that is being used has an internal time-response of about 1 second, meaning that the effective bandwidth of the system is about 0.25 cps and that only noise within these limits should contribute to the output deflections. This, however does neglect the noise picked-up through stray couplings between reference channel and signal channel and the drift due to variations in the lamp's output.

The Elliott Amplifier requires a sinusoidal (or triangular) wave form of 2 to 20 volts r.m.s. at an input impedance of approximately 10K to 20K ohms for the reference channel. The range of frequencies over which it is intended to operate is 400 to 4000 c.p.s. Since the reference signal here is derived from a phototransistor being driven by a square wave chopper it was necessary to integrate the output into a triangular form. (It might be noted here, more or less in passing, that it was necessary to use a square-wave chopper on the edge

of the polaroid disk, rather than obtaining a sine wave directly with crossed polarizers for two reasons. Primarily, the sensitivity of the OCP71 phototransistor is extended far enough into the infrared to exceed the polarization abilities of sheet Polaroid. Infra-red sensitive Polaroid is, annoyingly, poor in the visible. Secondly, phototransistors and photodiodes are usually grossly non-linear and the resulting sine wave would be rich in harmonics).

Figure (31) is a schematic diagram of the reference channel prior to the Elliott Amplifier. The OCP71, a junction transistor, is effectively bottomed by the nearfocused light from a peanut-lamp. This lamp is colour separated from the main optical beam by a red Wratten filter. The signal is direct coupled to the OC201 making a simple DC amplifier. Allowance for temperature compensation is made in the base voltage divider of the OCP71 to avoid thermal run-away. The output of this circuit is 4.5 volts RMS (as read on a VTM integration) and consists of a clean triangular waveform with slightly clipped peaks on the negative (or overdriven) side. It appears to drive the Elliott Amplifier satisfactorily.

31



REFERENCE SIGNAL AMPLIFIER

Because of the extremely high sensitivity of the Elliott Amplifier, extreme care must be used in separating the input channels. Input leads should always be kept short and well shielded.

REFERENCES

- Berry, K. 1960 "The Radio Constructor",
14, 1, 68.
- Bradick, H.J.J. 1956 The Physics of Experimental
Method, John Wiley & Sons,
New York, p.370.
- Bragg, W.L. 1929 Z. Krist 70, 475
- Hopkins, H.H. 1950 Wave Theory of Aberrations,
Oxford Press, London.
- Mertz, L. 1956 J.O.S.A. 46, 548
- Smith, R.A.,
Jones, F.E. and
Chasmar, R.P. 1957 The Detection & Measurement
of Infra-Red Radiation,
Oxford Press, London, p.430
- Zworykin, V.K. &
Ramberg, E.G. 1956 Photoelectricity, John Wiley
& Sons, New York, p.136.

C H A P T E R I I I

An Evaluation Process Compatible to Both Subjective and Instrumental Testing

INSTRUMENTAL EVALUATIONS

The Fourier transform of a general scenic image will contain frequency components over a finite range. The lower limit to this range will be set by the dimensions of the image boundaries, while the upper limit will depend on the frequency content of the image, the transfer functions of the optical system and the photographic process. The amplitude function of the Fourier components will not exhibit discontinuities for a general image, but will vary smoothly over the frequency range. These frequency components will occur, in general, in all phases and azimuthal angles throughout the image. Neither the phase nor the azimuthal angle of a particular frequency occurring in a particular elemental area of the image will, in general, be equal to the phase or azimuthal angle occurring in any other elemental area at the same frequency.

If the Fourier transform is obtained for the integrated area of such a general scene in only one azimuthal orientation and at a fixed or constant phase relation, the sum of the sine transform and the cosine transform will usually be less than the true modulus of the transform. This will be the effect of the apparent phase variations resulting from azimuthal tipping and real phase variations over the image field. These phase variations will, to some degree, cause signal interference and thus reduce the apparent amplitude of the transform at any particular frequency.

It is necessary then that test objects be chosen for the instrument just described which have a fixed or constant phase relation, at each particular frequency, over the entire field upon which the transformation is to be performed. It is also necessary to establish a control on the azimuthal orientation of the image by either holding the angle constant, maximizing the signal by rotating the image with respect to the fringe field, or having rotational symmetry in the image.

Instrumental design features make it difficult, in this case, to rotate the image in the

fringe field and it was found, as we shall see in the next section, to be more convenient to produce one dimensional blurring in the image, thus precluding the use of rotational symmetry. Thus we have two criteria in the production of images for a comparison study between their Fourier transforms, and a subjective evaluation of their quality; first, that the phase relation, at any particular frequency, be constant over the field and, second, that the rotational orientation be held constant between the different series of images being examined. The particular pattern chosen for this study was that of a square-line transmission grating.

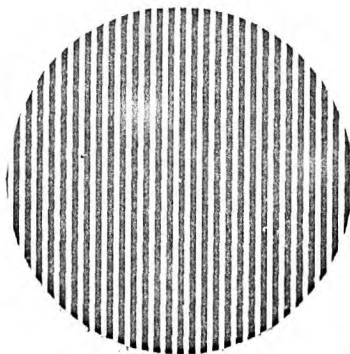
TEST OBJECT PRODUCTION

The master test object grating was produced by enlarging a photoengraver's equal-space half-tone grating onto an Ilford "Special Contrasty Lantern Plate". This plate was then normally developed in a fine-grain developer and, afterwards, intensified by dissolving away the undeveloped portions of the exposure, and bleaching and dying the remaining exposed portions. Great attention was paid to the alignment of the grating with the sides of the plate.

This process produced a grating of very high contrast and extremely sharp edges, with a spacing of about ten lines per inch. When an attempt was made to measure the profile of this master grating on the Hilger's microdensitometer it was found that the edges were sharper than the diffraction disk of the densitometer's scanning slit; this implies that the edges were sharp to better than a 4μ blur.

When this master grating was crossed, slightly, with another similar grating (which had been produced by the same process, but had been rejected because of irregularities in density) moiré fringes could be seen in transmission. These fringes appeared to be straight and evenly spaced over the whole aperture, thus indicating that the square-wave pattern itself contained no distortion of any importance. Further, when the grating was used as a transmission diffraction grating to view a narrow slit, the first order (second harmonic) spectrum was not visible to the naked eye, although the second and fourth orders were clearly seen. This indicates, of course, that the line to space ratio of the grating was 1:1 to a very high order of approximation, and again implies

that very little distortion was present in the grating.



32

Figure (32) is a direct copy of the grating and is included only to give a clearer idea of its size and scale.

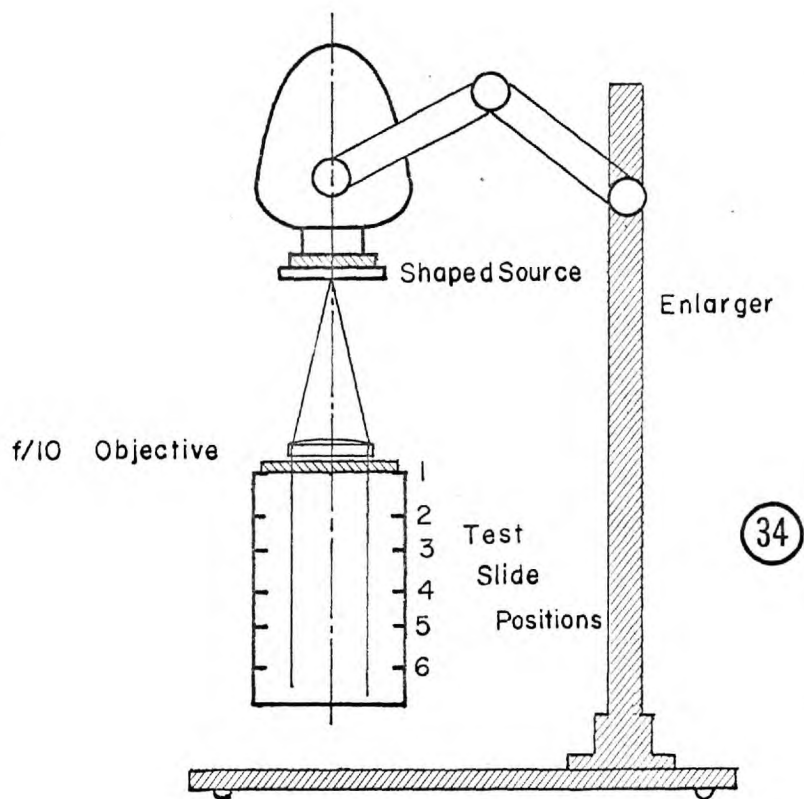
This grating was then used to produce

three sets of differently blurred photographic objects. Each set was composed of six slides covering the same range of blur resulting from three shaped sources. These shaped sources produced one-dimensional blur spots which had the form of a comatic distribution, a Gaussian distribution and a distribution similar to that produced by a first-order spherical aberration. Their shapes are shown in Figure (33) in the above order.

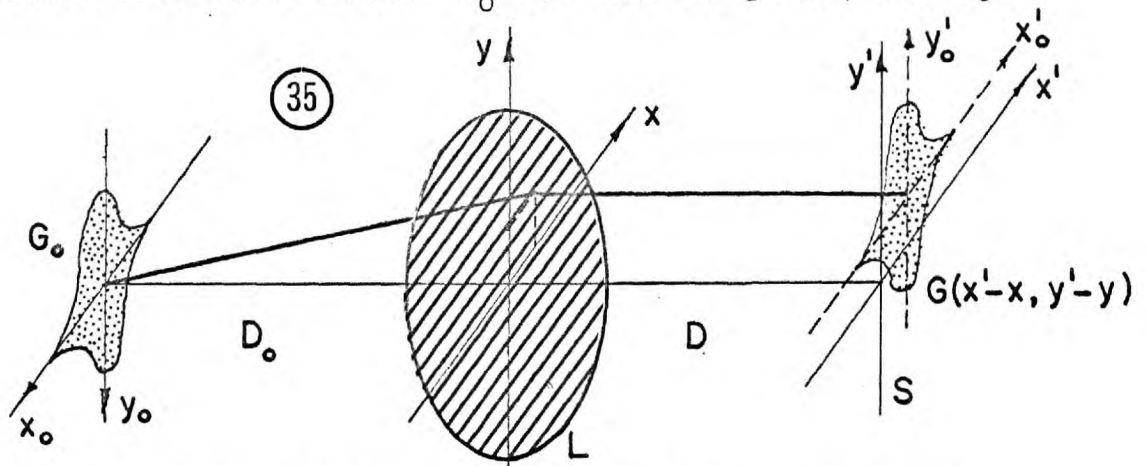


33

The optical system used to produce these sets of controlled blur is shown in Figure (34).



The theory underlying this process may be summarized as follows. G_o is a source plane, having



a distribution of intensity $G_o(x_o, y_o)$. Light from G_o , which is in the focal plane of a lens L , passes through a grating in contact with this lens and having

a transparency $B(x,y)$. Consider that light from all parts of the source which reaches a screen, S , through the point (x,y) of the grating. Clearly light from O_0 will go to the point $x'=x, y'=y$ on S ; and light from $P_0(x_0,y_0)$ will reach a point P'_0 on the screen, where $x'_0 = \frac{D}{D_0} x_0$ and $y'_0 = \frac{D}{D_0} y_0$. Thus each point (x,y) of the grating will give rise to a spread function on the screen, having intensity proportional to the transparency $B(x,y)$, centered on the point (x,y) on S and having a scale $\frac{D}{D_0}$ times that of the source G_0 itself.

Thus, if $G(x'-x, y'-y)$ is the form of this 'projected' source, constituting a spread function, the intensity distribution on the screen will be given by

$$B'(x',y') = \iint B(x,y) \cdot G(x'-x, y'-y) dx dy$$

and the transfer factor of the process is

$$g(\Xi, \Upsilon) = \iint G(x',y') \cdot e^{-i2\pi(x'\Xi, y'\Upsilon)} dx' dy'$$

or, in terms of G_0

$$\begin{aligned} g(\Xi, \Upsilon) &= \iint G_0 \left\{ \frac{D}{D_0} x', \frac{D_0}{D} y' \right\} e^{-i2\pi(x'\Xi, y'\Upsilon)} dx' dy' \\ &= \left(\frac{D}{D_0} \right)^2 \iint G_0(x_0, y_0) e^{-i2\pi \left[x_0 \frac{D}{D_0} \Xi + y_0 \frac{D}{D_0} \Upsilon \right]} dx_0 dy_0 \end{aligned}$$

Hence

$$g(\Xi, \Upsilon) = \left(\frac{D}{D_0} \right)^2 g_0 \left[\frac{D}{D_0} \Xi, \frac{D}{D_0} \Upsilon \right]$$

or, normalized

$$\frac{g(\Xi, r)}{g(0,0)} = \frac{g_0\left(\frac{D}{D_0}\Xi, \frac{D}{D_0}r\right)}{g_0(0,0)}$$

for a unidimensional object we need

$$D(\Xi) = \frac{g(\Xi, 0)}{g(0,0)} = \frac{g_0\left(\frac{D}{D_0}\Xi, 0\right)}{g_0(0,0)}$$

It may now be seen that with $\Xi_0 = \frac{D}{D_0}\Xi$,

$$g_0(\Xi_0, 0) = \iint_{+\infty}^{-\infty} G_0(x_0, y_0) \cdot e^{-i2\pi x_0 \Xi_0} dx_0 dy_0$$

or

$$g_0(\Xi_0, 0) = \int_{+\infty}^{-\infty} G_0(x_0) \cdot e^{-i2\pi x_0 \Xi_0} dx_0$$

where

$$G_0(x_0) = \int_{+\infty}^{-\infty} G_0(x_0, y_0) dy_0$$

is the integrated intensity along y_0 . It follows that a source of uniform intensity may be used, 'shaped' to simulate different forms of spread functions; the effective spread function being $G_0(x)$ as defined above.

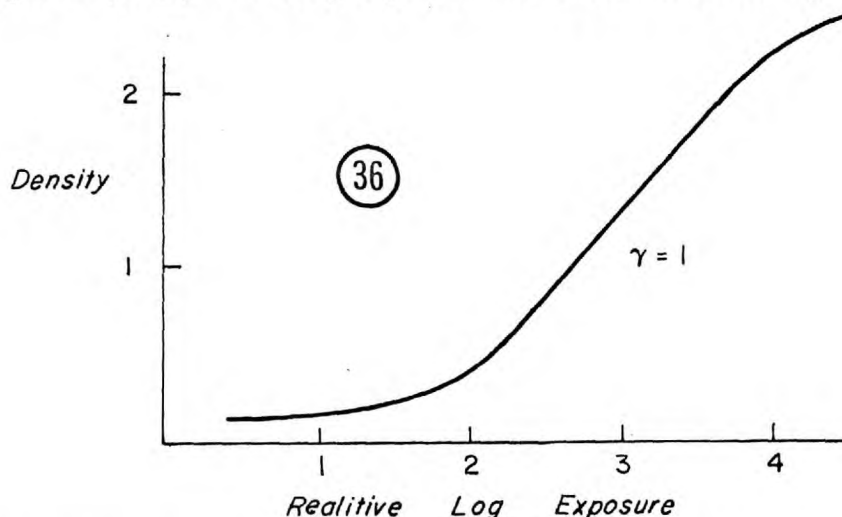
In practice the shaped masks were placed in an enlarger's even-illumination field, with the enlarger's objective removed. An $f/10$ objective then collimated the light which was transmitted by these masks.

As required above, the master grating was placed as close as possible to the objective. Exposures were then made with the unexposed slide and the grating in intimate contact and at five other fixed separations. This produced a series of six slides in each set ranging from the very sharp direct-copy print to a copy where the blur spot was very nearly equal to $1/4$ the grating spacing.

The plates used to produce these copies were the Ilford "Selochrome" emulsion. This plate was chosen because the gamma of the H-D curve could be held nearly equal to one while a large density range was covered. The plates were developed for four minutes, at 70°F. , in ID-2 developer mixed $1:2\frac{1}{2}$ with water. The plates for each set were processed all together in a specially adapted tank. The tank was continuously tip agitated to reduce the Eberhardt effect to a minimum. The plates were normally fixed and washed, with a final wetting-agent wash.

A test plate with varied steps of exposure was made with this emulsion using the above exposure and development process and from it an H-D curve was

calculated. It will be seen that this curve, shown in Figure (36), is roughly linear from a density of



0.6 to 1.8. By extrapolation, the corresponding exposure times, for these densities, were found and used for producing the slides. This helped to assure that the non-linearities of the photographic process were reduced to a minimum and that the images were degraded only by the mask contours. Reproductions of microdensitometer traces of the contours of these test slides, for all three series, are shown at the end of this chapter [Figures (48), (49) and (50)].

A variable R-C timer was designed and built to control the exposure times. A background exposure being put on each slide first, before exposing the grating structure, to bring the photograph into the linear density region.

PAIRED-COMPARISON QUALITY EVALUATIONS

These series of six slides in each set were then shown to a group of observers who were required to make a preference judgement; each of the three series was shown at three different distances. The distances chosen were calculated such that the normal eye could just resolve the fourth harmonic of the pattern (Distance I), the second harmonic (Distance II) and a spacing midway between the first and second harmonics of the test grating (Distance III).

The slides were back-illuminated with green light (to coincide with the other instrumental parameters) and shown to each observer in random pairs. The slides were placed side by side and both orientated in a vertical direction; this direction giving the most favourable acuity for the eye. Each pair was shown twice, in opposite arrangement, and all possible combinations of each set were employed. The pairs were kept in random order by marking each separate arrangement on a separate card; a different deck being used for each full set. Each pair was then shown in the order given on the card newly turned up, the deck being shuffled before each

new series of observations was made. The results of the observer's choice were marked on this card, with separate sections being used for each distance.

The only statement made to each observer was that he was to choose, right or left, which of each pair he found to be better. If he was not sure, he was to guess. This is the major advantage of the paired-comparison method; that only the bare minimum of information has to be given to the observer before he is able to make a judgement. Since an equality judgement is not allowed in this method, we are able to observe, quite clearly, the neighborhood of reactions close to the point where the observer is no longer able to make a conscious quality judgement. Also, since each pair was shown later in interchanged positions any inequalities of the observing parameters (such as unequal illumination) tend to cancel.

Since we are here interested primarily in the threshold of the quality discrimination for the observer, it is imperative that he be not able to discriminate between all of the pairs of slides with any degree of certainty; in fact, we wish the

observer to be forced to guess nearly half of the time.

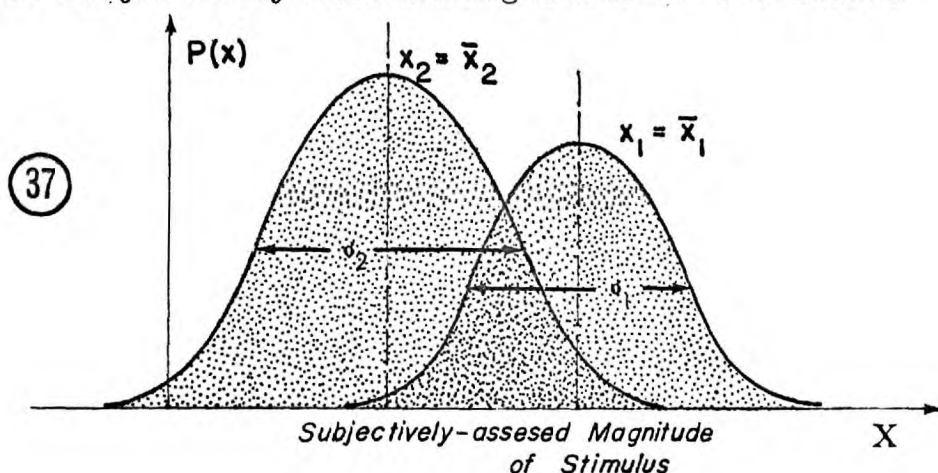
To control the quality of the image a circular patch of even illumination was overlaid on the viewed slide images. This was done by interposing a large beam-splitter between the observer and the slides being viewed. This reduced the contrast, that is the Michelson visibility, of the objects, equally. Several preliminary tests were made to establish a satisfactory level of visibility for the final tests.

The results of the judgements of such a pair-comparison give a preference ratio for each pair so compared. The preference ratio of one object relative to another is the ratio of the number of assessments of that object as superior in quality to the total number of assessments made. Clearly the greater the preference ratio for any pair the greater the difference between them as judged by observers. These preference ratios may be converted to give a linear scale of the magnitude of the subjectively perceived difference between any pair of objects.

This interpolation is based on Thurstone's (1927) 'Law of Comparative Judgement', which assumes

Cattell's principle that "equally often noticed differences are equal unless always or never noticed". Thurstone postulates that the dispersion of the subjectively-assessed magnitudes of a given stimulus will have the form of a normal distribution about a mean. In a pair-comparison two different physical stimuli are presented, each having normally distributed subjectively-assessed magnitudes about its own mean. The probability distribution for the difference between two normally distributed quantities is itself a normal distribution.

In Figure (37) for example the quantity x_1 is the subjectively-assessed magnitude of a stimulus



having a normal distribution of standard deviate σ_1 about the mean \bar{x}_1 . Thus

$$P(x_1) = \frac{1}{\sigma_1 \sqrt{2\pi}} e^{-\frac{1}{2} \left(\frac{x_1 - \bar{x}_1}{\sigma_1} \right)^2}$$

and similarly

$$P(x_2) = \frac{1}{\sigma_2 \sqrt{2\pi}} e^{-\frac{1}{2} \left(\frac{x_2 - \bar{x}_2}{\sigma_2} \right)^2}$$

If the subjective reactions to the two stimuli are completely uncorrelated, the probability of finding x_1, x_2 together is

$$P(x_1)P(x_2) = \frac{1}{2\pi\sigma_1\sigma_2} e^{-\frac{1}{2} \left[\left(\frac{x_1 - \bar{x}_1}{\sigma_1} \right)^2 + \left(\frac{x_2 - \bar{x}_2}{\sigma_2} \right)^2 \right]}$$

Now for any x_1 the value of x_2 will be $x_1 - \Delta$, if the difference $x_1 - x_2 = \Delta$; so the probability of finding x_1 and x_2 such that $x_1 - x_2 = \Delta$ is

$$P(x_1)P(x_1 - \Delta) = \frac{1}{2\pi\sigma_1\sigma_2} e^{-\frac{1}{2} \left[\left(\frac{x_1 - \bar{x}_1}{\sigma_1} \right)^2 + \left(\frac{x_1 - \Delta - \bar{x}_2}{\sigma_2} \right)^2 \right]}$$

and the probability of finding $x_1 - x_2 = \Delta$ is

$$\begin{aligned} P(\Delta) &= P(x_1 - x_2) \\ &= \int_{x_1 = -\infty}^{+\infty} \frac{1}{2\pi\sigma_1\sigma_2} e^{-\frac{1}{2} \left[\left(\frac{x_1 - \bar{x}_1}{\sigma_1} \right)^2 + \left(\frac{x_1 - \Delta - \bar{x}_2}{\sigma_2} \right)^2 \right]} dx_1 \end{aligned}$$

This integral may be integrated using the result

$$\int_{-\infty}^{+\infty} \frac{1}{\sigma \sqrt{2\pi}} e^{-\frac{1}{2} \left\{ \frac{x - \bar{x}}{\sigma} \right\}^2} dx = 1$$

Thus, expanding the square bracket in the first integral and completing the squares in x_1 and Δ gives, after considerable reduction

$$\left[\star \right] = \frac{\sigma_1^2 + \sigma_2^2}{\sigma_1^2 \sigma_2^2} \left[x_1 - \frac{\sigma_2^2 \bar{x}_1 + \sigma_1^2 \{\Delta + \bar{x}_2\}}{\sigma_1^2 + \sigma_2^2} \right]^2 + \left[\frac{\Delta - \{x_1 - \bar{x}_2\}}{\sqrt{\sigma_1^2 + \sigma_2^2}} \right]^2$$

Thus, after substitution and putting the integral above equal to

$$\frac{\sigma_1 \sigma_2}{\sqrt{\sigma_1^2 + \sigma_2^2}}$$

one finds that

$$P(\Delta) = \frac{1}{\sqrt{2\pi} \sqrt{\sigma_1^2 \sigma_2^2}} e^{-\frac{1}{2} \left[\frac{\Delta - \{\bar{x}_1 - \bar{x}_2\}}{\sqrt{\sigma_1^2 + \sigma_2^2}} \right]^2}$$

so that the probability of finding $x_1 - x_2 = \Delta$ is a normal distribution of standard deviate and mean given by

$$\sigma = \sqrt{\sigma_1^2 + \sigma_2^2}$$

$$\bar{\Delta} = \bar{x}_1 - \bar{x}_2$$

The situation is illustrated in Figure (38) where the magnitude of the subjective difference between the two stimuli x_1, x_2 is clearly the value of Δ for which $P(\Delta)$ is a maximum.

The difference $\bar{x}_1 - \bar{x}_2$ is thus given by the abscissa of Δ_{\max} on the curve of $P(\Delta)$. This coordinate is easily found from the method of pair-comparison. The totality of judgements that O_1 is better than O_2 ($\Delta = x_1 - x_2 > 0$) is equal to the area under the curve between $\Delta = 0$ and $\Delta = +\infty$. Conversely, the totality of judgements that O_2 is better than O_1 ($\Delta < 0$) is equal to the area under the curve between $\Delta = -\infty$ and $\Delta = 0$. Thus if X is the value of the variable of Δ in

$$\frac{1}{\sigma\sqrt{2\pi}} e^{-\frac{1}{2}\left[\frac{\Delta - \bar{\Delta}}{\sigma}\right]^2}$$

for which the preference ratio is R , then

$$R = \frac{\int_{-\infty}^X \frac{1}{\sigma\sqrt{2\pi}} e^{-\frac{1}{2}\left[\frac{\Delta - \bar{\Delta}}{\sigma}\right]^2} d\Delta}{\int_{-\infty}^{+\infty} \frac{1}{\sigma\sqrt{2\pi}} e^{-\frac{1}{2}\left[\frac{\Delta - \bar{\Delta}}{\sigma}\right]^2} d\Delta}$$

or

$$R = \int_{-\infty}^X \frac{1}{\sigma\sqrt{2\pi}} e^{-\frac{1}{2}\left[\frac{\Delta - \bar{\Delta}}{\sigma}\right]^2} d\Delta$$

and, therefore, X can be found by inverse interpolation from a table of the error function integral. This

value of X provides a scale-measure of the difference of the two stimuli, which is found directly from the preference ratio.

It will be seen now why the judgement "don't know" is excluded, for this is in a mathematical sense of measure zero, but would nevertheless be a too often preferred statement if this judgement were not excluded.

The difference in scale value for any two stimuli \underline{a} and \underline{b} is now defined to be

$$S_a - S_b = X_{ab} \sqrt{\sigma_a^2 + \sigma_b^2}$$

where X_{ab} is found, as described above, from a knowledge of the preference ratio. X_{ab} is the upper limit of the integral which makes the fraction of the area under the normal curve equal to the preference ratio; this upper limit is interpreted, in accordance with the above discussion, both in magnitude and sense, as the response difference between the two stimuli constituting the pair under comparison.

In our use of the above law we assume that there is no correlation between the two stimuli when they are being compared. This assumes that $r = 0$

in the more general formula

$$S_a - S_b = X_{ab} \sqrt{\sigma_a^2 + \sigma_b^2 - 2r\sigma_a\sigma_b}$$

where r is a correlation factor between individual discriminial dispersions during the same judgement. We further assume that $\sigma_a = \sigma_b$, which is reasonable in view of the close similarity of the two stimuli being compared. Inaccuracies in the scaling would result mostly from this latter assumption but, as we shall see, the errors are generally small. The law can now be stated as

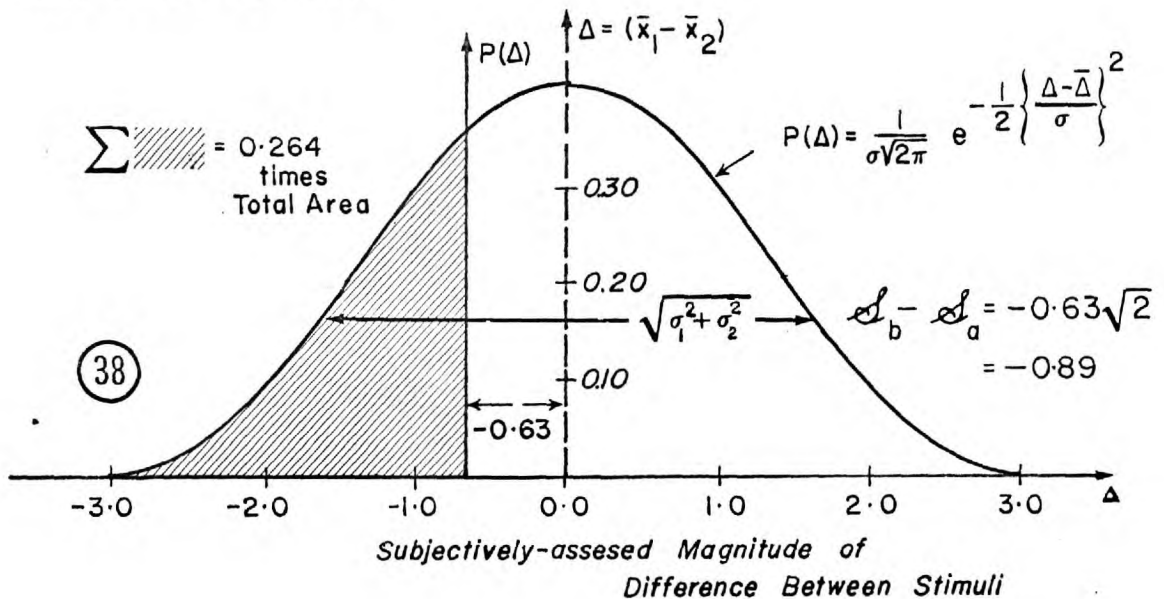
$$S_a - S_b = X_{ab} \sigma \sqrt{2} = S_d$$

or, if we use σ as the unit of scale

$$S_a - S_b = X_{ab} \sqrt{2} = S_d$$

From the judgement data for all of the observers, a preference ratio (the ratio of actual to possible number of times that one stimulus is judged better than the other) is thus computed for each pair. These ratios are arranged in a skew complementary matrix as shown in the following tables; the skew axis being the estimated 50% preference ratios which were not observed. The corresponding

observed response differences $\left[\frac{s_a - s_b}{\sqrt{2}} \right]$ are then obtained. Figure (38) illustrates an observed response difference of -0.89 , obtained from a preference ratio of 0.264 .



A second matrix, which is now skew symmetric is formed from these values of observed response difference. It should be noted that it has no elements shown in positions corresponding to zero or unity preference ratios. These missing elements are to be interpreted as response differences either too great or too small to be representable by finite standard normal deviates without an increase in the number of observers.

The occurrence of these "gaps" in the skew symmetric matrix are attributable to the fact that, if the number of stimuli cover (in terms of the responses which they evoke) a gamut which is large as compared to the discriminial unit, then many of the pairs will inevitably consist of stimuli which are so far apart that, unless the number of observers is made extremely large, no disagreement amongst observers occurs and hence no finite estimate of their scale separations can be made. For example, in order for the possibility to exist of detecting any finite standard normal deviate greater than 3.00 the number of observers would have to be at least 741.

The smallest number of finite response differences which can be used to scale n stimuli is, of course, $(n-1)$; the largest number of response differences which can result from n stimuli is $\frac{1}{2}n(n-1)$. If m , the number of pairs for which finite response differences are obtained, is such that

$$(n-1) \leq m < \frac{1}{2}n(n-1)$$

the response data are said to be incomplete, but

it will still be possible to compute the most probable values of response difference from the observed data. The data will be complete when $m = \frac{1}{2}n(n-1)$; in our case n , the number of stimuli, equals six.

The purpose in reducing the visibility of the slides by varying the intensity of the overlay previously mentioned was, then, really an effort to make the data more nearly complete in the above sense. For a Michelson visibility of 0.79 it was found that $m \approx 4$ and the data could not be used; for a visibility of 0.31, $m \approx 7$ making the data acceptable but doubtful. The value finally settled upon was such that with a visibility of 0.07 m was never less than 10 and often equaled 15, the value for the complete case.

Guildford (1936) has given a method of estimating the most probable response differences from the values obtained for the observed response differences. It is most effective when used with complete data, but it is of value still in the incomplete situation. In this method an $n \times (n-1)$ matrix is formed from the skew symmetric matrix of observed response differences by subtracting, element by element, each column of the latter from the column to

the left of it whenever such subtraction is possible. Each column of the $n \times (n-1)$ matrix, referred to as the 'basic response variations', then contains, in the complete case, n estimates, two direct and $(n-2)$ indirect, of the response differences between the two stimuli of one pair; one of the two direct estimates is usually regarded as redundant and is therefore not written.

The mean of the sum of each column times $\sqrt{2}$ is taken to be the best estimate of the response difference d_a between each pair. From these means a matrix of computed response differences is assembled and, then, a matrix of the corresponding computed preference ratios is computed. As a check on the reliability of the computed response differences the matrix of computed preference ratios is subtracted from the observed preference ratios matrix, element by element. Examination of this final difference matrix shows whether or not the computed response differences may be assumed to be valid.

This method assumes, of course, that the response differences between any pair of stimuli is both linear and additive as Thurstone points out in his original efforts to obtain a proper scale.

Morrissey (1955) points out that in Guildford's method a different set of $(n-1)$ column means used in computing the matrix of response differences will, in the incomplete case, be obtained from the differencing procedure if the order of the rows (and columns) in the skew symmetric observed response differences matrix is changed; in fact, there will be many separate sets of $(n-1)$ column means, corresponding to different permutations of the numbers 1 to \underline{n} . In the complete case these sets all correspond to one another and any one constitutes a unique set of basic response variations.

Morrissey goes on to suggest that a better estimate of the basic response variations could be made by making a least-squares solution such that the \underline{n} response values are chosen so as to minimize the sum of the squares of the \underline{m} differences between the \underline{m} observed response differences and the \underline{m} computed response differences. But in making this suggestion Morrissey seems to forget that since the probable error of each element in the observed response difference matrix is not linearly proportional to the value of the response difference itself, it is not

possible to directly compare the pooled observed and computed response difference values. He would have been more correct in suggesting a least-squares solution which minimized the sum of the squares of the m differences between the computed and observed preference ratios.

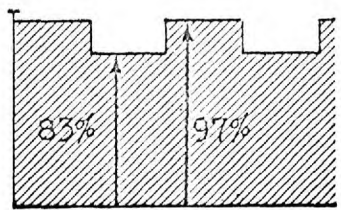
However, since Morrissey also fails to apply the necessary scaling factor of $\sqrt{2}$ to his computed response difference matrix his results are perpendicularly skew and produce larger apparent discrepancies between the observed and computed response differences than exist.

In any event, Guildford's differencing method has been applied in this work and, since most of the data sets are complete, it leads to very reasonable error values. Following the suggestion of Kettler (1957) any values of a difference between the observed and computed preference ratios greater than 0.080 is taken to be open to question; the value of 0.080 being four times the probable error of a discrepancy when the preference ratio is 0.750.

The following tables are the result of the observations of ten trained observers when they viewed

the above mentioned three sets of six slides at three separate distances. The Michelson visibility was held constant throughout the observations at 0.07.

COMA
 DISTANCE I
 10 x 2 OBSERVERS



$V = 0.07$

MATRIX OF OBSERVED PREFERENCE RATIOS:

	1	2	3	4	5	6
1	(0.500)	0.250	0.000	0.000	0.000	0.000
2	0.750	(0.500)	0.100	0.150	0.000	0.000
3	1.000	0.900	(0.500)	0.350	0.100	0.100
4	1.000	0.850	0.650	(0.500)	0.150	0.050
5	1.000	1.000	0.900	0.850	(0.500)	0.600
6	1.000	1.000	0.900	0.950	0.400	(0.500)

MATRIX OF OBSERVED RESPONSE DIFFERENCES

	1	2	3	4	5	6
1	0	-0.67	---	---	---	---
2	+0.67	0	-1.28	-1.04	---	---
3	---	+1.28	0	-0.39	-1.28	-1.28
4	---	+1.04	+0.39	0	-1.04	-1.65
5	---	---	+1.28	+1.04	0	+0.25
6	---	---	+1.28	+1.65	-0.25	0

CALCULATIONS OF FIVE BASIC RESPONSE VARIATIONS

	1-2	2-3	3-4	4-5	5-6
1	+0.67	---	---	---	---
2	---	+1.28	-0.24	---	---
3	---	---	+0.39	+0.89	0.00
4	---	+0.65	---	+1.04	+0.61
5	---	---	+0.24	---	-0.25
6	---	---	-0.37	+1.90	0.00
Σd	+0.67	+1.93	+0.26	+3.83	+0.36
M_d	+0.67	+0.97	+0.07	+1.28	+0.12
S_d	+0.95	+1.37	+0.10	+1.81	+0.17

COMPUTED RESPONSE DIFFERENCES

	1	2	3	4	5	6
1	0	-0.95	-2.32	-2.42	-4.23	-4.40
2	+0.95	0	-1.37	-1.47	-3.28	-3.45
3	+2.32	+1.37	0	-0.10	-1.91	-2.08
4	+2.42	+1.47	+0.10	0	-1.81	-1.98
5	+4.23	+3.28	+1.91	+1.81	0	-0.17
6	+4.40	+3.45	+2.08	+1.98	+0.17	0

COMPUTED PREFERENCE RATIOS:

	1	2	3	4	5	6
1	0.500	0.171	0.010	0.008	0.000	0.000
2	0.829	0.500	0.085	0.071	0.001	0.000
3	0.990	0.915	0.500	0.460	0.028	0.019
4	0.992	0.929	0.540	0.500	0.035	0.024
5	1.000	0.999	0.972	0.965	0.500	0.432
6	1.000	1.000	0.981	0.976	0.568	0.500

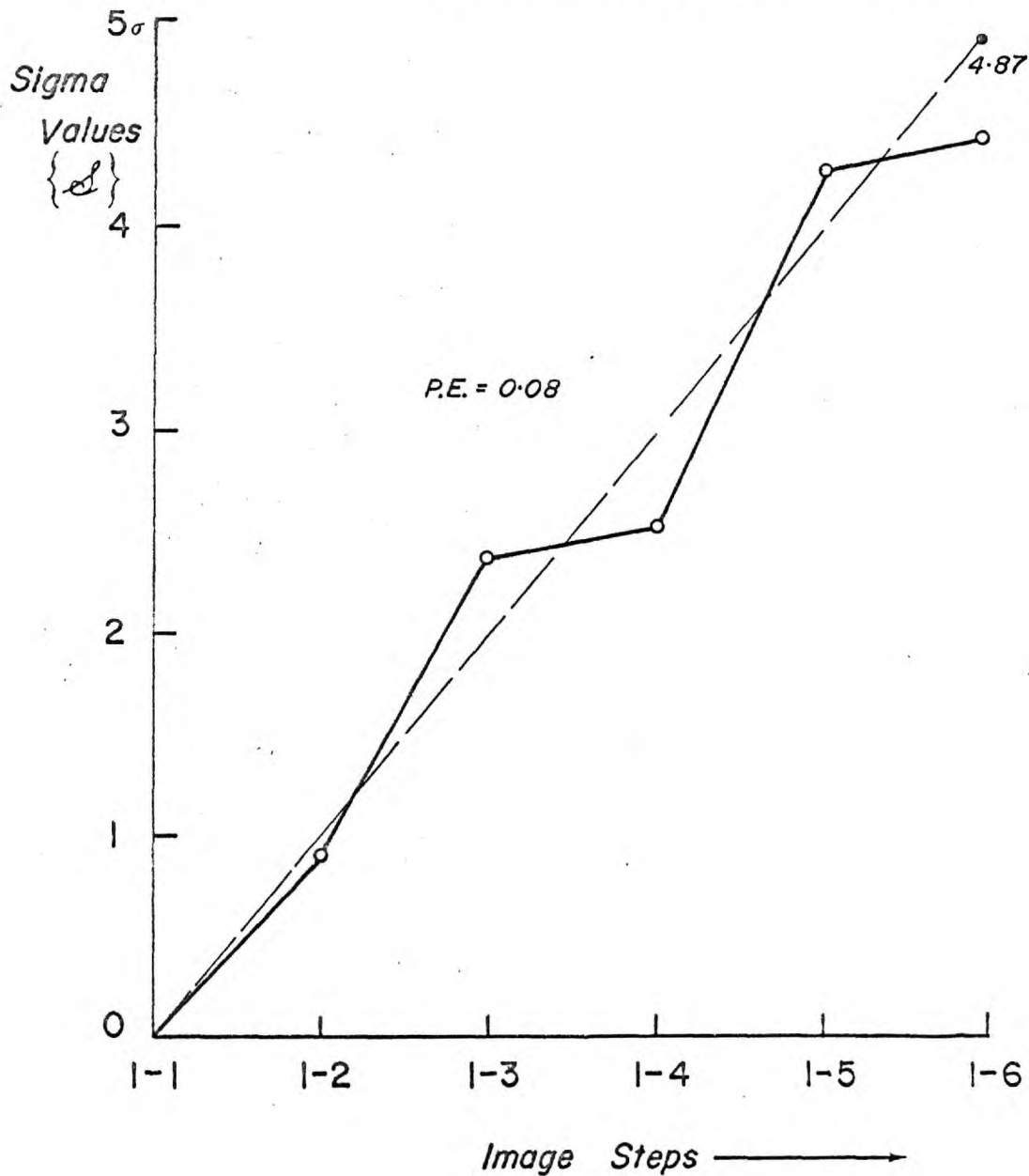
OBSERVED MINUS COMPUTED PREFERENCE RATIOS

	1	2	3	4	5	6
1	0.000	0.079	-0.010	-0.008	0.000	0.000
2	-0.079	0	0.015	0.079	-0.001	0.000
3	0.010	-0.015	0	-0.110	0.062	0.081
4	0.008	-0.079	0.110	0	0.115	0.026
5	0.000	0.001	-0.072	-0.115	0	0.168
6	0.000	0.000	-0.081	-0.026	-0.168	0
$\sum d$	-0.061	-0.014	-0.048	0.080	0.008	0.275
M_d	-0.010	-0.002	-0.008	-0.013	0.001	0.046
$M_d(2)^{-\frac{1}{2}}$	-0.007	-0.002	-0.006	-0.009	0.001	0.032

$$\sum M_d(2)^{-\frac{1}{2}} = 0.009$$

$$\text{Mean Error} = 0.002$$

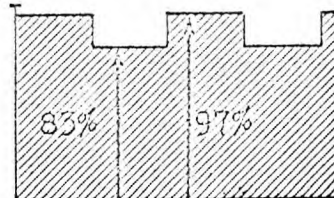
COMA DISTANCE I
WITH MEAN LINE APPROXIMATION



(39)

Unit $\{\sigma\}$ = 86% Preference Ratio

COMA
 DISTANCE II
 10 x 2 OBSERVERS



$$V = 0.07$$

MATRIX OF OBSERVED PREFERENCE RATIOS:

	1	2	3	4	5	6
1	(0.500)	0.300	0.200	0.050	0.050	0.150
2	0.700	(0.500)	0.400	0.400	0.250	0.000
3	0.800	0.600	(0.500)	0.500	0.150	0.350
4	0.950	0.600	0.500	(0.500)	0.200	0.300
5	0.950	0.750	0.850	0.800	(0.500)	0.650
6	0.850	1.000	0.650	0.700	0.350	(0.500)

MATRIX OF OBSERVED RESPONSE DIFFERENCES

	1	2	3	4	5	6
1	0	-0.52	-0.84	-1.65	-1.65	-1.04
2	+0.52	0	-0.25	-0.25	-0.67	---
3	+0.84	+0.25	0	0.00	-1.04	-0.39
4	+1.65	+0.25	0.00	0	-0.84	-0.52
5	+1.65	+0.67	+1.04	+0.84	0	+0.39
6	+1.04	---	+0.39	+0.52	-0.39	0

CALCULATIONS OF FIVE BASIC RESPONSE VARIATIONS:

	1-2	2-3	3-4	4-5	5-6
1	+0.52	+0.32	+0.81	0.00	-0.61
2	---	+0.25	0.00	+0.42	---
3	+0.59	---	0.00	+1.04	-0.65
4	+1.40	+0.25	---	+0.84	-0.32
5	+0.98	-0.37	+0.20	---	-0.39
6	---	---	-0.13	+0.91	---
Σd	+3.09	+0.45	+0.88	+3.21	-1.97
M_d	+0.77	+0.11	+0.18	+0.64	-0.39
S_d	+1.09	+0.16	+0.25	+0.91	-0.56

COMPUTED RESPONSE DIFFERENCES

	1	2	3	4	5	6
1	0	-1.09	-1.23	-1.50	-2.41	-1.85
2	+1.90	0	-0.16	-0.36	-1.27	-0.71
3	+1.25	+0.16	0	-0.25	-1.16	-0.60
4	+1.56	+0.36	+0.25	0	-0.91	-0.35
5	+2.41	+1.27	+1.16	+0.91	0	+0.56
6	+1.85	+0.71	+0.60	+0.35	-0.56	0

COMPUTED PREFERENCE RATIOS

	1	2	3	4	5	6
1	0.500	0.138	0.106	0.067	0.008	0.031
2	0.862	0.500	0.436	0.359	0.002	0.239
3	0.894	0.564	0.500	0.401	0.123	0.274
4	0.933	0.641	0.599	0.500	0.181	0.363
5	0.992	0.998	0.877	0.819	0.500	0.712
6	0.969	0.761	0.726	0.637	0.288	0.500

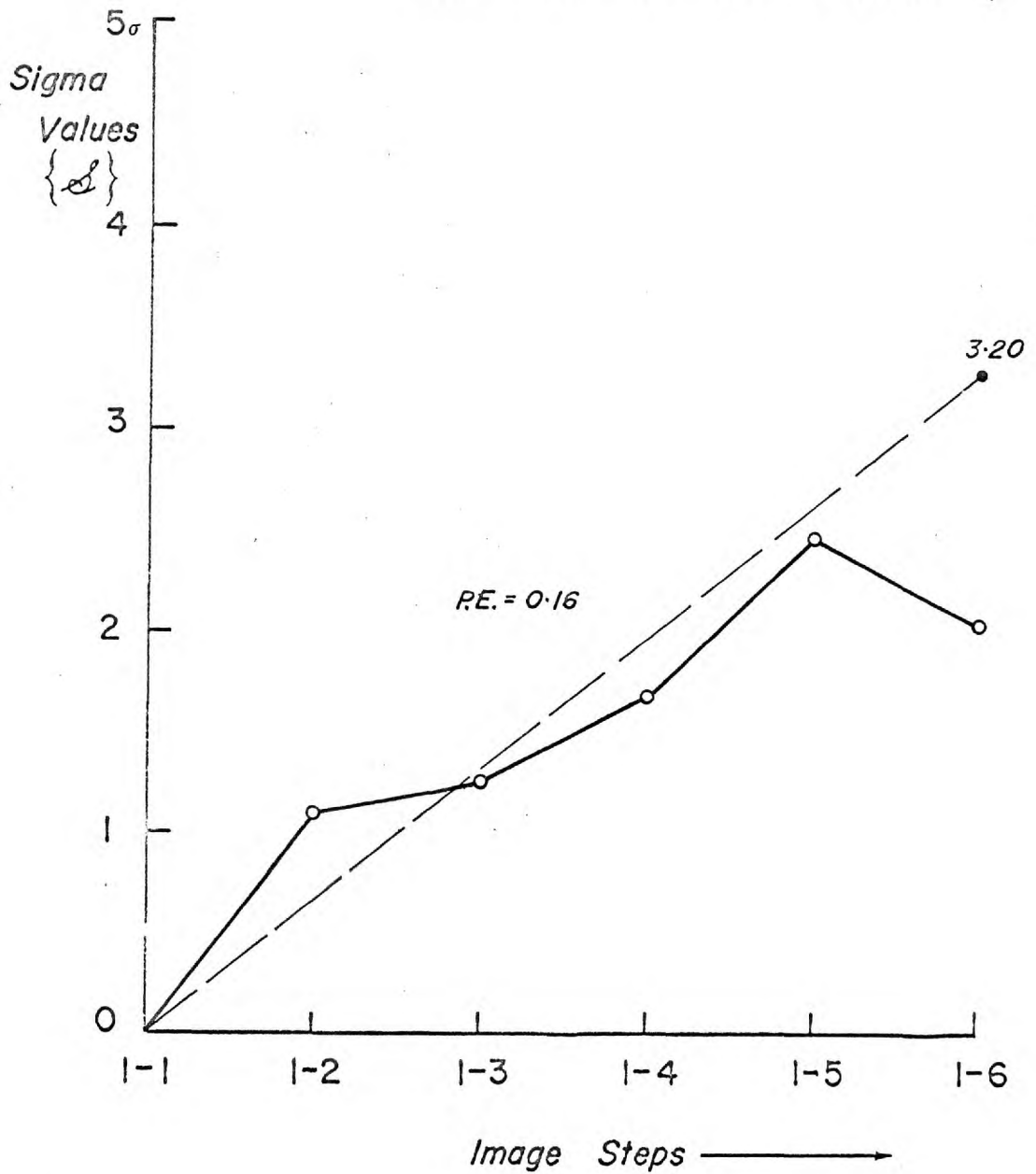
OBSERVED MINUS COMPUTED PREFERENCE RATIOS

	1	2	3	4	5	6
1	0	0.162	0.094	-0.017	0.042	0.119
2	-0.162	0	-0.036	0.041	0.248	0.239
3	-0.094	0.036	0	0.099	0.027	0.076
4	0.017	-0.041	-0.099	0	0.019	-0.063
5	-0.042	-0.248	-0.027	-0.019	0	-0.062
6	-0.119	0.239	-0.076	0.063	0.062	0
$\sum d$	-0.447	0.148	-0.144	0.167	0.338	0.309
M_d	-0.075	0.025	-0.024	0.028	0.056	0.051
$M_d(2)^{-\frac{1}{2}}$	-0.053	0.017	-0.017	0.020	0.040	0.036

$$\sum M_d(2)^{-\frac{1}{2}} = 0.043$$

$$\text{Mean Error} = 0.007$$

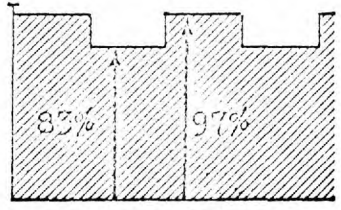
COMA DISTANCE II
WITH MEAN LINE APPROXIMATION



(40)

Unit { σ } = 86% Preference Ratio

COMA
 DISTANCE III
 10 x 2 OBSERVERS



V = 0.07

MATRIX OF OBSERVED PREFERENCE RATIOS:

	1	2	3	4	5	6
1	(0.500)	0.300	0.150	0.200	0.150	0.100
2	0.700	(0.500)	0.200	0.300	0.100	0.150
3	0.850	0.800	(0.500)	0.550	0.200	0.250
4	0.800	0.700	0.450	(0.500)	0.450	0.250
5	0.850	0.900	0.800	0.550	(0.500)	0.450
6	0.900	0.850	0.750	0.750	0.550	(0.500)

MATRIX OF OBSERVED RESPONSE DIFFERENCES:

	1	2	3	4	5	6
1	0	-0.52	-1.04	-0.84	-1.04	-1.28
2	+0.52	0	-0.84	-0.52	-1.28	-1.04
3	+1.04	+0.84	0	+0.12	-0.84	-0.67
4	+0.84	+0.52	-0.12	0	-0.12	-0.67
5	+1.04	+1.28	+0.84	+0.12	0	-0.12
6	+1.28	+1.04	+0.67	+0.67	+0.12	0

CALCULATIONS OF FIVE BASIC RESPONSE VARIATIONS:

	1-2	2-3	3-4	4-5	5-6
1	+0.52	+0.52	-0.20	+0.20	+0.24
2	---	+0.84	-0.32	+0.76	-0.24
3	+0.20	---	-0.12	+0.96	-0.17
4	+0.32	+0.64	---	+0.12	+0.55
5	-0.24	+0.44	+0.72	---	+0.12
6	+0.24	+0.37	0.00	+0.55	---
Σd	+1.04	+2.81	+0.06	+2.59	+0.50
M_d	+0.21	+0.56	+0.01	+0.52	+0.10
S_d	+0.30	+0.79	+0.01	+0.73	+0.14

COMPUTED RESPONSE DIFFERENCES

	1	2	3	4	5	6
1	0	-0.30	-1.09	-1.10	-1.83	-1.97
2	+0.30	0	-0.79	-0.80	-1.53	-1.67
3	+1.09	+0.79	0	-0.01	-0.74	-0.88
4	+1.10	+0.80	+0.01	0	-0.73	-0.87
5	+1.83	+1.53	+0.74	+0.73	0	-0.14
6	+1.97	+1.67	+0.88	+0.87	+0.14	0

COMPUTED PREFERENCE RATIOS:

	1	2	3	4	5	6
1	0.500	0.382	0.138	0.136	0.034	0.024
2	0.618	0.500	0.215	0.212	0.063	0.047
3	0.862	0.785	0.500	0.496	0.230	0.189
4	0.864	0.788	0.504	0.500	0.433	0.192
5	0.966	0.937	0.770	0.567	0.500	0.444
6	0.976	0.953	0.811	0.808	0.556	0.500

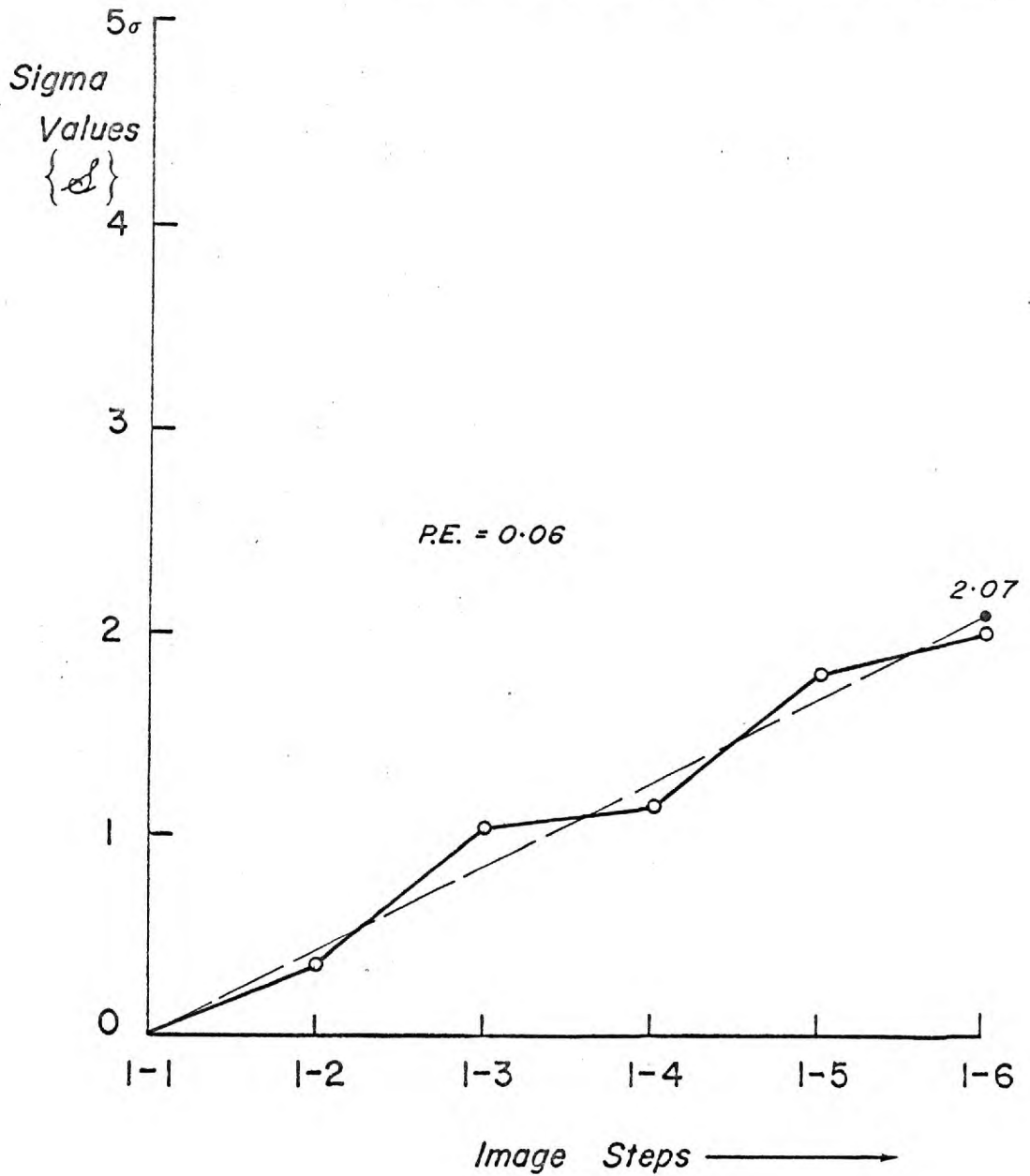
OBSERVED MINUS COMPUTED PREFERENCE RATIOS

	1	2	3	4	5	6
1	0	-0.082	0.012	0.064	0.116	0.076
2	0.082	0	-0.015	0.088	0.037	0.103
3	-0.012	0.015	0	0.054	-0.030	0.061
4	-0.064	-0.088	-0.054	0	0.017	0.058
5	-0.116	-0.037	0.030	-0.017	0	0.006
6	-0.076	-0.103	-0.061	-0.058	-0.006	0
$\sum d$	-0.180	-0.310	-0.088	0.131	0.134	0.304
M_d	-0.026	-0.050	-0.014	0.022	0.022	0.051
$M_d(2)^{-\frac{1}{2}}$	-0.018	-0.030	-0.010	0.015	0.016	0.036

$$\sum M_d(2)^{-\frac{1}{2}} = 0.009$$

$$\text{Mean Error} = 0.002$$

COMA DISTANCE III
WITH MEAN LINE APPROXIMATION

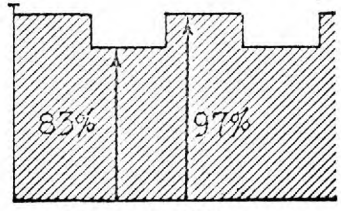


(41)

Unit { σ } = 86% Preference Ratio

-
-
-
-
-

GAUSSIAN
 DISTANCE I
 10 x 2 OBSERVERS



MATRIX OF OBSERVED PREFERENCE RATIOS:

	1	2	3	4	5	6
1	(0.500)	0.050	0.050	0.100	0.000	0.000
2	0.950	(0.500)	0.350	0.300	0.000	0.050
3	0.950	0.650	(0.500)	0.450	0.000	0.150
4	0.900	0.700	0.550	(0.500)	0.100	0.050
5	1.000	1.000	1.000	0.900	(0.500)	0.600
6	1.000	0.950	0.850	0.950	0.400	(0.500)

MATRIX OF OBSERVED RESPONSE DIFFERENCES

	1	2	3	4	5	6
1	0	-1.65	-1.65	-1.28	---	---
2	+1.65	0	-0.39	-0.52	---	-1.65
3	+1.65	+0.39	0	-0.13	---	-1.04
4	+1.28	+0.52	+0.13	0	-1.28	-1.65
5	---	---	---	+1.28	0	+0.25
6	---	+1.65	+1.04	+1.65	-0.25	0

CALCULATIONS OF FIVE BASIC RESPONSE VARIATIONS

	1-2	2-3	3-4	4-5	5-6
1	+1.65	0.00	-0.37	---	---
2	---	+0.39	+0.13	---	---
3	+0.26	---	+0.13	---	---
4	+0.76	+0.39	---	+1.28	+0.37
5	---	---	---	---	-0.25
6	---	+0.61	-0.61	+1.90	---
Σa	+2.67	+1.39	-0.52	+3.18	+0.12
M_d	+0.92	+0.35	-0.13	+1.59	+0.06
S_d	+1.30	+0.49	-0.18	+2.25	+0.09

COMPUTED RESPONSE DIFFERENCES

	1	2	3	4	5	6
1	0	-1.30	-1.89	-1.71	-3.96	-4.05
2	+1.30	0	-0.49	-0.31	-2.56	-2.65
3	+1.89	+0.49	0	+0.18	-2.07	-2.16
4	+1.71	+0.31	-0.18	0	-2.25	-2.34
5	+3.96	+2.56	+2.07	+2.25	0	-0.09
6	+4.05	+2.65	+2.16	+2.34	+0.09	0

COMPUTED PREFERENCE RATIOS

	1	2	3	4	5	6
1	0.500	0.097	0.029	0.044	0.000	0.000
2	0.903	0.500	0.312	0.378	0.005	0.004
3	0.971	0.688	0.500	0.571	0.019	0.015
4	0.956	0.622	0.429	0.500	0.012	0.010
5	1.000	0.995	0.981	0.988	0.500	0.464
6	1.000	0.996	0.985	0.990	0.536	0.500

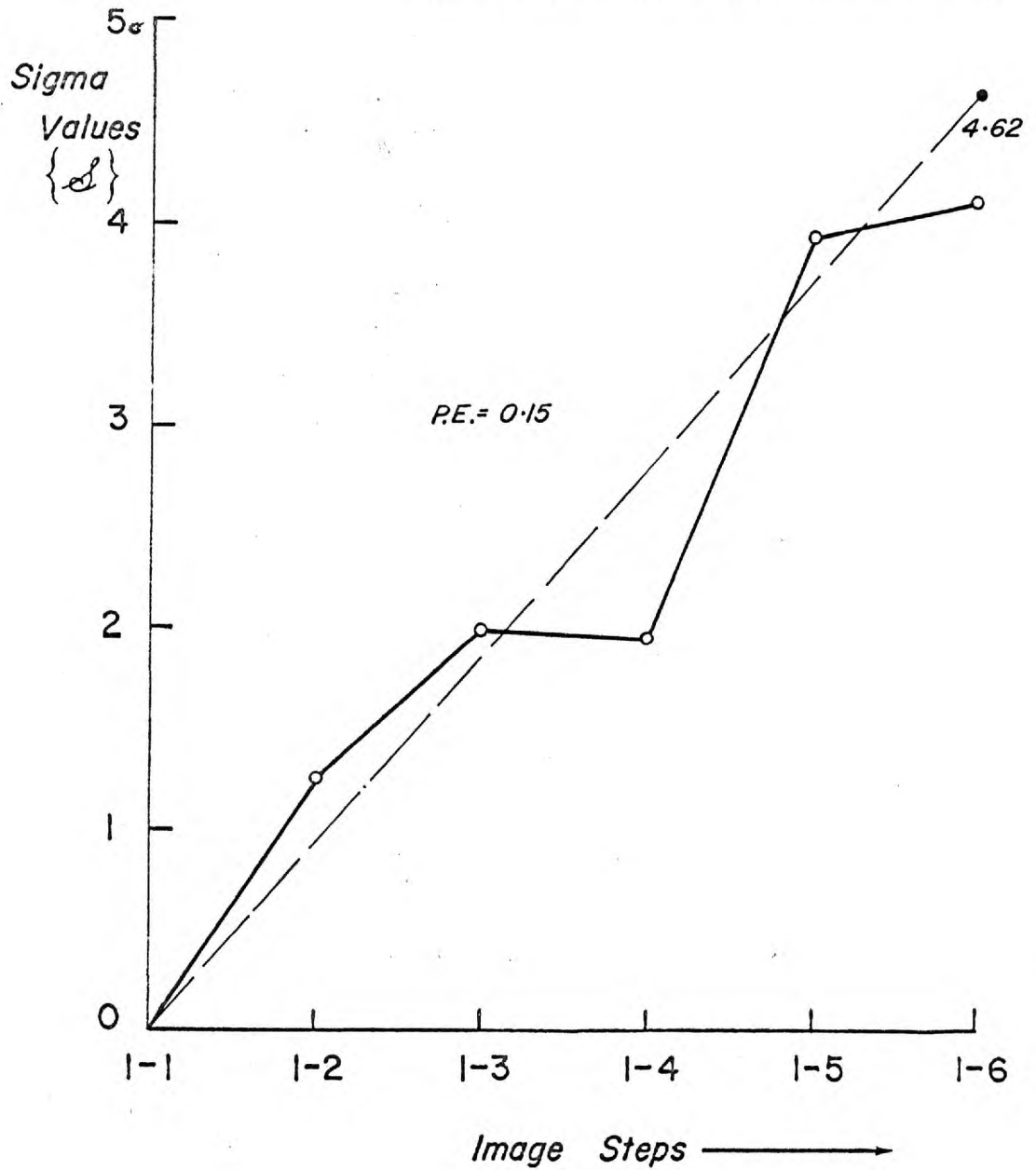
OBSERVED MINUS COMPUTED PREFERENCE RATIOS

	1	2	3	4	5	6
1	0	-0.047	0.021	0.056	0.000	0.000
2	0.047	0	0.038	-0.078	-0.005	0.046
3	-0.021	-0.038	0	-0.121	-0.019	0.135
4	-0.056	0.078	0.121	0	0.088	0.040
5	0.000	0.005	0.019	-0.088	0	0.136
6	0.000	-0.046	-0.135	-0.040	-0.136	0
$\sum d$	0.030	-0.048	0.064	0.271	-0.160	0.357
M_d	0.005	-0.008	0.011	0.045	-0.026	0.060
$M_d(2)^{-\frac{1}{2}}$	0.004	-0.006	0.008	0.032	-0.019	0.042

$$\sum M_d(2)^{-\frac{1}{2}} = 0.016$$

$$\text{Mean Error} = 0.001$$

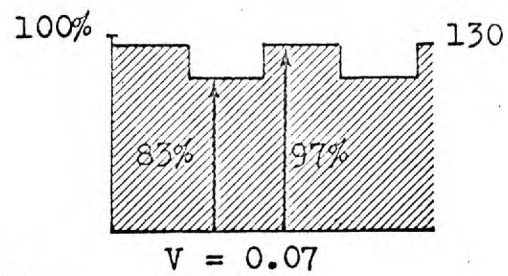
GAUSSIAN DISTANCE I
WITH MEAN LINE APPROXIMATION



(42)

Unit $\{\sigma\}$ = 86% Preference Ratio

□
 □ GAUSSIAN
 □ DISTANCE II
 □ 10 x 2 OBSERVERS
 □



MATRIX OF OBSERVED PREFERENCE RATIOS:

	1	2	3	4	5	6
1	(0.500)	0.050	0.100	0.050	0.150	0.000
2	0.950	(0.500)	0.200	0.350	0.250	0.200
3	0.900	0.800	(0.500)	0.500	0.300	0.250
4	0.950	0.650	0.500	(0.500)	0.300	0.300
5	0.850	0.750	0.700	0.700	(0.500)	0.450
6	1.000	0.800	0.750	0.700	0.550	(0.500)

MATRIX OF OBSERVED RESPONSE DIFFERENCES

	1	2	3	4	5	6
1	0	-1.65	-1.28	-1.65	-1.04	---
2	+1.65	0	-0.84	-0.39	-0.67	-0.84
3	+1.28	+0.84	0	0.00	-0.53	-0.68
4	+1.65	+0.39	0.00	0	-0.52	-0.52
5	+1.04	+0.67	+0.53	+0.52	0	-0.13
6	---	+0.84	+0.68	+0.52	+0.13	0

CALCULATIONS OF FIVE BASIC RESPONSE VARIATIONS:

	1-2	2-3	3-4	4-5	5-6
1	+1.65	-0.37	+0.37	-0.61	---
2	---	+0.84	-0.49	+0.28	+0.17
3	+0.44	---	0.00	+0.53	+0.15
4	+1.26	+0.39	---	+0.52	0.00
5	+0.37	+0.14	+0.01	---	+0.13
6	---	+0.16	+0.16	+0.39	---
Σd	+3.72	+1.16	+0.05	+1.11	+0.45
M_d	+0.93	+0.23	+0.01	+0.22	+0.11
S_d	+1.32	+0.32	+0.01	+0.31	+0.15

COMPUTED RESPONSE DIFFERENCES

	1	2	3	4	5	6
1	0	-1.32	-1.64	-1.65	-1.96	-2.11
2	+1.32	0	-0.32	-0.33	-0.64	-0.79
3	+1.64	+0.32	0	-0.01	-0.34	-0.49
4	+1.65	+0.33	+0.01	0	-0.31	-0.46
5	+1.96	+0.64	+0.34	+0.31	0	-0.15
6	+2.11	+0.79	+0.49	+0.46	+0.15	0

COMPUTED PREFERENCE RATIOS

	1	2	3	4	5	6
1	0.500	0.093	0.050	0.049	0.025	0.017
2	0.907	0.500	0.374	0.371	0.261	0.215
3	0.950	0.626	0.500	0.496	0.367	0.312
4	0.951	0.629	0.504	0.500	0.378	0.323
5	0.975	0.739	0.633	0.622	0.500	0.440
6	0.983	0.785	0.688	0.677	0.560	0.500

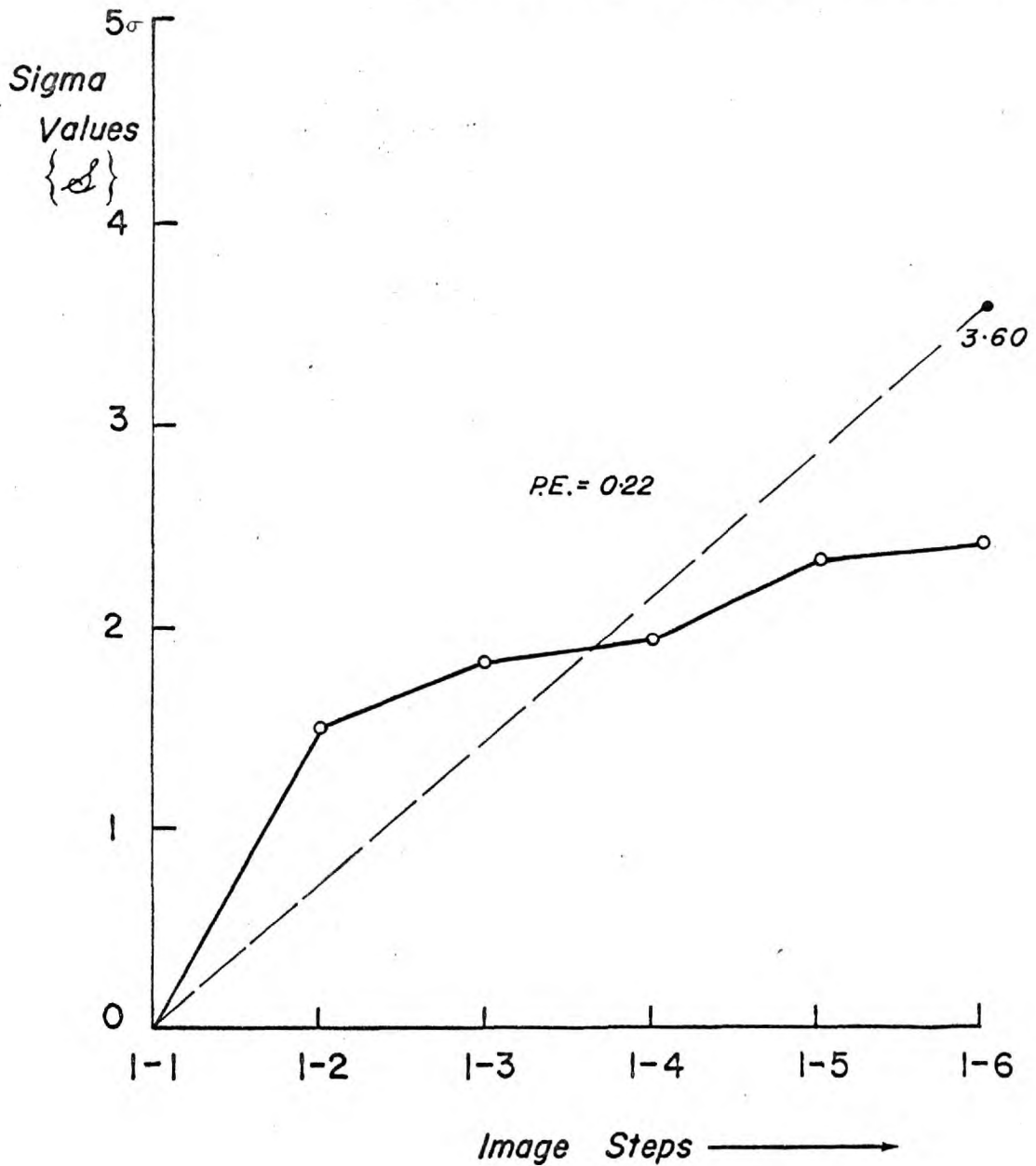
OBSERVED MINUS COMPUTED PREFERENCE RATIOS

	1	2	3	4	5	6
1	0	-0.043	0.050	0.001	0.125	-0.017
2	0.043	0	-0.174	-0.021	-0.011	-0.015
3	-0.050	0.174	0	0.004	-0.067	-0.062
4	-0.001	0.021	-0.004	0	-0.078	-0.023
5	0.125	0.011	0.067	0.078	0	0.010
6	0.017	0.015	0.062	0.023	-0.010	0
$\sum d$	0.134	0.178	0.001	0.085	-0.041	-0.107
M_d	0.057	0.030	0.000	0.014	-0.007	-0.018
$M_d(2)^{-\frac{1}{2}}$	0.040	0.021	0.000	0.010	-0.005	-0.013

$$\sum M_d(2)^{-\frac{1}{2}} = 0.053$$

$$\text{Mean Error} = 0.009$$

GAUSSIAN DISTANCE II
WITH MEAN LINE APPROXIMATION

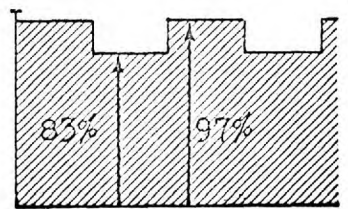


(43)

Unit {d} = 86% Preference Ratio

-
-
-
-
-
-

GAUSSIAN
 DISTANCE III
 10 x 2 OBSERVERS:



V = 0.07

MATRIX OF OBSERVED PREFERENCE RATIOS:

	1	2	3	4	5	6
1	(0.500)	0.200	0.150	0.250	0.100	0.100
2	0.800	(0.500)	0.350	0.400	0.300	0.250
3	0.850	0.650	(0.500)	0.200	0.350	0.400
4	0.750	0.600	0.800	(0.500)	0.300	0.250
5	0.900	0.700	0.650	0.700	(0.500)	0.550
6	0.900	0.750	0.600	0.750	0.450	(0.500)

MATRIX OF OBSERVED RESPONSE DIFFERENCES

	1	2	3	4	5	6
1	0	-0.84	-1.04	-0.67	-1.28	-1.28
2	+0.84	0	-0.39	-0.25	-0.52	-0.67
3	+1.04	+0.39	0	-0.84	-0.39	-0.25
4	+0.67	+0.25	+0.84	0	-0.52	-0.67
5	+1.28	+0.52	+0.39	+0.52	0	+0.13
6	+1.28	+0.67	+0.25	+0.67	-0.13	0

CALCULATIONS OF FIVE BASIC RESPONSE VARIATIONS:

	1-2	2-3	3-4	4-5	5-6
1	+0.84	+0.20	-0.37	+0.61	0.00
2	---	+0.39	-0.14	+0.27	+0.15
3	+0.65	---	+0.84	-0.45	-0.14
4	+0.42	-0.59	---	+0.52	+0.15
5	+0.76	+0.13	-0.13	---	-0.13
6	+0.61	+0.42	-0.42	+0.80	---
Σa	+2.86	+1.05	-0.22	+2.20	+0.03
M_a	+0.57	+0.21	-0.04	+0.44	+0.01
S_a	+0.81	+0.30	-0.06	+0.61	+0.01

COMPUTED RESPONSE DIFFERENCES

	1	2	3	4	5	6
1	0	-0.81	-1.01	-0.95	-1.56	-1.57
2	+0.81	0	-0.30	-0.24	-0.85	-0.86
3	+1.01	+0.30	0	+0.06	-0.55	-0.56
4	+0.95	+0.24	-0.06	0	-0.61	-0.62
5	+1.56	+0.85	+0.55	+0.61	0	-0.01
6	+1.57	+0.86	+0.56	+0.62	+0.01	0

COMPUTED PREFERENCE RATIOS:

	1	2	3	4	5	6
1	0.500	0.209	0.156	0.171	0.059	0.058
2	0.791	0.500	0.382	0.405	0.198	0.195
3	0.844	0.618	0.500	0.524	0.291	0.288
4	0.829	0.595	0.476	0.500	0.271	0.268
5	0.941	0.802	0.709	0.729	0.500	0.496
6	0.942	0.805	0.712	0.732	0.504	0.500

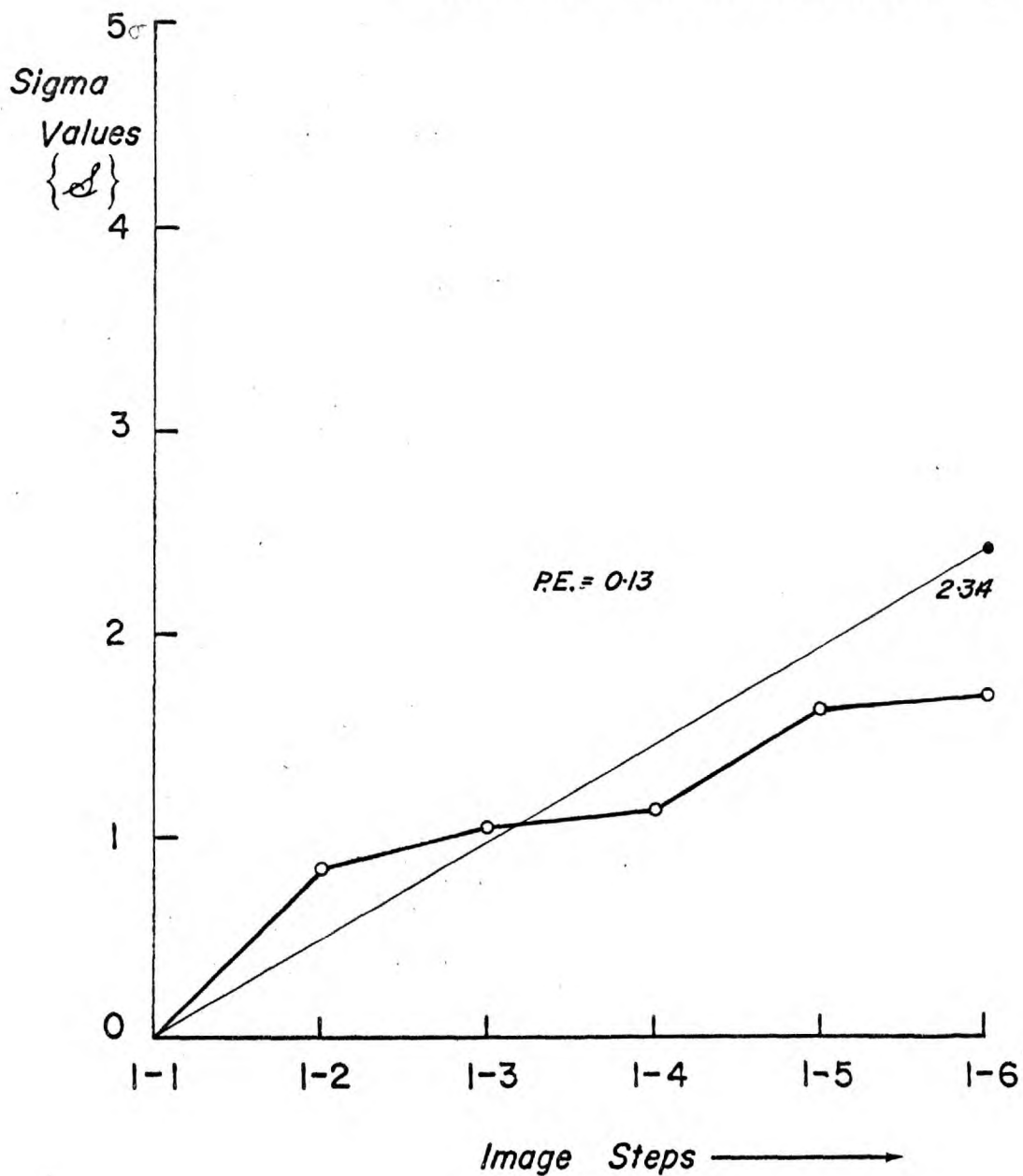
OBSERVED MINUS COMPUTED PREFERENCE RATIOS

	1	2	3	4	5	6
1	0	-0.009	-0.006	0.079	0.041	0.042
2	0.009	0	-0.032	-0.005	0.102	0.055
3	0.006	0.032	0	-0.324	0.059	0.112
4	-0.079	0.005	0.324	0	0.029	-0.018
5	-0.041	-0.102	-0.059	-0.029	0	0.054
6	-0.042	-0.055	-0.112	0.018	-0.054	0.500
$\sum d$	-0.147	-0.129	0.115	-0.261	0.177	0.245
M_d	-0.025	-0.022	0.019	-0.043	0.029	0.041
$M_d(2)^{-\frac{1}{2}}$	-0.017	-0.015	0.014	-0.031	0.021	0.029

$$\sum M_d(2)^{-\frac{1}{2}} = 0.001$$

$$\text{Mean Error} = 0.000$$

GAUSSIAN DISTANCE III
WITH MEAN LINE APPROXIMATION

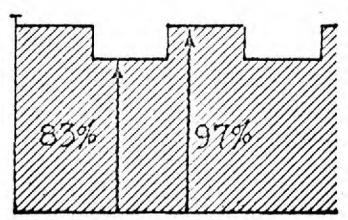


(44)

Unit $\{d\} = 86\%$ Preference Ratio

-
-
-
-
-

SPHERICAL
DISTANCE I
10 x 2 OBSERVERS



$V = 0.07$

MATRIX OF OBSERVED PREFERENCE RATIOS:

	1	2	3	4	5	6
1	(0.500)	0.100	0.050	0.050	0.000	0.000
2	0.900	(0.500)	0.100	0.000	0.000	0.000
3	0.950	0.900	(0.500)	0.150	0.000	0.000
4	0.950	1.000	0.850	(0.500)	0.250	0.150
5	1.000	1.000	1.000	0.750	(0.500)	0.400
6	1.000	1.000	1.000	0.850	0.600	(0.500)

MATRIX OF OBSERVED RESPONSE DIFFERENCES

	1	2	3	4	5	6
1	0	-1.28	-1.64	-1.64	---	---
2	+1.28	0	-1.28	---	---	---
3	+1.64	+1.28	0	-1.04	---	---
4	+1.64	---	+1.04	0	-0.67	-1.04
5	---	---	---	+0.67	0	-0.25
6	---	---	---	+1.04	+0.25	0

CALCULATIONS OF FIVE BASIC RESPONSE VARIATIONS

	1-2	2-3	3-4	4-5	5-6
1	+1.28	+0.36	0.00	---	---
2	---	+1.28	---	---	---
3	+0.36	---	+1.04	---	---
4	---	---	---	+0.67	+0.37
5	---	---	---	---	+0.25
6	---	---	---	+0.79	---
Σd	+1.64	+1.64	+1.04	+1.46	+0.62
M_d	+0.82	+0.82	+0.52	+0.73	+0.31
S_d	+1.17	+1.17	+0.74	+1.05	+0.44

COMPUTED RESPONSE DIFFERENCES

	1	2	3	4	5	6
1	0	-1.17	-2.34	-3.08	-4.13	-4.57
2	+1.17	0	-1.17	-1.91	-2.96	-3.40
3	+2.34	+1.17	0	-0.74	-1.79	-2.23
4	+3.08	+1.91	+0.74	0	-1.05	-1.49
5	+4.13	+2.96	+1.79	+1.05	0	-0.44
6	+4.57	+3.40	+2.23	+1.49	+0.44	0

COMPUTED PREFERENCE RATIOS

	1	2	3	4	5	6
1	0.500	0.121	0.010	0.001	0.000	0.000
2	0.879	0.500	0.121	0.028	0.001	0.000
3	0.990	0.879	0.500	0.230	0.037	0.013
4	0.999	0.972	0.770	0.500	0.147	0.068
5	1.000	0.999	0.963	0.853	0.500	0.330
6	1.000	1.000	0.987	0.932	0.760	0.500

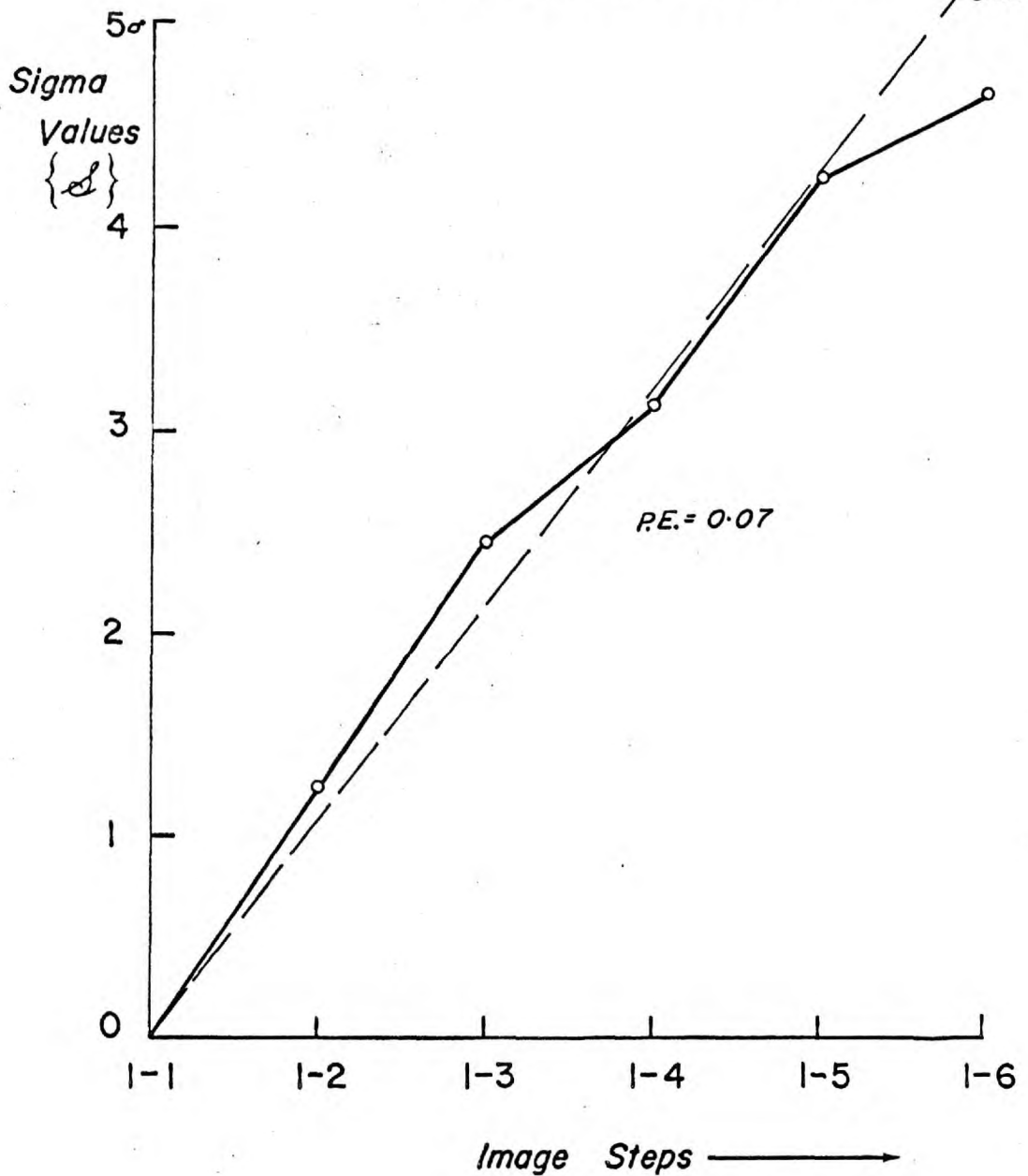
OBSERVED MINUS COMPUTED PREFERENCE RATIOS

	1	2	3	4	5	6
1	0	-0.021	0.040	0.049	0.000	0.000
2	0.021	0	-0.021	-0.028	-0.001	0.000
3	-0.040	-0.021	0	-0.080	-0.037	-0.013
4	-0.049	0.028	0.080	0	0.103	0.082
5	0.000	0.001	0.037	-0.103	0	0.070
6	0.000	0.000	0.013	-0.082	-0.070	0
$\sum d$	-0.068	-0.013	0.159	-0.244	-0.008	0.139
M_d	-0.011	-0.022	0.026	-0.040	-0.001	0.023
$M_d(2)^{-\frac{1}{2}}$	-0.008	-0.015	0.018	-0.028	0.000	0.016

$$\sum M_d(2)^{-\frac{1}{2}} = -0.017$$

$$\text{Mean Error} = -0.003$$

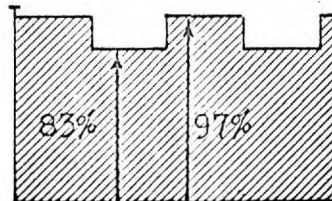
SPHERICAL DISTANCE I
WITH MEAN LINE APPROXIMATION



(45)

Unit $\{\sigma\}$ = 86% Preference Ratio

□
 □ SPHERICAL
 □ DISTANCE II
 □ 10 x 2 OBSERVERS
 □



$$V = 0.07$$

MATRIX OF OBSERVED PREFERENCE RATIOS:

	1	2	3	4	5	6
1	(0.500)	0.250	0.200	0.050	0.050	0.100
2	0.750	(0.500)	0.250	0.150	0.100	0.100
3	0.800	0.750	(0.500)	0.200	0.200	0.200
4	0.950	0.850	0.800	(0.500)	0.350	0.350
5	0.950	0.900	0.800	0.650	(0.500)	0.450
6	0.900	0.900	0.800	0.650	0.550	(0.500)

MATRIX OF OBSERVED RESPONSE DIFFERENCES

	1	2	3	4	5	6
1	0	-0.68	-0.84	-1.65	-1.65	-1.28
2	+0.68	0	-0.68	-1.04	-1.28	-1.28
3	+0.84	+0.68	0	-0.84	-0.84	-0.84
4	+1.65	+1.04	+0.84	0	-0.39	-0.39
5	+1.65	+1.28	+0.84	+0.39	0	-0.13
6	+1.28	+1.28	+0.84	+0.39	+0.13	0

CALCULATIONS OF FIVE BASIC RESPONSE VARIATIONS

	1-2	2-3	3-4	4-5	5-6
1	+0.68	+0.16	+0.81	0.00	-0.31
2	---	+0.68	+0.36	+0.24	0.00
3	+0.16	---	+0.84	0.00	0.00
4	+0.61	+0.20	---	+0.39	0.00
5	+0.37	+0.44	+0.45	---	+0.13
6	0.00	+0.44	+0.45	+0.26	---
Σd	+1.82	+1.92	+2.91	+0.89	-0.18
M_d	+0.36	+0.38	+0.58	+0.18	-0.04
S_d	+0.51	+0.54	+0.82	+0.25	-0.06

COMPUTED RESPONSE DIFFERENCES

	1	2	3	4	5	6
1	0	-0.51	-1.05	-1.87	-2.12	-2.06
2	+0.51	0	-0.54	-1.36	-1.61	-1.55
3	+1.05	+0.54	0	-0.82	-1.07	-1.01
4	+1.87	+1.36	+0.82	0	-0.25	-0.19
5	+2.12	+1.61	+1.07	+0.25	0	+0.06
6	+2.06	+1.55	+1.01	+0.19	-0.06	0

COMPUTED PREFERENCE RATIOS

	1	2	3	4	5	6
1	0.500	0.308	0.167	0.031	0.017	0.020
2	0.692	0.500	0.295	0.087	0.054	0.061
3	0.853	0.705	0.500	0.206	0.142	0.156
4	0.969	0.913	0.794	0.500	0.401	0.425
5	0.983	0.946	0.858	0.599	0.500	0.524
6	0.980	0.939	0.844	0.575	0.476	0.500

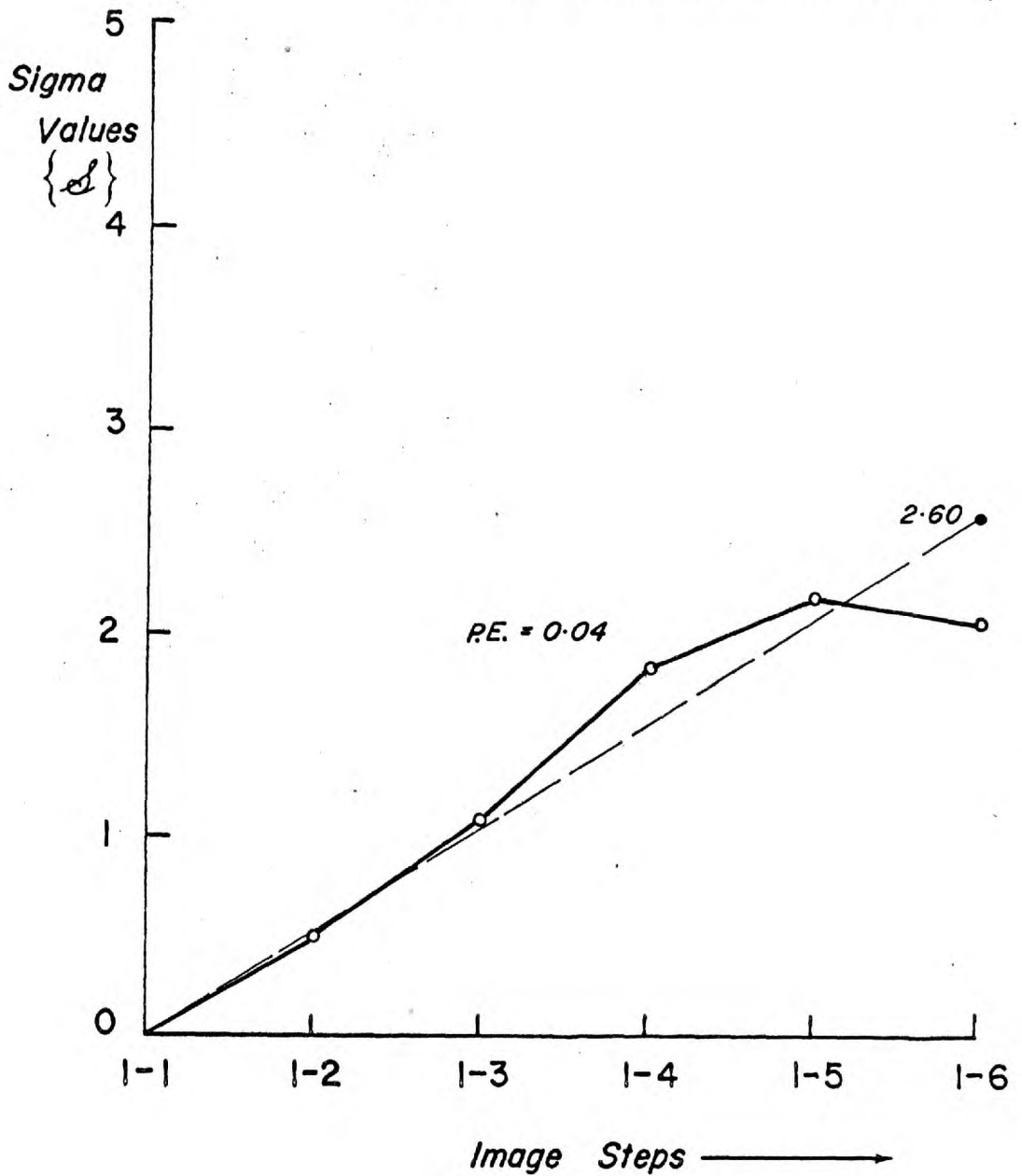
OBSERVED MINUS COMPUTED PREFERENCE RATIOS

	1	2	3	4	5	6
1	0	-0.058	0.033	0.019	0.033	0.080
2	0.058	0	-0.045	0.063	0.046	0.034
3	-0.033	0.045	0	-0.006	0.058	0.044
4	-0.019	-0.063	0.006	0	-0.051	-0.075
5	-0.033	-0.046	-0.058	0.051	0	-0.074
6	-0.080	-0.039	-0.044	0.075	0.074	0
$\sum d$	-0.107	-0.161	-0.120	0.202	0.140	0.009
M_d	-0.018	-0.027	-0.020	0.034	0.023	0.002
$M_d(2)^{-\frac{1}{2}}$	-0.012	-0.019	-0.014	0.024	0.016	0.001

$$\sum M_d(2)^{-\frac{1}{2}} = 0.004$$

$$\text{Mean Error} = 0.001$$

SPHERICAL DISTANCE II
WITH MEAN LINE APPROXIMATION

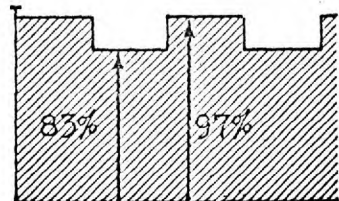


(46)

Unit {d} = 86% Preference Ratio

□
□
□
□
□

SPHERICAL
DISTANCE III
10 x 2 OBSERVERS



$V = 0.07$

MATRIX OF OBSERVED PREFERENCE RATIOS:

	1	2	3	4	5	6
1	(0.500)	0.300	0.250	0.150	0.200	0.050
2	0.700	(0.500)	0.350	0.250	0.250	0.150
3	0.750	0.650	(0.500)	0.250	0.200	0.350
4	0.850	0.750	0.750	(0.500)	0.300	0.350
5	0.800	0.750	0.800	0.700	(0.500)	0.650
6	0.950	0.850	0.650	0.650	0.350	(0.500)

MATRIX OF OBSERVED RESPONSE DIFFERENCES:

	1	2	3	4	5	6
1	0	-0.52	-0.68	-1.04	-0.84	-1.65
2	+0.52	0	-0.39	-0.68	-0.67	-1.04
3	+0.68	+0.39	0	-0.67	-0.84	-0.39
4	+1.04	+0.68	+0.67	0	-0.52	-0.39
5	+0.84	+0.67	+0.84	+0.52	0	+0.39
6	+1.65	+1.04	+0.39	+0.39	-0.39	0

CALCULATIONS OF FIVE BASIC RESPONSE VARIATIONS:

	1-2	2-3	3-4	4-5	5-6
1	+0.52	+0.16	+0.36	-0.20	+0.81
2	---	+0.39	+0.29	-0.01	+0.37
3	+0.29	---	+0.67	+0.17	-0.45
4	+0.36	+0.01	---	+0.52	-0.13
5	+0.17	-0.17	+0.32	---	-0.39
6	+0.61	+0.65	0.00	+0.78	---
Σd	+1.95	+1.44	+1.64	+1.24	+0.21
M_d	+0.38	+0.29	+0.33	+0.25	+0.04
S_d	+0.54	+0.41	+0.47	+0.35	+0.06

COMPUTED RESPONSE DIFFERENCES

	1	2	3	4	5	6
1	0	-0.54	-0.91	-1.38	-1.73	-1.80
2	+0.54	0	-0.41	-0.88	-1.23	-1.27
3	+0.91	+0.41	0	-0.47	-0.82	-0.88
4	+1.38	+0.88	+0.47	0	-0.35	-0.41
5	+1.73	+1.23	+0.82	+0.35	0	-0.06
6	+1.80	+1.27	+0.88	+0.41	+0.06	0

COMPUTED PREFERENCE RATIOS

	1	2	3	4	5	6
1	0.500	0.295	0.181	0.084	0.042	0.036
2	0.705	0.500	0.341	0.189	0.109	0.102
3	0.819	0.659	0.500	0.319	0.203	0.189
4	0.916	0.811	0.681	0.500	0.363	0.341
5	0.958	0.891	0.797	0.637	0.500	0.476
6	0.964	0.898	0.811	0.659	0.524	0.500

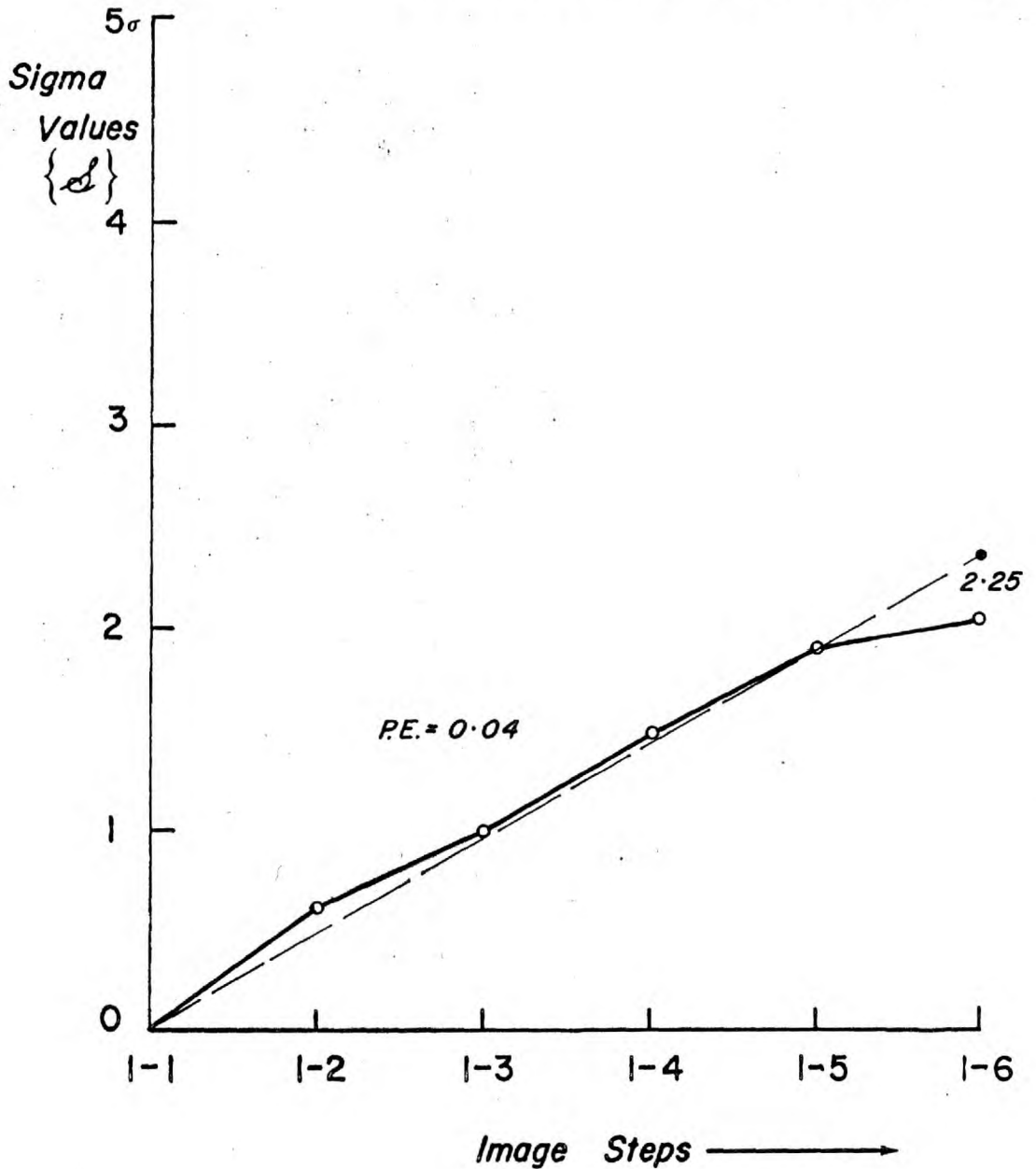
OBSERVED MINUS COMPUTED PREFERENCE RATIOS

	1	2	3	4	5	6
1	0	0.005	0.069	0.066	0.158	0.014
2	-0.005	0	0.009	0.061	0.141	0.048
3	-0.069	-0.009	0	-0.069	-0.003	0.161
4	-0.066	-0.061	0.069	0	-0.063	0.009
5	-0.158	-0.141	0.003	0.063	0	0.174
6	-0.014	-0.048	-0.161	-0.009	-0.174	0
$\sum d$	-0.312	-0.254	-0.031	0.112	0.059	0.406
M_d	-0.052	-0.042	-0.005	0.019	0.010	0.068
$M_d(2)^{-\frac{1}{2}}$	-0.037	-0.030	-0.004	0.013	0.007	0.048

$$\sum M_d(2)^{-\frac{1}{2}} = 0.003$$

$$\text{Mean Error} = 0.001$$

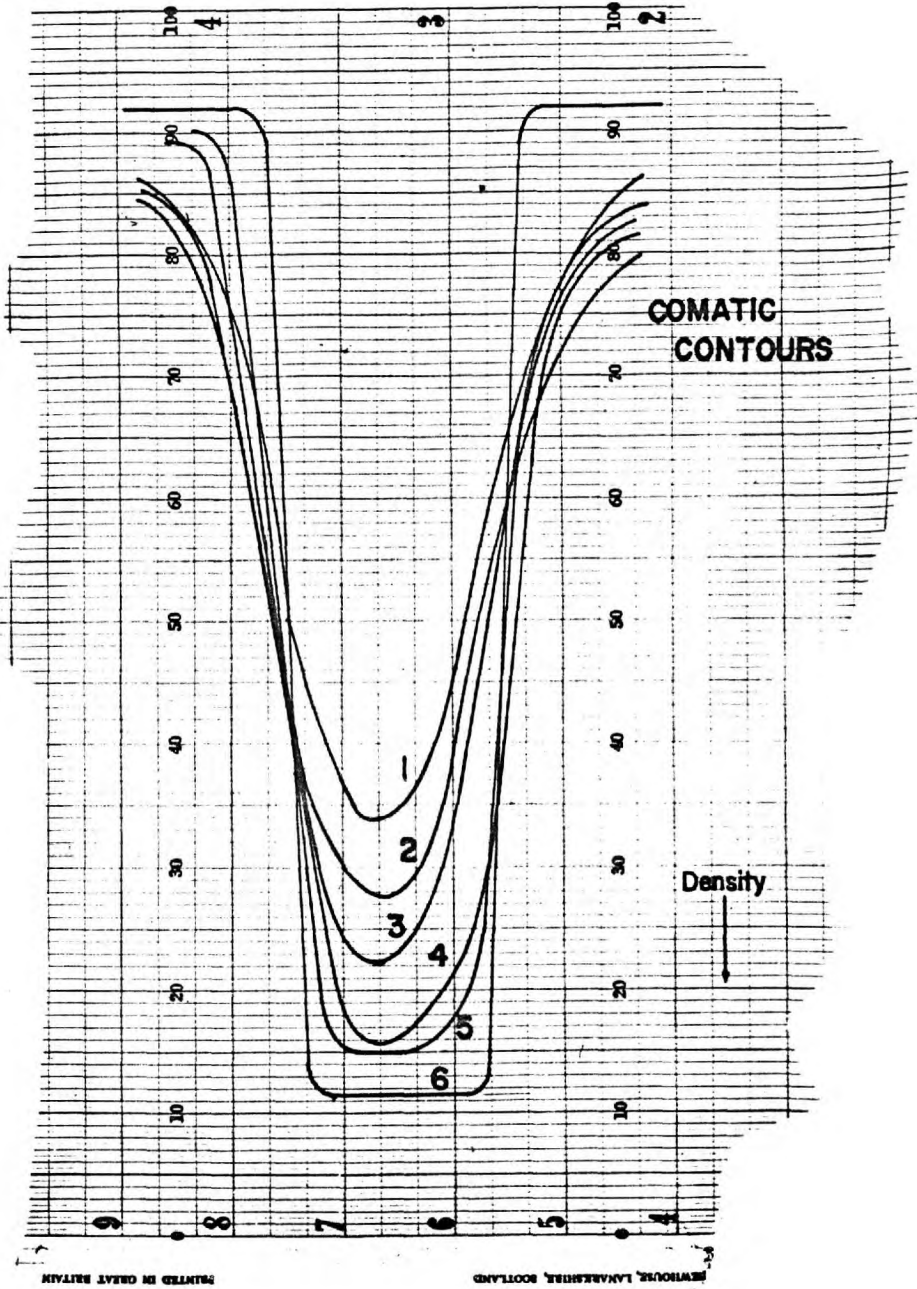
SPHERICAL DISTANCE III
WITH MEAN LINE APPROXIMATION



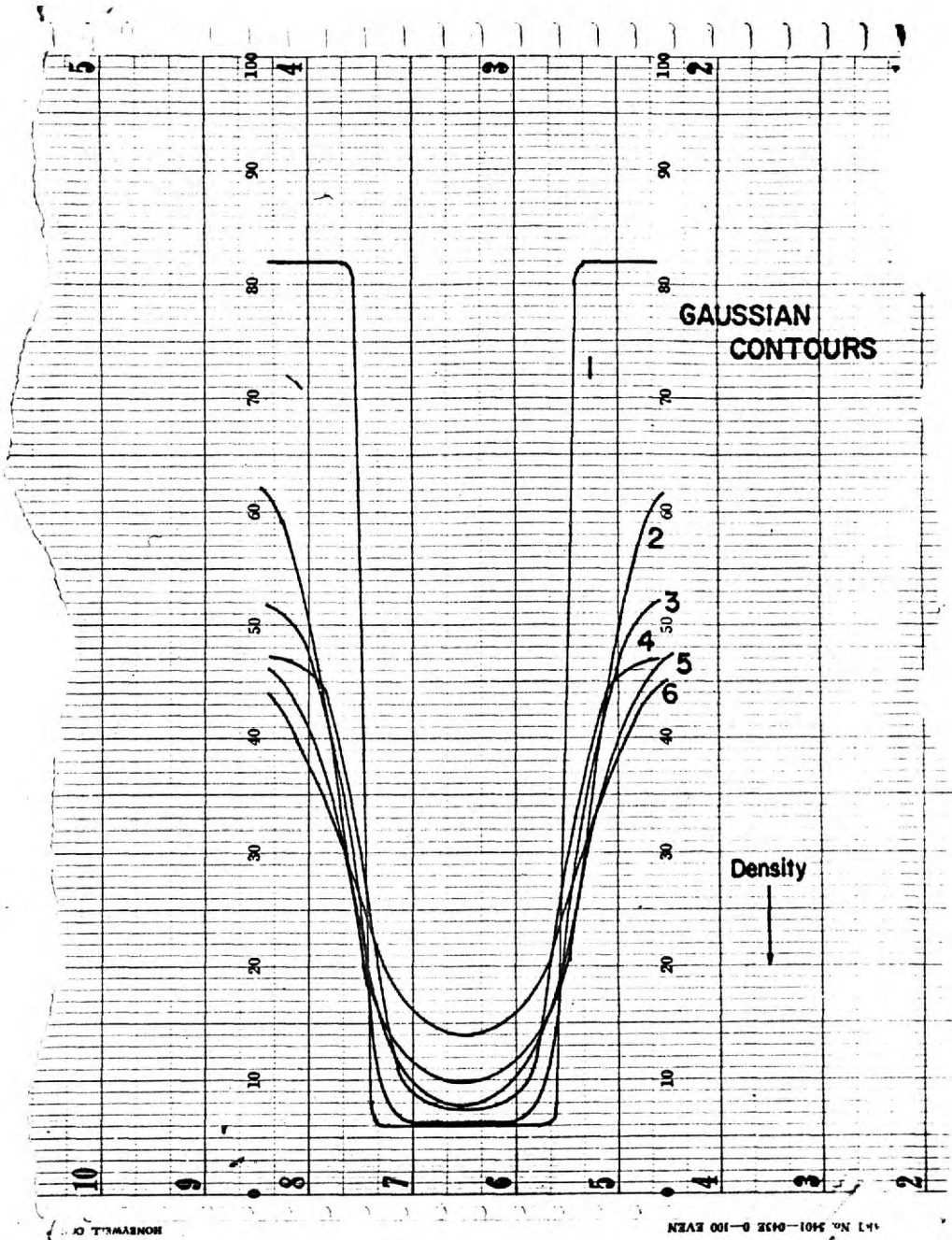
(47)

Unit {d} = 86% Preference Ratio

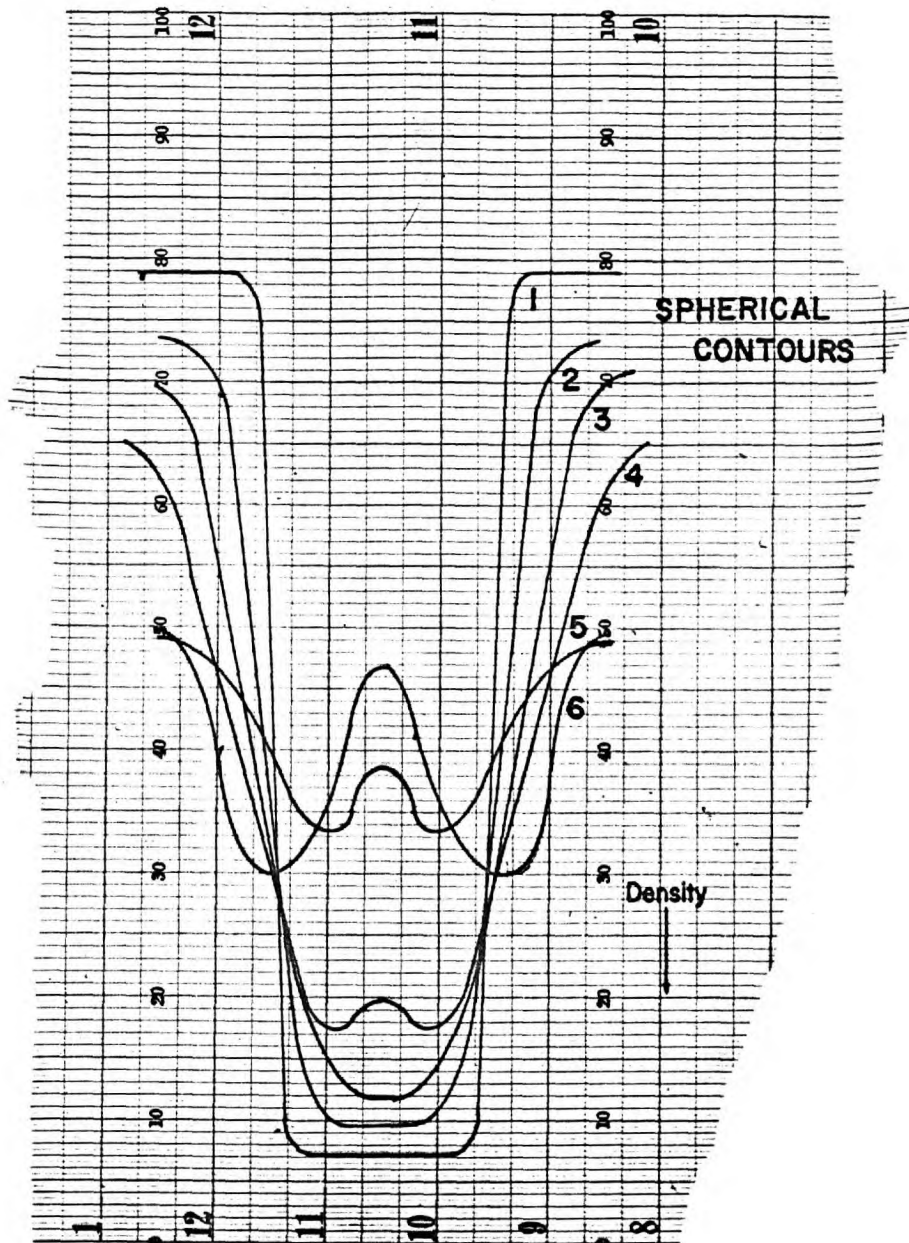
Microdensitometer Traces of One Period From Each Slide



Microdensitometer Traces of One Period From Each Slide




Microdensitometer Traces of One Period From Each Slide



PRINTED IN GREAT BRITAIN

GLEN, SCOTLAND

REFERENCES

- Guildford, J.P. (1936) Psychometric Methods, McGraw-Hill Book Co., pp. 207-378.
- Ilford Ltd. (1959) "Technical Information Handbook", Ilford Limited.
- Kettler, R.B. (1957) unpublished work
- Morrissey, J.H. (1955) J.O.S.A., 45, 373-378.
- Thurstone, L.L. (1927) Am. J. Psychol., 38, 368-389.
- 

CHAPTER IVRelating Visual and Instrumental Concepts
of Quality

FOURIER TRANSFORMS OF TEST SLIDES

The Fourier transform of any extended but finite two-dimensional area will be the convolution of the transforms of the basic function and its boundary function. While the previously described equipment is being used to obtain the transforms of grating-like objects it is useful to consider the effects of the boundary function on the interpretability of the final data; if the boundary function is such that large side-bands are produced beside the grating peaks it may become difficult visually to differentiate between the harmonics that we wish to measure and these side-band effects.

The least complicated or confusing spread function which is readily produced is a Gaussian distribution and, since the transform of a Gaussian distribution is itself a Gaussian distribution, this shape will be a suitable boundary for grating-like objects. Since we are obtaining only a one-dimensional transform

of these objects, a mask with a Gaussian shape, inserted at the fringe plane of the instrument, will be sufficient to eliminate any later difficulties in data reduction.

The size of this limiting aperture, as seen by the slide under test, was about $5/8$ " across the peak. The choice of size was somewhat arbitrary, being limited on the one hand by the signal-to-noise ratio of the equipment and on the other hand by a residual curvature of the fringe pattern (the effect of which we wished to minimize).

As a test run, to check the reproducibility and accuracy of the instrument, the transforms of a sharp, equal-spaced square-wave pattern were obtained. The spacing of this pattern was about eleven lines per inch. The values of the modulus of this transformation were found to be reproducible to within 2% and the values of amplitude were all within 3% of the calculated values through to the 7th harmonic. Noise level and signal stability at both full and zero modulation were better than 2% at all times. These values were felt to be adequate and useable.

The transforms of the eighteen slides used in the subjective evaluation tests were then obtained.

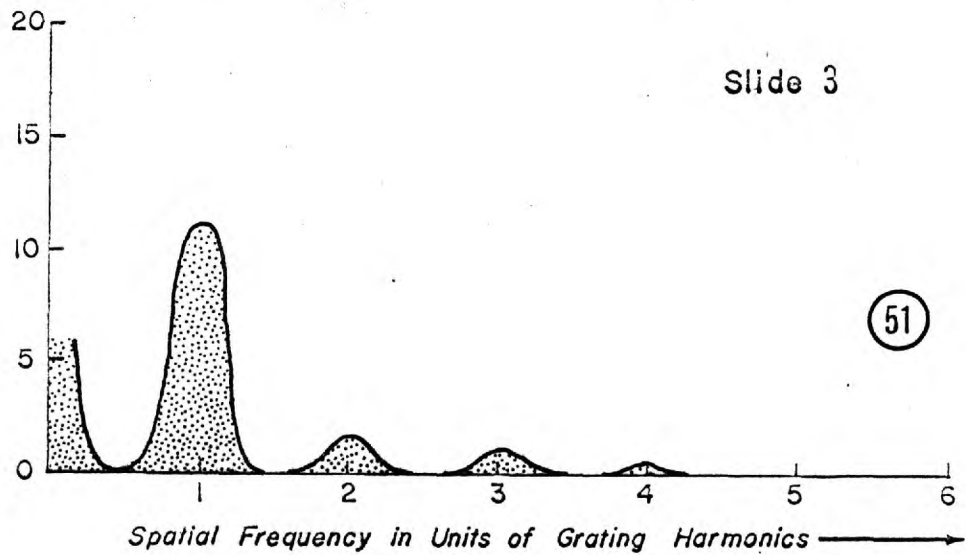
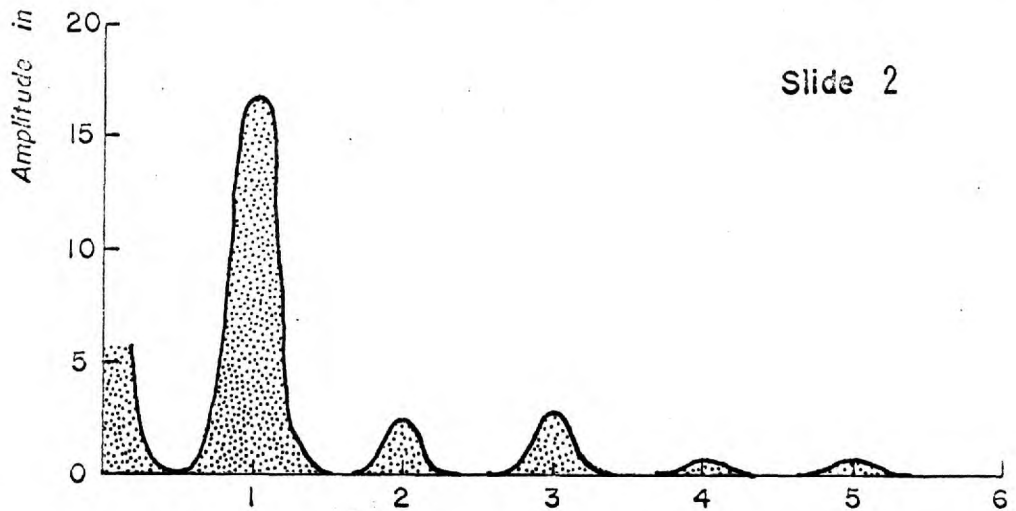
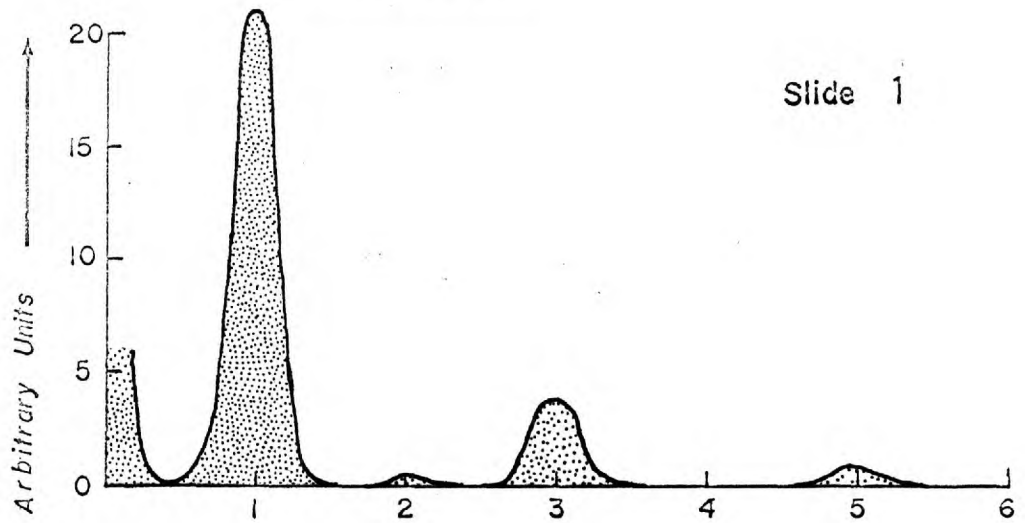
The following procedure was found to be useful and is noted here for future reference.

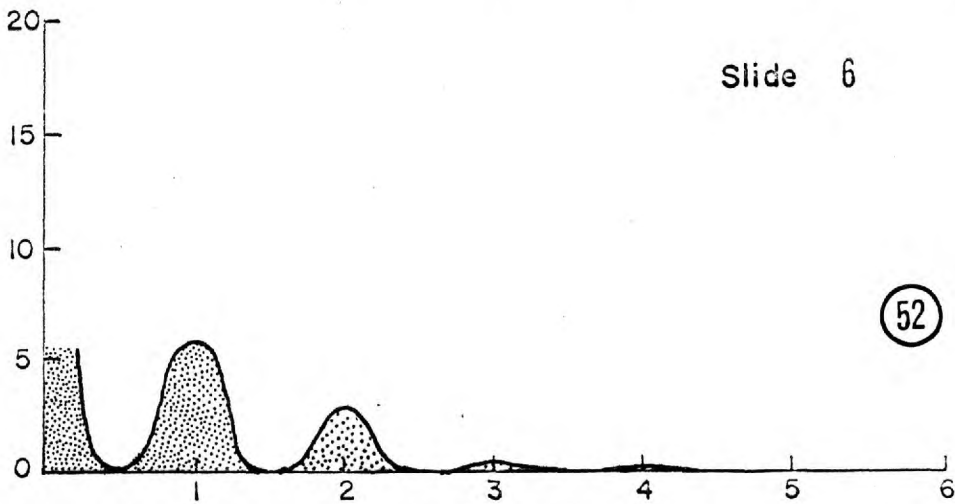
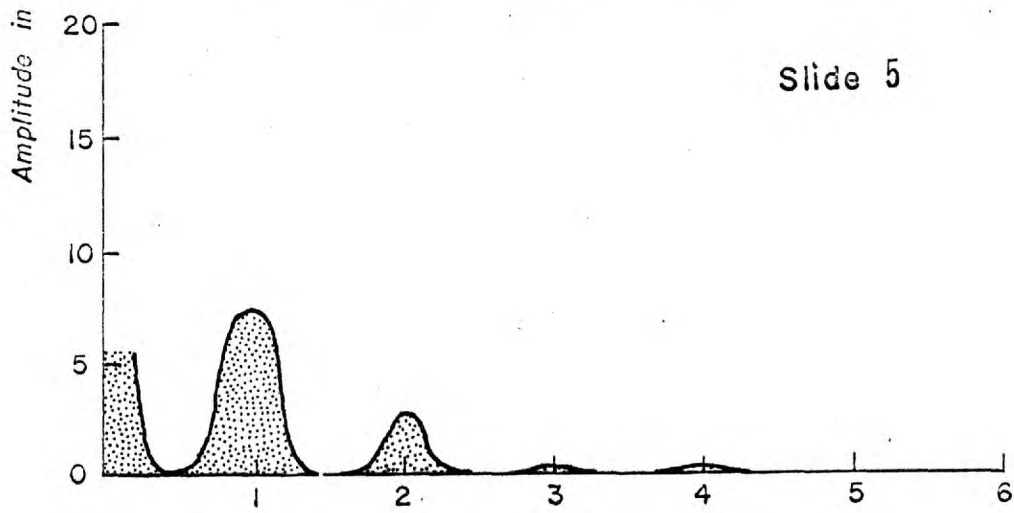
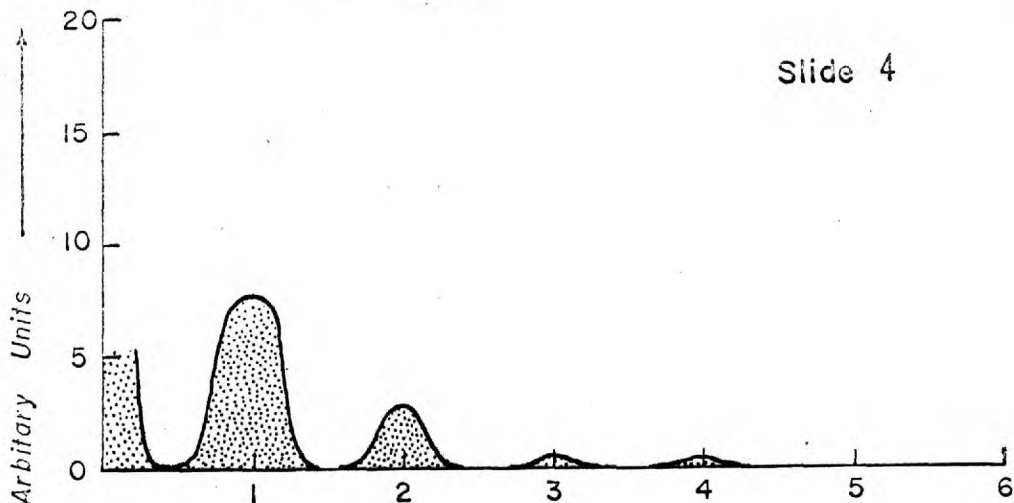
1. A one hour warm-up period was allowed on all the equipment.
2. Knob ① was pulled out (producing full modulation) and the reading was adjusted to nearly full scale and then noted.
3. Knob ① was pushed back. The amplifier was then reduced in attenuation by 4db and a scan was made.
4. Step 2 was repeated for the complimentary transform (with Knob ② pulled out) and the full-scale reading was adjusted to the previous reading.
5. Step 3 was repeated to obtain the complementary transform (with Knob ② still pulled out).

This procedure eliminates any variation in scale introduced by the insertion of the quarter-wave plate and keeps a continual check on the instrument's stability. It is important also that the slides being tested are kept in the same orientation with one another. All readings were repeated twice in these observations.

The following curves [Figures (51), (52), (53), (54), (55) and (56)] are the smoothed values of the root-mean-square sums of the sine and cosine transforms of the three series of slides previously shown

SMOOTHED MODULUS of FOURIER TRANSFORMS
COMA SLIDES





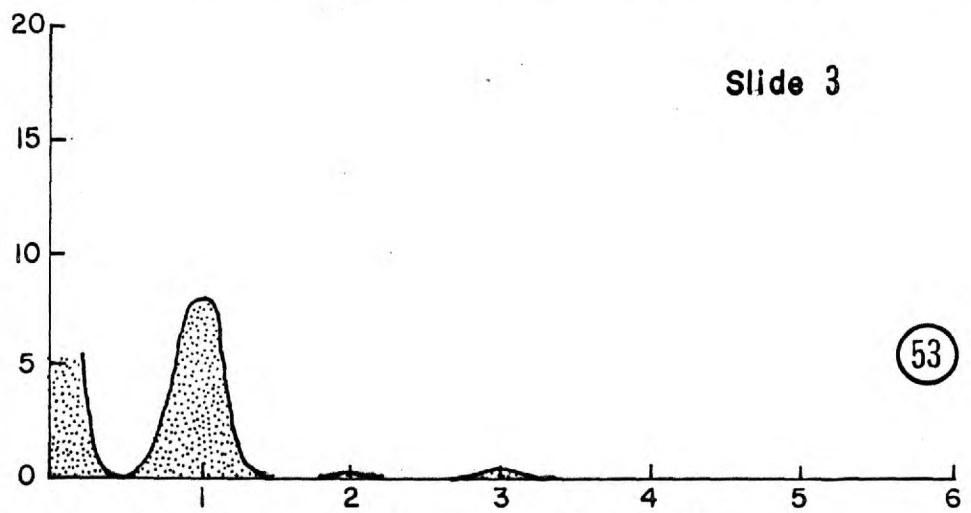
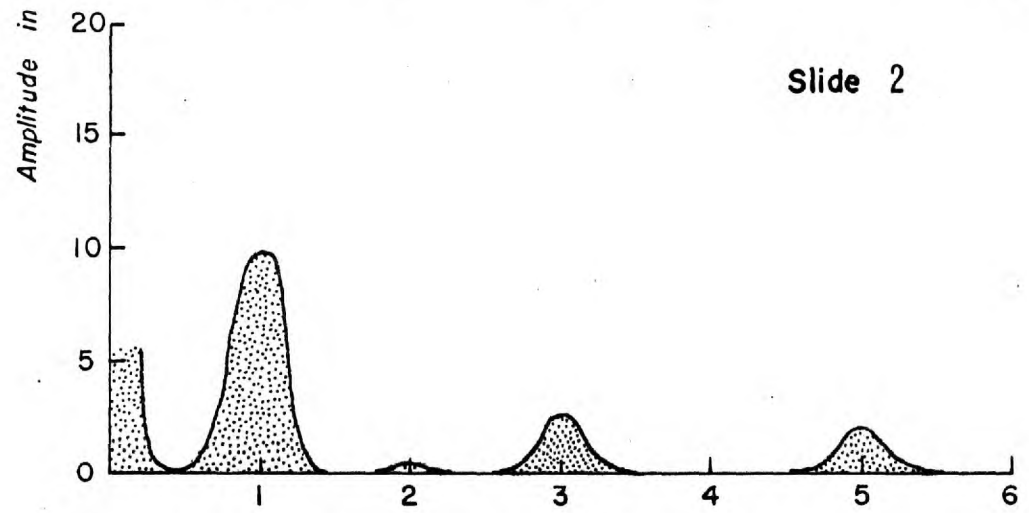
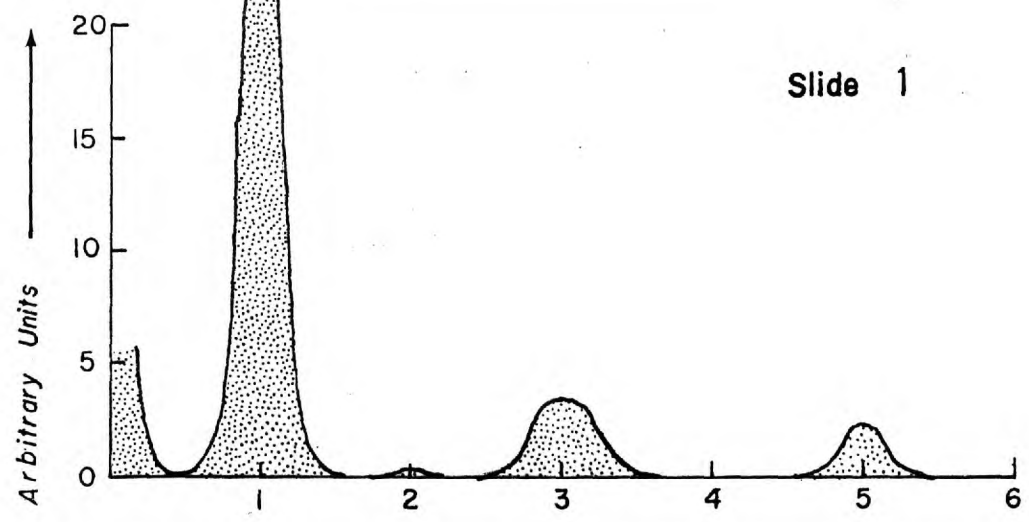
52

Spatial Frequency in Units of Grating Harmonics

Spatial Frequency in Lines per Inch

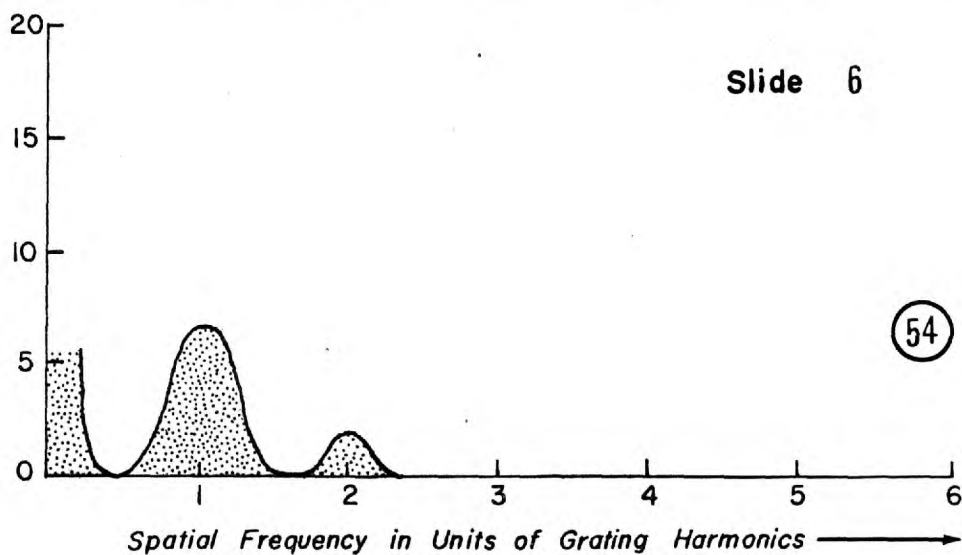
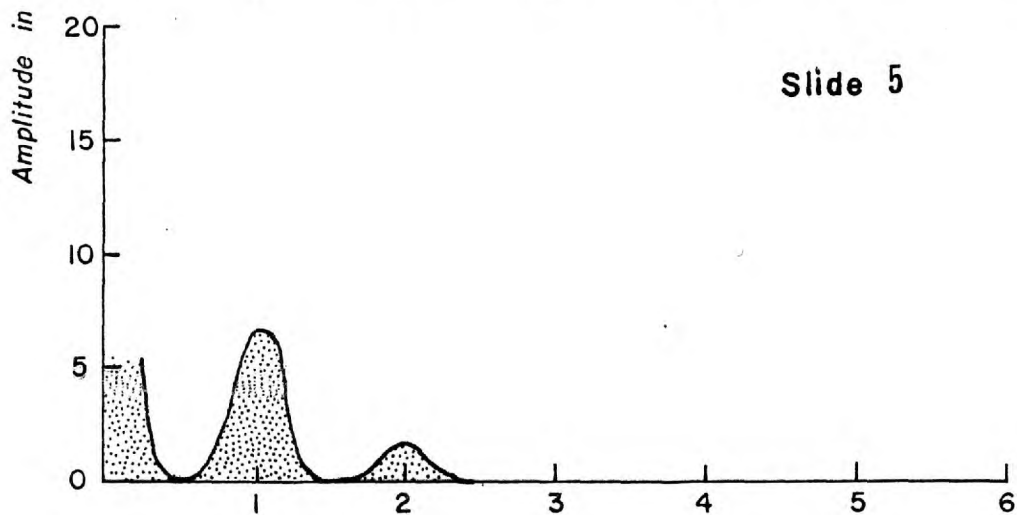
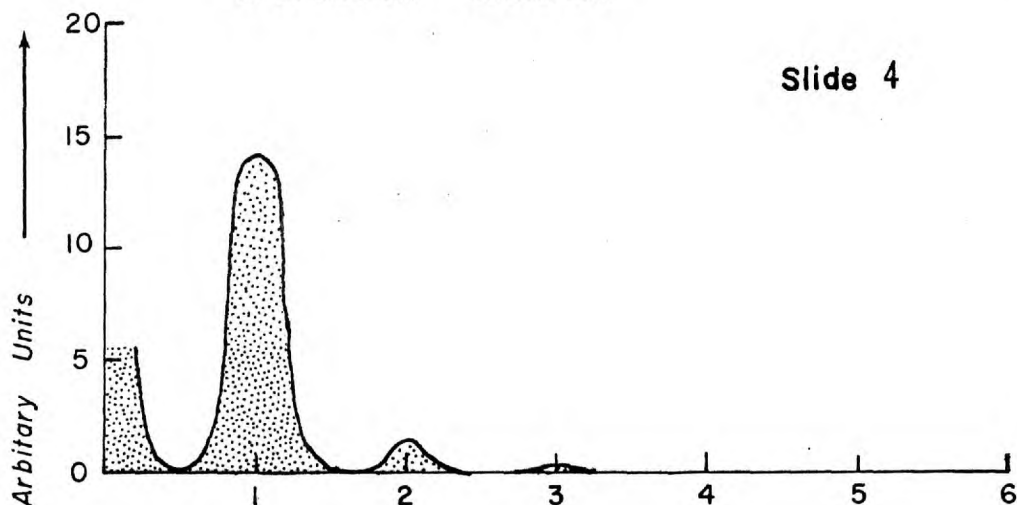
Spatial Frequency in Lines per Inch

SMOOTHED MODULUS of FOURIER TRANSFORMS GAUSSIAN SLIDES

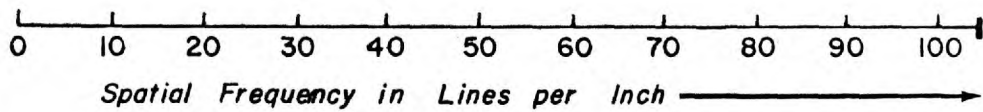


Spatial Frequency in Units of Grating Harmonics →

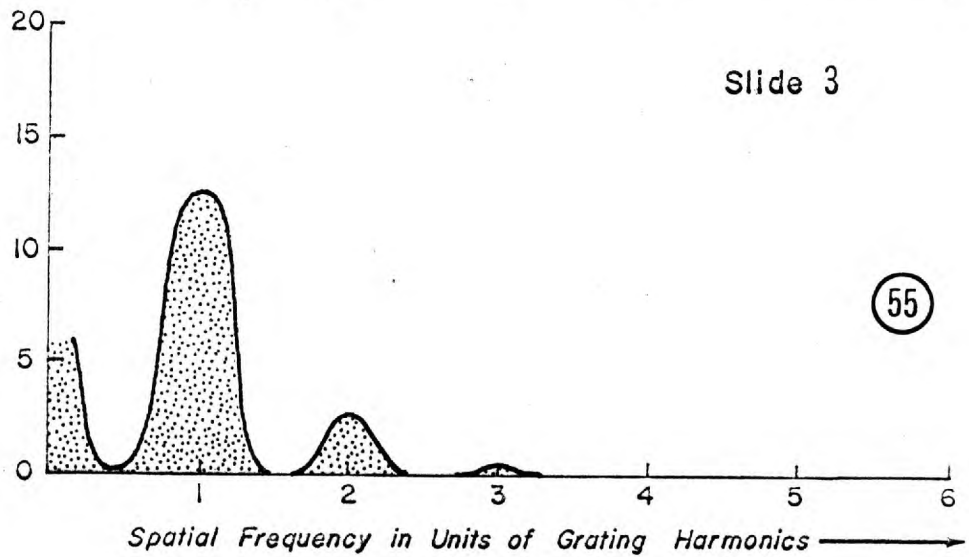
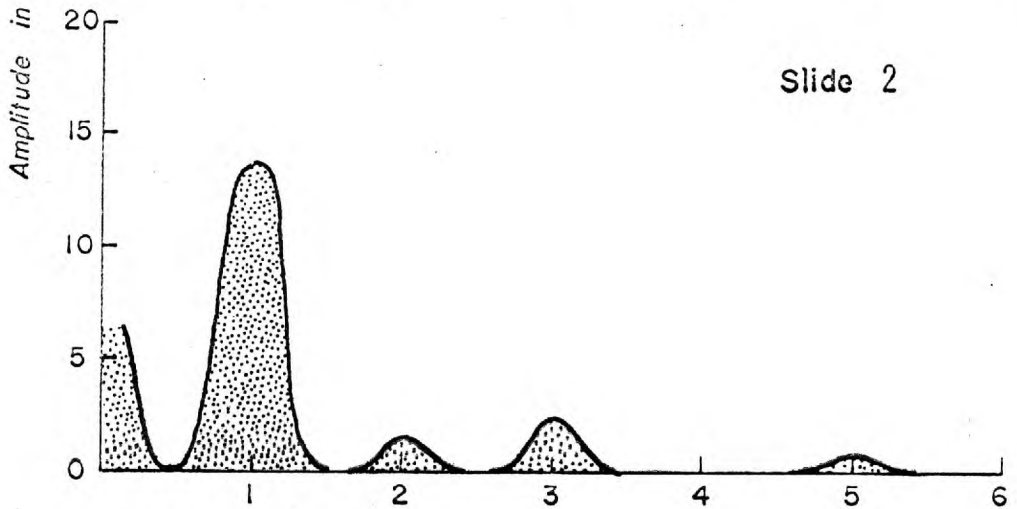
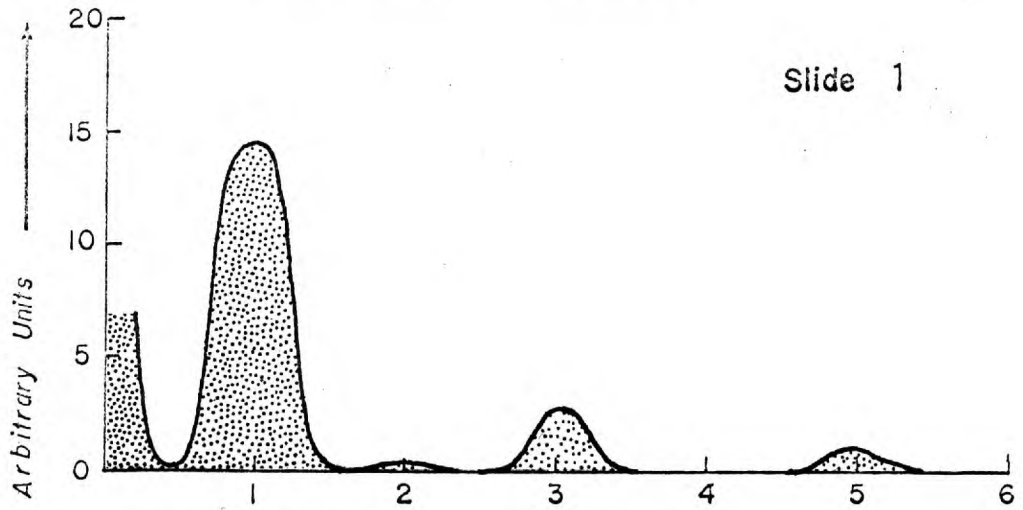
GAUSSIAN SLIDES

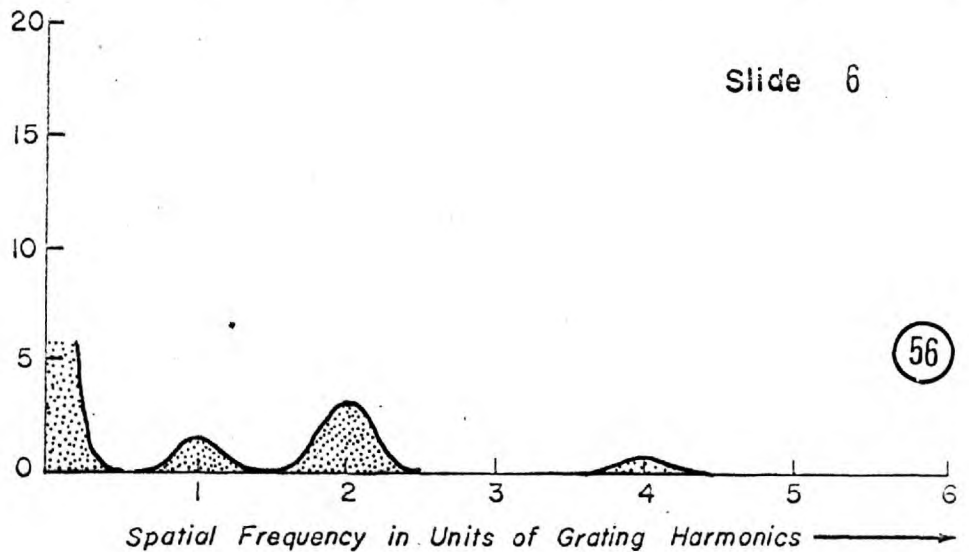
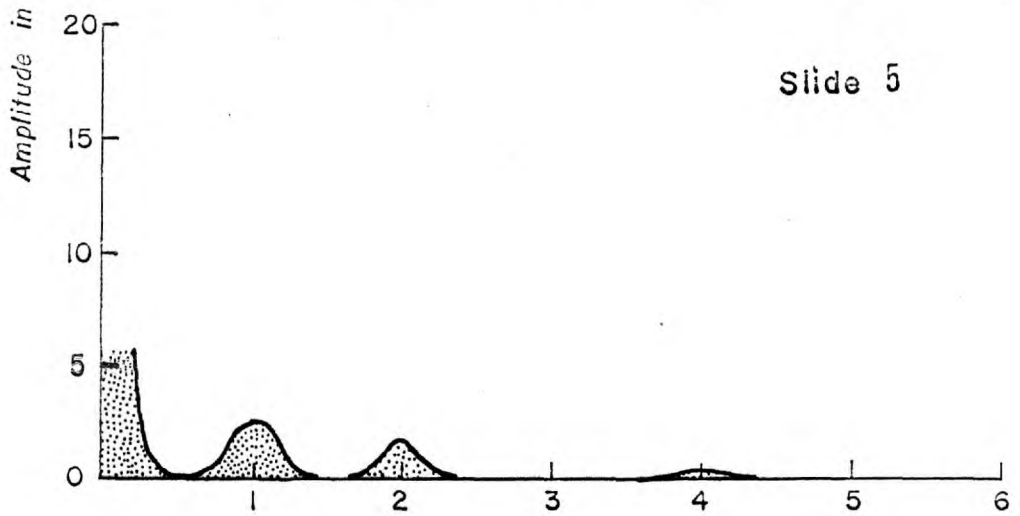
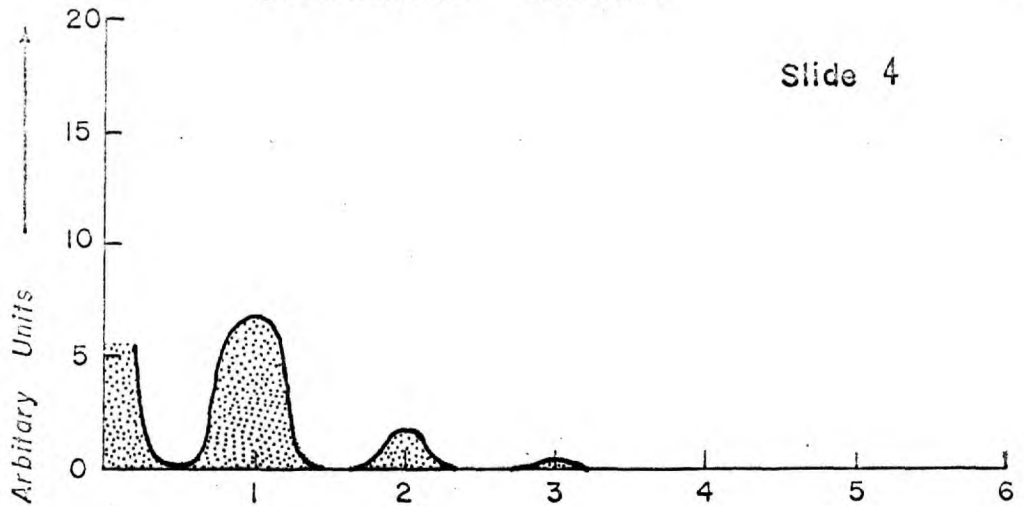


54

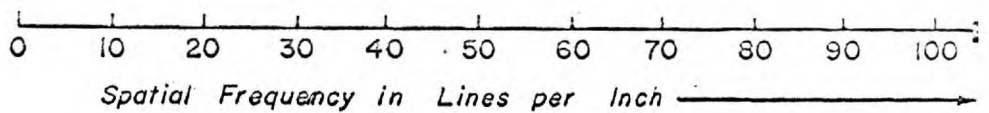


SMOOTHED MODULUS of FOURIER TRANSFORMS

SPHERICAL SLIDES



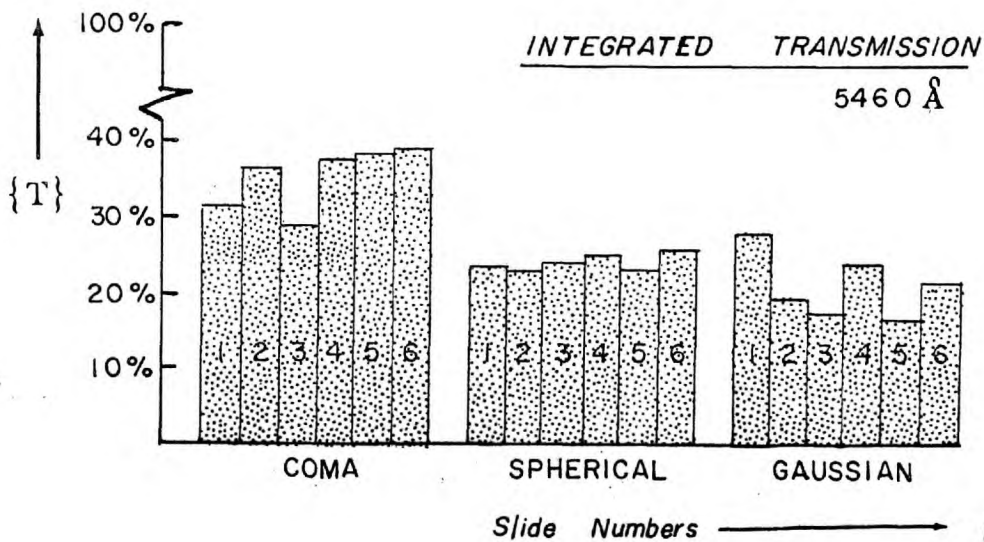
56



to the group of observers. The amplitude units are arbitrary but constant throughout the readings.

It will be noticed that there is a variation in amplitude between the first slides of each series; that the transforms are similar but apparently differently scaled. These and other variations in the progressive reductions of amplitude in the frequency spectrum are due, in spite of the care taken, to a variation in the photographic and development processes. It is most probable that these variations were the result of unequal exposure times, thereby causing an unequal and irregular variation in the expected Michelson visibility of the printed-on grating structure.

Figure (57) shows these variations as changes of the integrated transmission for each slide.



These variations were clearly to be expected from the densitometer traces shown in Figures (48), (49) and (50). The values of the integrated transmission were obtained for an area of $\frac{1}{2}$ " diameter, with a Beckman spectro-photometer at a wavelength of 5460\AA . It will be seen, shortly, that these variations in integrated transmission and, therefore, variations from even steps in the Fourier transforms are closely related to the non-linear progression of response difference noticed by the observers.

COMPARISON BETWEEN TRANSFORMS AND SUBJECTIVE TESTS

If the steps of image degradation, as measured instrumentally, proceed in a linear or, at least smooth, simple manner and if the scaling techniques used on the observer's judgements of quality are valid in their linearity assumptions, it would be reasonable to assume that the curves of response differences, shown in the previous chapter, would also be at least smooth. With the possible exception of the spherically blurred slides, this is not the case. Both the coma and Gaussian response difference curves exhibit strong departures from a smooth

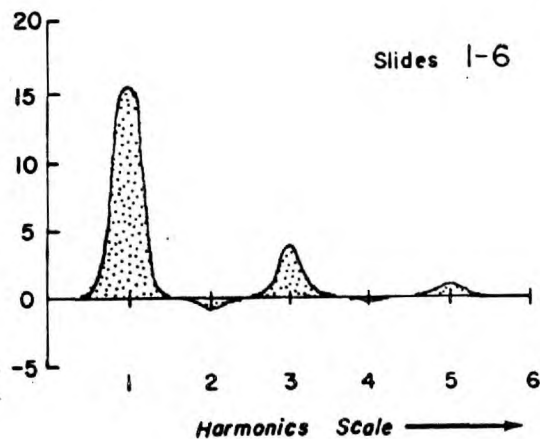
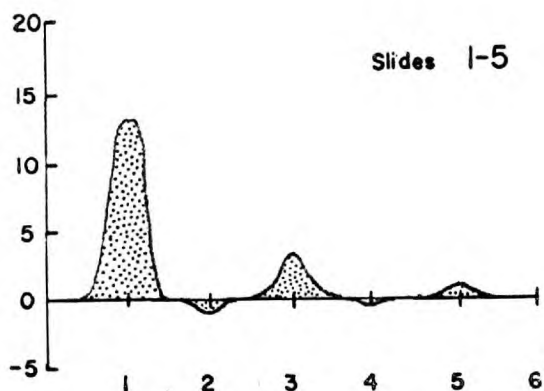
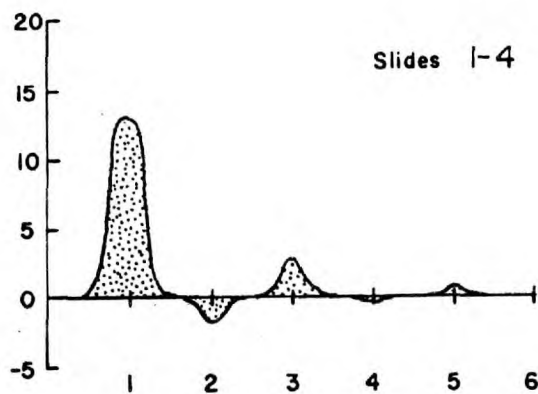
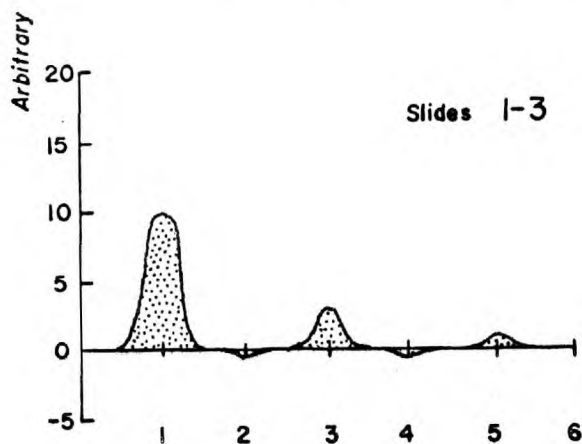
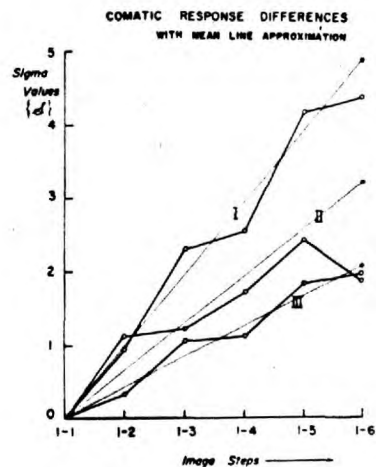
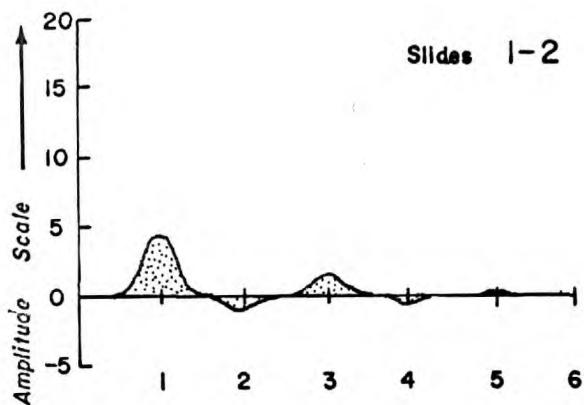
progression. We notice, however, from both the densitometer traces [Figures (48), (49) and (50)] and the values of integrated transmission [Figure (57)] that it is exactly the spherically blurred slides which exhibit the greatest degree of constancy in their integrated transmission and zero shift.

It will be of interest to see whether we are able to obtain scaling values from the Fourier transforms of the slides which will enable us to smooth the response difference curves. This would, at the same time, show us more clearly the relationship between the variation of response difference for the observer and the variation in the Fourier transforms seen instrumentally.

Figures (58), (59) and (60) show the progressive differences between slides resulting from the subtraction of the amplitudes of the transforms of two slides. Included for reference, in these figures, are the response difference measurements for all three distances for each series of slides. It will be noticed more clearly in these plots of response difference that there is a strong similarity between the shapes of the curves for all three distances; that although the observer's certainty of quality decreases with dis-

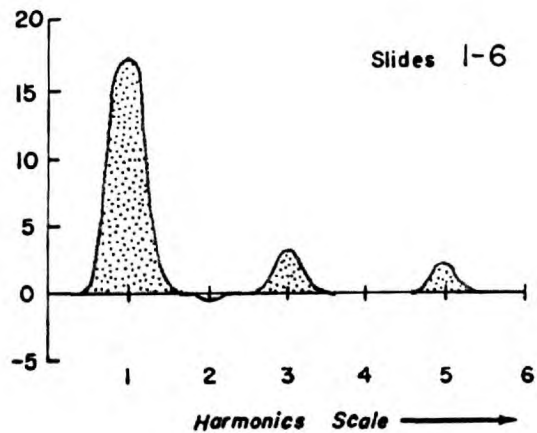
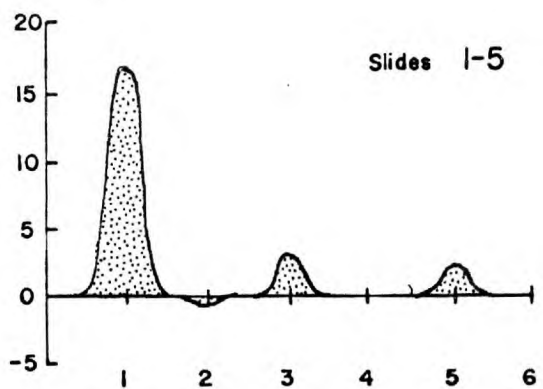
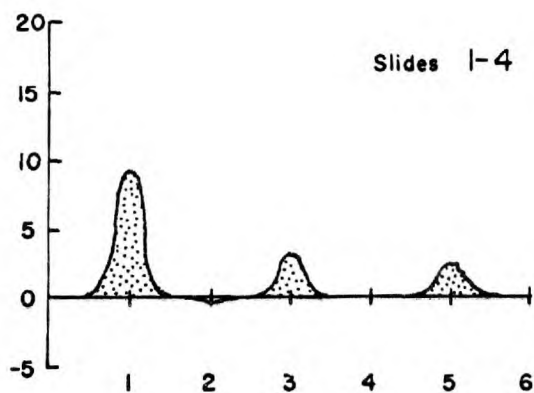
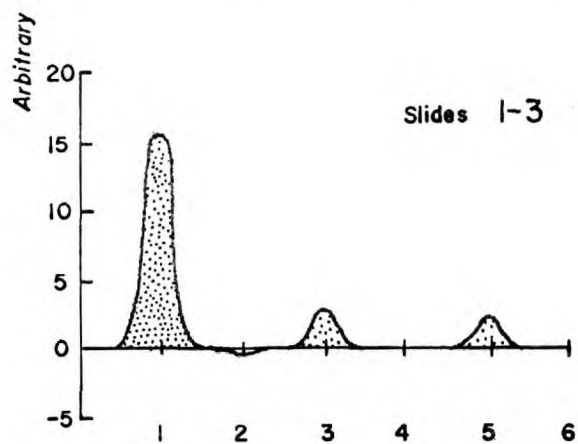
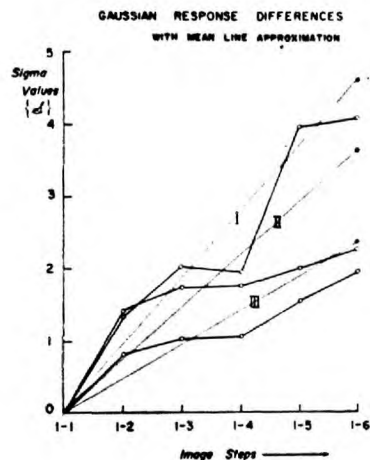
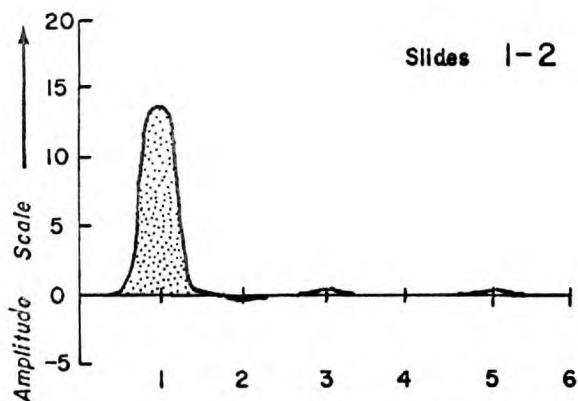
COMA SLIDES

SUBTRACTED DIFFERENCES BETWEEN TRANSFORMS



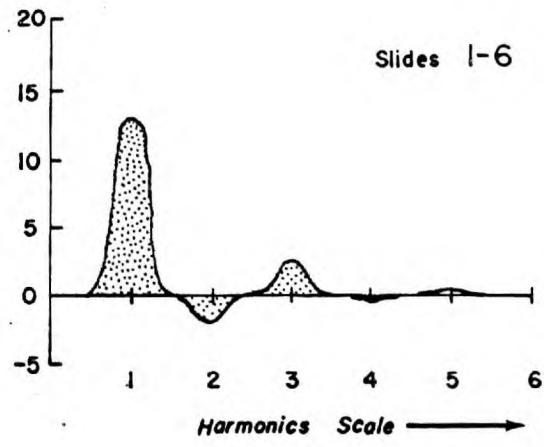
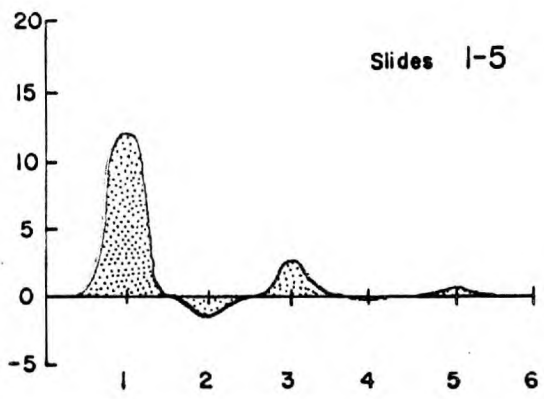
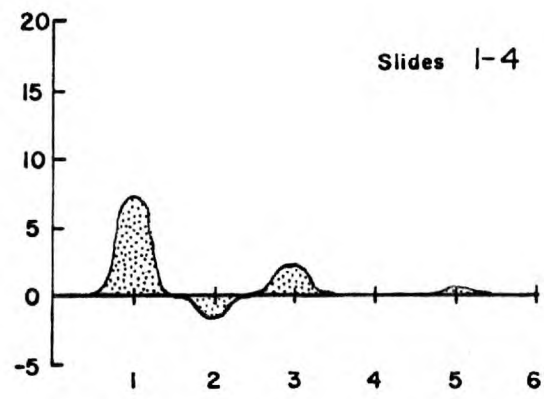
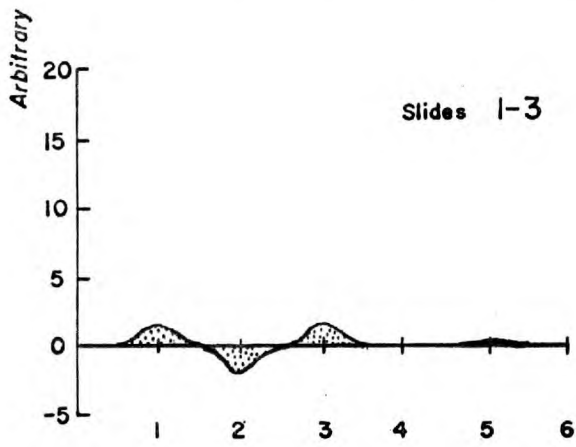
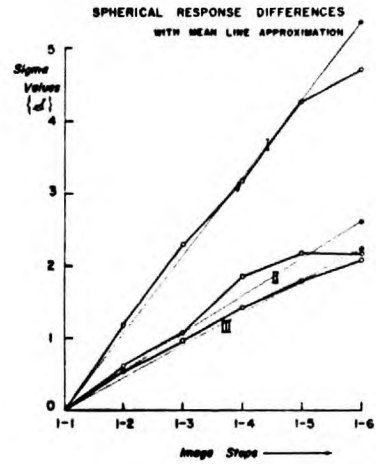
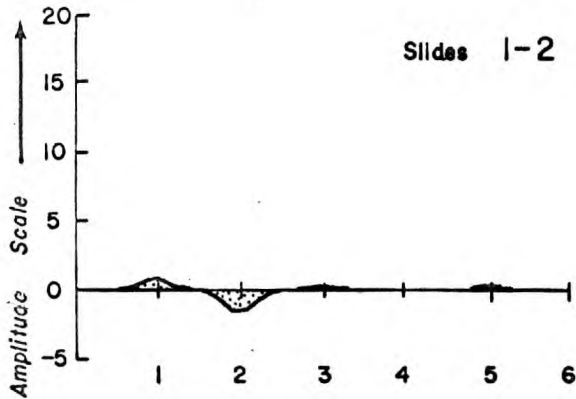
GAUSSIAN SLIDES

SUBTRACTED DIFFERENCES BETWEEN TRANSFORMS



SPHERICAL SLIDES

SUBTRACTED DIFFERENCES BETWEEN TRANSFORMS



tance, the discontinuity effects are present throughout.

Two simple scaling techniques were tried in an effort to smooth these discontinuities. Neither was wholly satisfactory but there was, at least, evidence that such a correlation might exist. In the first instance the sums of the peaks of the transform differences were obtained for each pair. The deviations of these differences from a linear progression were used as scaling factors to weight the calculated response difference values. These weights tended to smooth the response difference curves somewhat, but the effects were far from complete. Secondly, the same weighting method was tried, using only the amplitudes of the fundamental frequency, rather than the sum of the entire frequency spectrum. This technique was just slightly more satisfactory.

Since the shape of the response difference curve does not seem to be dependent on the observing distance it was felt that perhaps the observer was basing his entire judgement only on those frequencies which were within his resolution limits at all three distances (namely the fundamental). The poorer performance of the weighting method involving the entire

frequency spectrum indicates that this is perhaps partially true.

At Distance I (the nearest viewing distance) the maximum sigma value of observed response difference is at most less than five. We may interpret this to mean that the majority (86%) of the observers will be able to just distinguish five steps of image degradation in each set of slides at this distance. Instrumentally we find, however, that there has been an average decrease in amplitude of the fundamental frequency of 77% throughout each series of slides. If we take the instrumental errors to be as much as 5% we would still be able to detect fifteen steps of image degradation by this technique. In other words, the instrument is at least three times more sensitive in detection of image quality than the human eye when that eye is able to resolve the 4th harmonic of pattern. An increase of observing distance, of course, increases the instrumental advantage, by reducing the information available to the eye.

CONCLUSIONS

Looking back to the modulus of the Fourier transforms for each slide, it will be noticed that the Gaussian blur slides lose, with the exception of the second harmonic, most of their upper frequencies rather quickly. This is not the case with the other blur shapes. The observer, however, does not greatly prefer these other slides in his efforts to make a quality judgement. Furthermore, changing the observing distance so that he is only able to see the lower end of the frequency spectrum does not change the character of the observer's ability to discriminate between slides, although it does always make the choice more difficult. Strong discontinuities in the computed response differences for the observer do correspond to changes in the amplitude of the frequency spectrum (such as the slide pair 1-4 in the Gaussian series). These factors all tend to the impression that the observer is mostly concerned with reductions of contrast in the fundamental frequency; complex blur functions are no less detrimental to image quality than more simple blur functions.

While there was a definite and large decrease in the observer's discriminial ability when he was moved in so that he could not see both the third and fourth harmonics (Distance II), the decreased information available at Distance III, namely the lack of first and second harmonics, did very little in decreasing his discriminial ability. His response difference values were only slightly degraded with this increase of distance.

It seems reasonable then that the failure of the weighting procedures was due more to inaccuracies in the response difference data, from perhaps too few observers, than to a basic invalidity of the idea.

It is clear, however, that these instrumental measurements of the transform of the image constitute a superior method of discrimination of image content and quality than the human observer with his visual abilities.

In agreement with the preliminary experiments, it appears that quality judgements for many optical images are primarily dependent on the lower

frequency components of the Fourier transform of the image. That, in fact, a loss of higher frequencies in an image need not be detrimental to the quality judgement provided that there has occurred, at the same time, an increase in contrast for the fundamental frequency.



ACKNOWLEDGEMENTS

I wish to express my deepest gratitude to Dr. H. H. Hopkins for his unending suggestions, assistance, outright help and patient criticism; from his original suggestion of this work to his final corrections of this manuscript, I am indebted to him.

I wish also to thank the Ministry of Aviation who, by way of their contract and grant, have made this work possible and the National Physical Laboratory who made, polished and corrected the Wollaston prism used in the equipment.

